THE BOOK WAS DRENCHED

RECHERCHES ASTRONOMIQUES
DE L'OBSERVATOIRE D'UTRECHT

XIII

PART I

THE HYDROGEN SPECTRUM OF THE SUN

BY

C. DE JAGER

DRUK: EXCELSIORS FOTO-OFFSET - 's-GRAVENHAGE

1952

CONTENTS

CHAPTER I

INTRODUCTION AND SUMMARY

The line spectrum of the sun (and also of the stars) is mainly determined by (*a*) the *structure of the solar atmosphere* and its *chemical composition* and (*b*) the *atomic processes* which determine the way in which radiation is *absorbed* and *re-emitted* by the atoms.

Several *models of the solar atmosphere* have already been derived in the course of the last ten years, both observational and theoretical ones. As the observational models do not yet describe the solar radiation with sufficient precision and still less so the theoretical models, it seems necessary to determine a new model of the atmosphere, which model has to explain as completely as possible the continuous radiation of the sun as well as the Fraunhofer lines.
In general it appears quite possible to compute the excitation and the ionisation of the atoms in a reliable way (laws of Boltzmann and Saha) and also the total absorbing power of the atoms is known. But it is not yet known with sufficient certainty in what way the absorption is distributed over the wavelengths in the region of the Fraunhofer lines, nor do we know the way in which the re-emission varies with the wavelength.
These difficulties fully manifest themselves when an explanation of the profiles of the *strong* Fraunhofer lines is attempted; on the other hand these lines give the possibility of studying the processes of absorption and redistribution in detail, as each point of the line profile may be investigated separately and as also the dependence on depth of these processes may be found by investigating the centre to limb variation of the line profiles.
In this investigation the *hydrogen lines* of the solar spectrum are studied, to which lines the above remarks fully apply.
The remarkable width of the hydrogen lines is caused by the Stark effect of the surrounding charged particles, but there is not yet a complete theory which describes with sufficient exactness the combined influence of all disturbing particles, either the quick or the slow ones. It is generally assumed that for the temperature and pressure which are found in the solar atmosphere, it is only the positive ions which have an appreciable influence.
It is the purpose of this investigation (*a*) to derive a model of the solar atmosphere which explains the profiles of the hydrogen lines and (*b*) to obtain a more precise description of the way in which the absorption coefficient is broadened and in which the re-emission takes place.

Observations are published of
1. the Balmer lines H_{2-3} ... H_{2-16} excepting three strongly blended lines. The lines H_{2-15} and H_{2-16} are hardly visible because of the blending by other solar lines and of the overlapping of the high Balmer lines. The profiles have been determined at Utrecht for 20 values of r/R (Chapter II);
2. the Balmer lines H_{2-3} ... H_{2-6} observed at four points on the disc, and the line H_{2-3} in the chromosphere, the profile of which has been determined up to about 9000 km beside the limb. The observations have been made at Meudon. (Chapter III);
3. thirteen infrared Paschen and Brackett lines, observed only in the central parts of the disc at the Sphynx observatory of the Jungfraujoch (Chapter IV).

As a first step towards a precise model of the solar atmosphere the existing observations of the limb darkening and the energy-wavelength curve of the continuous radiation between 4000 and 6000 A are rediscussed (Chapter V). This yields a new model (*model V*; cf. table 34), which model is supposed to be more reliable than the existing ones.
Nevertheless, it may be proved that many other models could equally well explain the continuous radiation (§ 11 of chapter V). A more definite solution is obtained by modifying model V in such a way, that the observed profiles of H_{2-3} ... H_{2-6} are explained.
In Chapter VI this is done for the deep layers, using only the wings of these lines and in Chapter VII this model is completed for the high solar layers, using the cores (*model VII*). However, to obtain a consistent model, it appears necessary to assume that the line absorption coefficients are greater in the wings of the lines and smaller in the cores, than is predicted by the classical theory for the widening by ions.
It is very satisfactory to notice later on that control calculations show indeed that model VII does not only explain the profiles of the Balmer lines, calculated with the new widening law, (see figures 23 and 25 in Chapter VIII) but

also the energy-wavelength curve of the continuous radiation (figure 28) and the continuous limb darkening between 4000 and 23000 Angström (figures 29 and 30 of Chapter IX).

The corrections, which had to be applied to the profiles of the line absorption coefficients, given by the ordinary theory, show that the true profiles are more widened than the computed profiles. It is true, that the total line absorption $\int \kappa_\nu d\nu$ has remained unchanged for each line but its profile becomes uniformly wider in the wings and correspondingly shallower in the cores. The widening factors are for the Balmer, Paschen and Brackett lines respectively 1,3; 2,3 and 3,1. (Chapters X and XI).
It is true that the *Balmer* lines may thus be explained by assuming that both electrons and ions share equally in the statistical stark widening but this explanation is in any case insufficient for the Paschen and Brackett lines. It does not seem impossible that the physical theory of the widening of the hydrogen lines is susceptible of improvement.

In Chapter XII some problems of blending are examined; it is shown that the faintly indicated profile of the hydrogen line H_{3-7}, blended with the strong H line of Ca^+ may be explained quantitatively; is is further shown that the invisibility of the deuterium lines in the solar spectrum (which invisibility had already led to an extremely low upper limit for the abundance of D) may be explained by the blending with the wing of the corresponding hydrogen line. It is assumed that the upper limit for the abundance of D is of the same order as the terrestrial value ($N_D/N_H \approx 10^{-4}$).

In the last two chapters a far more unsettled subject is dealt with than in the preceding ones. To be able to explain our observations of H_{2-3} in the chromosphere, a model of the chromosphere is necessary. It is shown that - with great uncertainty - such a model may be derived which is in agreement both with the optical and the radio measurements (Chapter XIII).
On the basis of this model the intensity of H_α in the chromosphere may be explained up to a distance of about 3000 km from the limb, using the populations of the low hydrogen levels, computed by GIOVANELLI. The deviations between the observations and the calculations, which increase considerably when progressing towards greater heights, may probably be explained by the very intense upward motions which exist in the region of the spicules.

Acknowledgements
The author wishes to express his deep gratitude to all those who have shown their interest or who have offered help in the course of this investigation, but especially
to Prof. M.MINNAERT, who suggested this subject and who contributed most kindly of his time and knowledge to the discussions, for his unflagging interest and for his constructive criticism;
to Prof. A.DANJON, director of the observatory of Paris and to Dr D'AZAMBUJA for having placed the facilities of the Astrophysical Observatory of Meudon at his disposal;
to Mme D'AZAMBUJA for introducing him to the obvational technique of the Meudon spectroheliograph;
to Dr H.MINEUR, director of the Institut d'Astrophysique of Paris, for his kind permission to work at his institute;
to Dr D.CHALONGE for his kind and helpful advice in photometric problems;
to Prof. P.SWINGS and Prof. M.MIGEOTTE for their permission to use the infrared spectrograph of the Institut d'Astrophysique at Liège; to the latter for explaining the use of his fine instrument so clearly and enthousiastically;
to Mr. L.NEVEN from the Observatory of Uccle, Belgium, for his generous assistance, both in the observations at the Jungfraujoch and in the discussions afterwards; for his permission to publish our combined results in this paper;
to Dr J.HOUTGAST for many instructive hints with respect to the work with the Utrecht spectrograph;
to Dr E.SCHATZMAN and Dr J.KORRINGA for discussions on the widening of the hydrogen lines;
to Mrs. E.van ALBADA-van DIEN for permitting him to use unpublished data on the absorption coefficients in the hydrogen lines;
to Dr H.C.van de HULST for discussions on the chromosphere and its hydrogen spectrum;
to Dr J.C.PECKER and Mr. R.MICHARD for many interesting discussions on the model of the solar atmosphere;
to Mr. E.DENNISON for photometric work on H_β;
to Miss J.BLOM for active and accurate help in many computations;
to Mr. Th.van DIJK for placing some infrared Z-plates at the disposal of the author;
to Mr. J.DAMEN STERCK, for drawing the figures and for his aid in reducing the records of the Balmer lines.

The author is under great obligation for the financial aids which have made this investigation possible:
The stay at Paris was the result of an exchange

of astronomers, sponsored by the Centre National de la Recherche Scientifique (France) and the UNESCO through the intermediary of Prof. STRATTON, president of commission 38 of the International Astronomical Union.
The journey to the Jungfraujoch was also made possible by financial aid of the UNESCO through the intermediary of the I.A.U.

The board of the Jungfraujoch Scientific Station offered financial facilities which made it possible to work at this station.
The publication of this volume of the Recherches de l'Observatoire d'Utrecht was made possible by a grant of the Netherlands Central Organisation for Scientific Research (Nederlandse Organisatie voor Zuiver Wetenschappelijk onderzoek).

CHAPTER II

PHOTOGRAPHIC OBSERVATIONS OF THE PROFILES OF THE BALMER LINES MADE AT UTRECHT

§ 1. *Observational technique.*

The Balmer lines H_{2-3} .. H_{2-16} have been investigated by photographic photometry during the months of January to June 1947. The observations have been made with the solar grating spectrograph of Sonnenborgh Observatory, Utrecht (Ø = 15 cm; F = 7 m); the apparatus has already been described by others[74,75,62,51]. Most observations were made in the second order spectrum (dispersion 2 A/mm), with the exception of the H_α spectra, which were made in the first order. In all spectral regions, except for H_β the intensity of straylight in the spectrograph was reduced by means of placing colour filters in front of the slit. For H_β no suitable filters were available.

A complete set of observations consisted of three plates I, II and III. The spectra numbered from I,1 to I,8 are found on the first plate; the spectra II,1 to II,8 are found on the second plate, each number corresponding with another distance from the centre; on the third plate were taken four spectra III,1 to III,4 at points near the northern limb and four spectra III,5 to III,8 at the corresponding points near the southern limb. The values of cosθ, corresponding with these spectra are given in table 1. The slit was adjusted radially with respect to the solar disc for all points with $r/R < 0,85$; for the spectra nearer to the limb it was always adjusted tangentially. The height of each spectrum was 2 mm.

All spectra on the same plate were made with the same exposure time; to have the same photographic densities in the spectra, the intensity of light in the central parts of the sun was reduced with the aid of a photographic wedge, placed 5 cm above the slit. In all cases, however, the parts of the sun with $r/R > 0,91$ were photographed without any weakener.

Two standardizing spectra were made on each plate with the aid of a Zeiss platinum step weakener, using the light of the central parts of the disc. For these two spectra the orientation of the weakeners differed by 180° with respect to the slit in order to eliminate the influence of non parallelism (if existing) of the slit jaws. In order to compensate possible irregularities of the slit jaws, the slit-width, used in making the standardizing spectra was always much greater than the normal width. The latter was, according to Van CITTERT[27,28] 0,05 mm for Hβ; the former was respectively 0,3 and 0,6 mm for both standardizing spectra in the H_α region and 0,6 and 0,9 mm in the violet region. The too great intensity of the light for the calibration spectra was reduced in turn by a homogeneous weakener, placed about 5 cm above the slit.

TABLE 1. Points on the solar disc which have been investigated

Designation of spectrum	r/R	cos θ	slit Tangential or Radial
I,1	0,000	1,000	R
I,2	0,442	0,897	R
I,3	0,605	0,796	R
I,4	0,722	0,692	R
I,5	0,817	0,577	R
I,6	0,886	0,464	T
I,7	0,928	0,373	T
I,8	0,964	0,266	T
II,1	0,322	0,947	R
II,2	0,528	0,849	R
II,3	0,671	0,742	R
II,4	0,770	0,638	R
II,5	0,844	0,537	R
II,6	0,910	0,415	T
II,7	0,950	0,312	T
II,8	0,978	0,209	T
III,1; III,5	0,975	0,222	T
III,2; III,6	0,983	0,184	T
III,3; III,7	0,987	0,161	T
III,4; III,8	0,993	0,123	T

§ 2. *Photographic plates.*

The following plate types were used.

For H_α: Kodak 103 U and Agfa 700 Hart.

For the other lines: Gevaert Replica and Guilleminot Ortho.

The exposure times ranged between 3^s and 1^m, except for the ultra violet region, where exposure times up to 10^m were used. The total number of plates which were photometrized was 107; the total number of recorded spectra was 926.

All plates, except fifteen, were developed in a metol-hydroquinone-borax developer during 4½ minutes at 18° - 22° C. This developer gives clear images and a soft gradation, which was appropriate (great intensity variation in the lines). If I is the intensity of the light and T the transmission of the plate, then $dT/d(\log I)$ varies between 0,5 and 0,9 for this developer. The other fifteen plates were developed in a hydroquinone developer during 1½ minute giving a high gradation ($dt/d(\log I)$ ranged between 1,1 and 1,6); this developer was used for the ultra violet region.
Two plates I and II (cf. § 1 and table 1) were always made immediately after each other with exactly the same exposure times and under the same circumstanced. These plates were always developed together and very often these two plates had been cut from the same 9x12 cm^{2}plate. The gradation curves of these two plates were nearly always identical.

§ 3. *Photometry.*
The plates were recorded by the Moll type self recording photometer of the Utrecht observatory, constructed in our workshop by Mr. N.van STRATEN after the design of Dr J.HOUTGAST[63]. The widths of the photometer slits always ranged between 0,8 and 0,10 mm; this corresponds with about 0,01 mm as projected on the plate and with 0,02 A in the second order spectra. The height of the slit was about 10 mm, corresponding with 1 mm on the plate.

§ 4. *The apparatus function of the spectrograph.*
It is not necessary to know the apparatus function of the spectrograph very accurately, for the lines we are engaged on in this investigation are all wide.
The apparatus profile was determined for each individual plate, but only for the lines H_α to H_δ, by representing the profiles of some well isolated solar lines (no hydrogen lines) by a Voigt profile[65]; this was done by determining the Voigt parameters β_1 and β_2^2
The same lines have been looked up in the Utrecht Atlas of the Solar spectrum[108], the Voigt parameters of these profiles have also been determined. As the obliteration of a Voigt profile with another one is performed by the addition of the corresponding Voigt parameters, the Voigt profile of the Utrecht apparatus function is known relative to that of the Solar Atlas. Since the apparatus function of the Atlas is known[64], the Utrecht apparatus profile can be found.
The mean Voigt parameters of the apparatus profile and their theoretical values are given in table 2. The parameters β_1, β_2, h and p are introduced by Van de HULST[64]; β_1 and β_2 are the „Voigt parameters", h is the half width of the profile and $p = S/hc$, where S is the area of the profile of which c is the central value.

TABLE 2. Mean Voigt parameters of the apparatus profile of the Utrecht solar telescope.

line	order	β_1	β_2^2	p	h(μλ)	h(A)	h(mm)
H_α	I	7	1380	1.16	69	0,45	0,11
H_β	I	4,6	3800	1.13	110	0.53	0.13
H_γ	II	2.2	790	1.11	49	0.24	0.12
H_δ	II	0	510	1.06	38	0.17	0.08
	II	6.0	460	1.20	41	0.17	0.08
theory							
H_β	I					0.48	0.12
H_β	II					0.24	0.12

There is a good agreement between the theoretical half width and the mean of the observed values; they are practically equal. This shows, that the spectrograph may be considered to be excellent.

The influence of the limited resolving power was determined by obliterating the lineprofiles by the apparatus function, this was performed numerically. The correction to the central intensity is for H_α (first order) 0,04 to 0,05 (centre to limb of disc), while it is for the central parts of the second order lines of the order of 0,02. The correction is for these lines practically zero at 1 A distance from the line centre; for H_α in the first order this is at a distance of 2 A.

§ 5. *Corrections for Rowland ghosts.*
The same data and formulae were used as in HOUTGAST's thesis[62]. Corrections for the first and second Rowland ghosts at 6,5 and 13 A from the line centra were also applied.

§ 6. *Corrections for scattered light.*
The total intensity of the scattered light depends principally on the state of the mirrors and the objective. It was determined on three different days by measuring the intensity of the light beyond the sun's limb for different distances to the centre of the disc and for the wavelengths 3700 and 6500 A. Cf. table 3. The results, which are given in table 5, are expressed in the intensity of the centre of the disc.

Next we want to find the law of the scattering and to correct our observations. It is supposed that the intensity of scattered light I_{sc} at a point (x,y) at a distance r from a luminous point with intensity I is

$$I_{sc}\, dxdy = c.e^{-\alpha r^2} dxdy$$

TABLE 3. Periods of observations, grouped according to the intensity of stray light

period 1947	plate nr.	mirrors	objective	stray light measured on	λ
16 I - 26 III	H 28-H 72	clean	clean		
10 V - 3 VI	H 80-H136	somewhat affected	somewhat dusty	31 V '47	3700
18 VI - 25 VI	H143-H171	clean	dusty	24 VI '47	3750; H_α
15 VII - 16 VII	H172-H197	affected	clean	16 VII '47	3700; H_α
25 IX - 21 X	H198-H215	clean	clean		

It is further supposed that only a fraction d of the light I is scattered, hence:

$$\iint_{-\infty}^{\infty} c.e^{-\alpha r^2} dxdy = c\pi/\alpha = d$$

For a homogeneous disc the intensity of light in a point, outside the solar disc with coordinates $(x_1,0)$ - see figure 1 - is:

$$I_{sc}\ (x_1,0) = \frac{\alpha d}{\pi}\int_{-1}^{+1} e^{-\alpha(x_1-x)^2}dx \int_{-\sqrt{1-x^2}}^{\sqrt{1-x^2}} e^{-\alpha y^2}dy =$$

$$= \frac{\alpha d}{\pi}\int_{-1}^{+1} e^{-\alpha(x_1-x)^2} E_2(\sqrt{1-x^2})\,dx \qquad (II,1)$$

$E_2(y)$ is the error function.

In order to take the variation of the intensity of light over the solar disc into account, the limb darkening is represented by a discontinuous curve:

6560 A	3700 A
$0,0 < x < 0,5$: $I = 1,0$	$0,0 < x < 0,5$: $I = 1,0$
$0,5 < x < 0,9$: $I = 0,8$	$0,5 < x < 0,88$: $I = 0,8$
$0,9 < x < 1,0$: $I = 0,5$	$0,88 < x < 1,0$: $I = 0,3$

Thus the calculation of the intensity of the scattered light is reduced to a summation of three integrals of the type (II,1). The integration has been performed numerically according to GAUSS' method. It is simplified by supposing that I is only a function of x and that $I(x_0,y)$ can be replaced by a constant mean value over the y interval; roughly we put

$$\bar{I}(x_0;y) = I(x_0;\ 0,75\sqrt{1-x_0^2})$$

since, according to MINNAERT[105] this is the case for the disc as a whole. It does not exactly apply to a particular x_0, but the error, made with this simplification is not thought to be very great.

It was further determined from the well known limb darkening curves, that

$I(0;0,75)/I(0;0) = \bar{I}(0;y)/I(0;0)$ =

= 0,85 for 6560 A

= 0,70 for 3700 A

After some trials it was found that the best

TAPLE 4. Intensity of scattered light around the solar disc. (logarithmic scale; the values are expressed in the intensity of the centre of the disc).

A. OBSERVED VALUES

plate	λ	distance to sun's limb expressed in solar radius						
		0,03	0,06	0,09	0,15	0,18	0,45	0,90
129	3700	-1,32	-1,33	-1,41				
157	3750			-1,91		-1,99		
158	6560	-1,86		-2,02	-2,14			
189	3700	-1,98		-2,04			-2,68	-2,80
190	6560	-2,02		-2,28			-2,52	-2,66

B. THEORETICAL RESULTS

α=0,50	d=0,32	-1,32	-1,34	-1,40				
0,50	0,10			-1,91		-1,99		
0,40	0,11	-1,95		-1,99	-2,07			
0,50	0,072	-2,00		-2,06			-2,59	-2,95
0,40	0,063	-2,16		-2,28			-2,38	-2,81

agreement with the observations occurs for α = 0,4 at 6560 A and for α = 0,5 at 3700 A, though the agreement is not complete (table 4). However, for our purpose it will do.

FIGURE 1

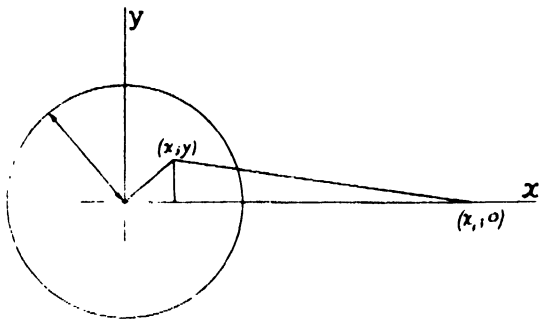

The measured intensities of the "sky" are, concerning their order of magnitude, comparable with those, measured by WANDERS[188] with the same apparatus. They are also of the same order of magnitude as the sky intensities, measured by us at the "grand spectrohéliographe" at Meudon (see chapter III).

With formula (II,1) the corrections for scattered light have been computed for H_α, $\Delta\lambda$ = 1,25 A and for H_ζ, $\Delta\lambda$ = 0,4 A. For these two wavelengths the function

$$\frac{d}{d(\sin\theta)}\left\{\frac{I_{\Delta\lambda}(\sin\theta)}{I_{cont.}(\sin\theta)}\right\}$$

has its maximal value, so in this way the greatest possible value of the correction was calculated – see table 5. It is obvious, that the influence of scattered light is negligible in nearly all cases. Only in the second period of observations (corresponding with plate 129) it would have some influence near the limb of the sun but in that period no limb observations have been made.

§ 7. *The accuracy of the limb observations.*
Atmospheric scintillation and driving errors in the clockwork may result in deviations up to 0,2 or 0,3 mm in the position of the solar image. In the extreme limb spectra this may introduce considerable errors (e.g. an error of 0,3 mm in the observations at $\cos\theta$ = 0,123 gives values of $\cos\theta$ of 0,070 or 0,148 respectively). Another consequence of this fact is that the intensity of straylight from the central parts of the disc is greater than should be the case according to table 5. In figure 2 it is shown that for the outmost points the mean value of $I_{cont.}(r)$ is about 90% of its true value, so that the correction is about 10% greater than the value, which would be obtained from table 5; but even then it remains negligible.

FIGURE 2

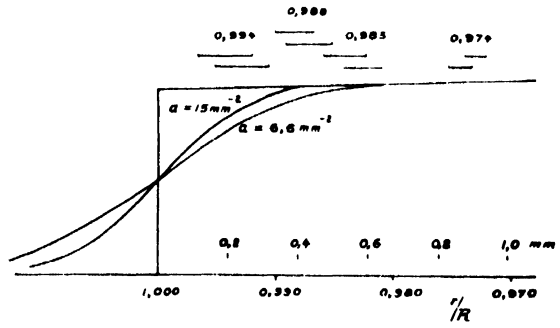

Deformation of the solar limb by scintillation and driving errors. The value α = 15 mm^{-2} corresponds with a mean deviation of ± 0,2 mm; α = 6,6 mm^{-2} corresponds with ± 0,3 mm. The parts of the sun's profile which are used for the limb spectra are indicated in the upper part of the figure.

§ 8. *The final profiles.*
They are given in tables 6 to 15. In the tables for H_α to H_δ the mean values are put between brackets if they have only been derived from one wing of the line or if these values are means of less than five individual measurements or if the differences between the mean values for the same wavelength distances in the red and the violet wings exceed 2% without any obvious reason.
For the lines H_{2-8} and higher, all data are obviously subject to greater uncertainty; this is expecially the case for H_{2-15} and H_{2-16}, which lines are very difficult to observe.

TABLE 5. Maximal influence of scattered light for H_α and H_ζ (the intensities are expressed in the intensity of the centre of the disc.; x = sinθ).

plate	wavelength	α	d	x=1,00	0,90	0,80	0,60	0,00
129	3700	0,50	0,32	-0,018	-0,008	-0,006	-0,002	+0,005
157	3750	0,50	0,10	-0,005	-0,003	-0,002	-0,001	+0,002
158	6560	0,40	0,11	-0,003	-0,001	-0,001	000	+0,001
189	3700	0,50	0,072	-0,003	-0,002	-0,001	000	+0,001
190	6560	0,40	0,063	-0,002	-0,001	-0,001	000	+0,001

TABLE 6. Residual Intensities of H_α (x 1000). λ = 6562,82 A.

Δλ(A) / cos θ	0,0	0,2	0,4	0,6	0,8	1,0	1,25	1,5	2,0	3	4	5	6	7	8	9	10	12	14	16	18	20
1,000	172	204	279	429	575	657	703	733	768	823	862	892	910	922	941	949	955	969	976	977	984	(982)
0,947	(167)	(213)	(274)	435	(575)	660	711	736	773	822	868	891	907	922	927	946	957	969	978	983		
0,897	195	257	331	453	599	(719)	747	774	805	849	882	929	935	944	947	952	962	973	978	986	(989)	
0,849	203	226	302	(445)	586	677	727	760	793	843	874	900	920	933	943	951	955	966	972	977	980	(981)
0,796	209	258	328	450	593	681	732	766	800	849	892	909	922	933	943	950	961	974	983	985	(989)	
0,742	203	235	322	470	610	699	768	818	820	860	903	919	930	939	946	953	962	971	978	984	984	(991)
0,692	201	224	312	480	640	725	763	786	820	873	899	922	936	943	946	955	964	969	980	988	(991)	(991)
0,638	197	225	303	455	633	740	785	808	831	880	899	920	930	937	946	955	967	978	980	986	(987)	(989)
0,577	218	241	323	467	657	745	793	814	850	893	921	939	947	951	956	964	973	978	987	(984)		
0,537	222	241	337	506	678	768	812	823	870	903	924	938	946	953	956	964	966	975	978	981	(986)	
0,464	215	247	330	513	661	775	827	849	879	909	935	946	953	958	965	966	974	977	985			
0,415	197	226	305	485	692	798	841	868	889	918	942	956	962	966	970	974	978	980	982	983		
0,373	227	243	341	524	724	839	875	905	915	950	959	967	975	977	978	977	979	(989)				
0,312	193	224	321	492	695	805	862	888	910	937	951	956	966	966	969	974	981	981	(985)			
0,266	203	230	323	518	690	847	882	907	914	936	950	961	967	976	980	979	981	987	(992)			
0,222	(185)	(201)	(281)	518	676	(823)	881	899	921	954	961	970	979	981	987	(989)	(991)	(992)				
0,209	215	236	327	523	728	868	906	915	936	955	964	969	972	975	978	978	980	981	(982)			
0,184	(194)	(224)	(300)	(505)	(722)	(856)	(905)	(917)	(933)	958	964	973	978	981	984	985	986	(988)	(991)			
0,161	(206)	(242)	(333)	526	722	886	926	926	944	965	973	974	977	(982)	(984)	986	(987)	(991)				
0,123	(224)	(266)	(349)	(573)	712	865	926	929	950	976	979	985	990	992	(991)	989	(992)					

TABLE 7. Residual Intensities of H_β (x 1000). λ = 4861,33 A.

Δλ(A) / cos θ	0,0	0,2	0,4	0,6	0,8	1,0	1,25	1,5	2	3	4	5	6	7	8	9	10	12	14
1,000	176	239	403	562	612	647	685	718	765	824	864	890	914	925	937	955	964	(975)	(975)
0,947	(179)	230	406	563	620	665	709	739	776	826	868	893	913	928	941	(945)	(945)		
0,897	180	253	416	538	610	644	676	713	773	827	867	890	908	916	926	937	946	966	
0,849	(172)	231	440	599	656	675	714	750	797	867	894	910	927	936	937	(945)	(945)		
0,796	193	247	420	583	629	669	708	718	781	839	886	911	929	943	946	955	(966)		
0,742	177	223	447	608	669	700	725	760	773	842	866	897	924	936	942	946			
0,692	187	256	455	636	684	701	729	771	817	862	888	909	929	934	939	946	948	966	(980)
0,638	173	246	435	640	688	716	744	770	797	855	876	892	910	923	933	942	950		
0,577	196	262	445	603	709	733	761	792	838	886	923	945	956	961	(966)	(964)	(976)		
0,537	200	227	472	655	693	736	764	783	(811)	858	881	901	919	929	935	940	(940)		
0,464	183	248	(425)	612	670	713	737	762	843	853	880	898	923	933	943	955	(949)	(969)	
0,415	195	276	469	681	720	766	802	833	858	899	920	927	943	945	948	953			
0,373	189	255	464	678	751	788	817	841	880	908	935	946	961	970	971	972	977		
0,312	222	296	516	751	814	843	867	888	906	912	930	942	954	954	(955)				
0,266	189	250	470	680	762	815	836	853	875	896	914	935	952	954	962	962	(965)	(973)	
0,222	(179)	(240)	(475)	(735)	804	851	872	892	913	(922)	(950)								
0,209	202	272	(503)	745	817	850	871	885	912	930	943	953	(961)						
0,184	(207)	(236)	(470)	(754)	(867)	(875)	(910)	(906)	(918)	(940)									
0,161	(216)	(272)	(499)	(778)	843	877	898	912	922	(930)									
0,123	(212)	(298)	(483)	(781)	853	880	897	915	924	(933)	(954)								

TABLE 8. Residual Intensities of H_γ (x 1000). λ = 4340,47 A.

Δλ(A) / cos θ	0,0	0,2	0,4	0,6	0,8	1,0	1,25	1,5	2,0	3	4	5	6	7	8	9
1,000	185	259	400	508	577	(627)	(686)	(732)	(780)	(858)	897	929	960	(979)	(989)	
0,947	(183)	272	415	499	559	(612)	(652)	(722)	(779)	(852)	887	934	963	974	(982)	(989)
0,897	191	261	(434)	552	615	(663)	(740)	(769)	(828)	(863)	919	951	970	978	(982)	(987)
0,849	(178)	262	425	535	581	(632)	(692)	(743)	(796)	(863)	918	951	968	976	987	989
0,796	189	285	449	572	627	(711)	(743)	(774)	(830)	(894)	918	947	969	976	(965)	(984)
0,742	181	282	450	562	614	(661)	(707)	(764)	(826)	(893)	928	950	963	976	982	
0,692	207	295	481	595	653	(699)	(745)	(786)	(841)	(912)	934	960	971	980	983	(987)
0,638	194	273	472	588	(669)	(702)	(748)	(800)	(847)	(912)	936	964	978	984		
0,577	215	303	495	632	694	(745)	(796)	(826)	(887)	(928)	960	984	987	(988)		
0,537	185	283	508	626	681	(720)	(775)	(823)	(875)	(928)	963	972	984			
0,464	205	323	538	660	(734)	(780)	(832)	(863)	(921)	(953)	960	987	993			
0,415	195	(309)	548	665	(723)	(774)	(824)	(862)	(911)	(955)	965	977	990	(998)		
0,373	242	(352)	607	752	(793)	(829)	(873)	(906)	(937)	(953)	970	981	(902)			
0,312	214	356	580	711	(771)	(807)	(854)	(886)	(928)	(951)	970	985				
0,266	250	381	644	778	(821)	(848)	(890)	(921)	(943)	(973)	985					
0,222	(210)	324	624	769	(806)	(870)	(906)	(937)	(977)							
0,209	197	329	614	748	(821)	(846)	(882)	(912)	(968)	(967)	977	(992)				
0,184	(250)	352	675	838	(855)	(893)	(925)	(943)	(970)							
0,161	(207)	(333)	666	837	(850)	(891)	(918)	(949)	(978)							
0,123	(224)	(337)	661	825	867	(912)	(937)	(979)	(981)							

TABLE 9. Residual Intensities of H_δ (x 1000). λ = 4101,74 A.

Δλ(') / cos θ	0,0	0,2	0,4	0,6	0,8	1,0	1,25	1,5	2,0	3	4	5	6	7	8	9	10
1,000	226	305	447	(561)	(615)	(654)	(696)	718	773	833	871	(892)	(912)	(931)	950	(960)	
0,947	(188)	242	413	(541)	(592)	(643)	(712)	734	780	(874)	(923)	(947)	(970)	(971)	(976)		(980)
0,897	231	327	481	(597)	(642)	(686)	(723)	760	807	878	906	(933)	(952)	(969)	(967)	976	
0,849	198	281	431	(548)	(619)	(662)	(707)	743	792	878	958	(931)	951	961	(963)	(972)	
0,796	(229)	(320)	(477)	(590)	(654)	(690)	(728)	(769)	(828)	(875)	(916)	(931)	(944)	(956)	(968)		
0,742	201	294	462	(590)	(646)	(688)	(738)	750	804	878	917	938	951	(965)	(959)	(973)	
0,692	(257)	328	511	(647)	(703)	(745)	(780)	807	847	900	922	(931)	(947)	(966)	(969)	(980)	
0,638	208	318	471	(593)	(662)	(718)	(770)	783	837	900	937	955	963	(974)	(986)		
0,577	245	(388)	566	(672)	(725)	(769)	(800)	832	869	921	(943)	(958)	(970)	(976)	(979)	(984)	
0,537	253	355	527	(629)	(698)	(727)	(788)	807	848	886	919	944	(965)	(974)	(980)		
0,464	(277)	(386)	(558)	(687)	(740)	(783)	(815)	(842)	(899)	(931)	(952)	(966)	(978)	(982)	(985)		
0,415	264	366	544	(696)	(742)	(774)	(795)	833	874	921	943	(966)	(970)	(981)	(987)		
0,373	288	407	605	(732)	(779)	(810)	(844)	862	896	952	(971)						
0,312	(293)	419	615	(746)	(808)	(844)	(862)	895	919	(947)	(957)	(962)	(974)	(988)			
0,266	(308)	437	679	(777)	(835)	(874)	(895)	917	932	967							
0,222	316	461	642	(807)	(840)	(878)	(897)	917	944	961	(979)						
0,209	299	438	655	(775)	(827)	(853)	(871)	(890)	906	(939)	(955)	(962)	(978)	(978)			
0,184	308	469	694	(838)	(879)	(895)	(922)	938	955	964	978						
0,161	338	479	700	(855)	(899)	(899)	(919)	924	936	966	978	(988)	(955)				
0,123	345	484	695	(837)	(869)	(885)	(904)	922	944	964	(984)						

TABLE 10. Residual Intensities of H_ζ (x 1000). λ =3889,05 A.

cos θ \ Δλ(A)	0,0	0,2	0,4	0,6	0,8	1,0	1,25	1,5	2	3	4	5	6	7
1,000	263	334	500	567	606	629	684	719	779	853	922			
0,947	283	326	469	530	569	605	628	674	727	828	894			
0,897	334	343	495	553	596	647	676	726	779	867	941			
0,849	288	393	517	573	619	644	680	715	765	833	896			
0,796	268	369	497	555	592	622	669	761	775	864	943	980		
0,742	263	393	535	577	612	652	677	705	774	860	930			
0,692	303	407	533	578	613	635	667	711	773	882	938	980		
0,638	273	393	533	593	632	666	690	720	774	838	873	917		966
0,577	367	509	598	627	654	674	696	737	768	853	925			
0,537	304	398	610	637	660	691	721	754	786	871	939	967		
0,464		485	643	682	702	728	759	795	844	948	990			
0,415	323	467	674	702	718	753	775	812	821	904	951			
0,374	312	486	707	728	752	773	789	811	869	942	975			
0,312	351	472	683	695	720	748	763	797	848	918	951			
0,266	353	453	685	724	738	763	785	805	864	932	978			
0,222	418	485	758	807	823	844	863	878	899	938	960	983		
0,209	400	483	704	766	779	799	820	844	867	911	962			
0,184	438	516	765	806	822	836	858	881	895	926	970	967		983
0,161	465	580	794	832	843	864	877	893	915	939	969			
0,123	503	617	839	871	881	900	912	932	940	967	987			

All observations are made in the *red wing* of the line.

The central intensities of these profiles are uncertain.

TABLE 11. Residual intensities of H_{2-10}. λ = 3797,90 A.

cos θ \ Δλ(A)	0	1	2	4	6	10
1,000	0,35	0,56	0,75	0,82	0,90	0,95
0,947	0,37	0,50	0,66	0,85	0,93	0,94
0,897	0,40	0,55	0,71	0,85	0,92	0,97
0,849	0,33	0,55	0,69	0,88	0,89	0,94
0,796	0,36	0,53	0,66	0,83	0,88	0,97
0,742	0,38	0,62	0,69	0,83	0,94	0,96
0,692	0,41	0,55	0,68	0,82	0,94	0,98
0,638	0,42	0,64	0,73	0,85	0,92	0,96
0,577	0,45	0,64	0,76	0,88	0,93	0,97
0,537	0,47	0,60	0,75	0,88	0,96	0,98
0,464	0,50	0,68	0,79	0,91	0,96	0,99
0,415	0,45	0,66	0,77	0,91	0,96	
0,373	0,50	0,65	0,79	0,88	0,92	0,97
0,312	0,50	0,71	0,83	0,94	0,97	
0,266	0,45	0,64	0,76	0,91	0,95	0,96
0,222	0,57	0,72	0,82	0,92	0,95	0,97
0,209	0,51	0,73	0,83	0,92	0,96	
0,184	0,54	0,69	0,84	0,91	0,93	0,98
0,161	0,64	0,76	0,84	0,92	0,97	0,98
0,123	0,62	0,73	0,85	0,92	0,94	

TABLE 12. Residual intensities of H_{2-11}. λ = 3770,63 A.

cos θ \ Δλ(A)	0	1	2	4	6	10
1,000	0,46	0,68	0,84	0,90	0,94	0,99
0,947	0,51	0,67	0,79	0,94	0,94	0,95
0,897	0,52	0,70	0,80	0,89	0,95	0,99
0,849	0,52	0,72	0,84	0,93	0,95	0,99
0,796	0,46	0,67	0,81	0,87	0,95	0,99
0,742	0,57	0,76	0,88	0,92	0,97	0,99
0,692	0,50	(0,67)	0,80	0,90	0,96	0,97
0,638	0,52	0,76	0,88	0,94	0,96	0,99
0,577	0,51	0,71	0,83	0,88	0,94	0,98
0,537	0,57	0,77	0,91	0,95	0,97	0,98
0,464	0,55	0,77	0,88	0,92	0,94	0,98
0,415	0,57	0,76	0,87	0,92	0,98	
0,373	0,58	0,79	0,91	0,96	0,98	
0,312	0,61	0,80	0,88	0,94	0,95	0,97
0,266	0,56	0,79	0,88	0,92	0,94	0,99
0,222	0,60	0,86	0,92	0,97	0,99	
0,209	0,59	0,82	0,91	0,95	0,97	0,98
0,184	0,68	0,87	0,95	0,97	0,99	
0,161	0,67	0,88	0,96	0,96	0,98	
0,123	0,67	0,90	0,93	0,98	0,99	

TABLE 13. Residual intensities of H_{2-12}. λ = 3750,15 A.

cos θ \ Δλ(A)	0	1	2	4
1,000	0,58	0,72	0,86	0,97
0,947	0,65	0,78	0,87	0,98
0,897	0,57	0,78	0,92	0,99
0,849	0,63	0,84	0,92	0,95
0,796	0,53	0,72	0,88	0,96
0,742	0,61	0,85	0,92	0,99
0,692	0,60	0,83	0,92	0,96
0,638	0,64	0,86	0,94	
0,577	0,68	0,83	0,90	0,93
0,537	0,69	0,81	0,94	0,99
0,464	0,63	0,84	0,91	0,96
0,415	0,63	0,77	0,97	0,99
0,373	0,64	0,82	0,92	0,98
0,312	0,70	0,83	0,94	0,98
0,266	0,64	0,84	0,92	0,97
0,222	0,71	0,88	0,93	0,98
0,209	0,73	0,87	0,94	0,99
0,184	0,75	0,90	0,96	0,99
0,161	0,69	0,85	0,94	0,98
0,123	0,73	0,87	0,94	0,98

TABLE 14. Residual intensities of H_{2-15}. λ = 3711,97 A.

cos θ \ Δλ(A)	0	1	2	4
1,000	0,71	0,90	0,96	0,99
0,947	0,72	0,90	0,96	0,97
0,897	0,73	0,90	0,97	
0,849	0,75	0,91	0,96	0,99
0,796	0,70	0,90	0,97	0,99
0,742	0,77	0,93	0,97	
0,692	0,71	0,88	0,96	
0,638	0,71	0,91	0,96	0,98
0,577	0,72	0,90	0,98	0,99
0,537	0,70	0,86	0,94	0,97
0,464	0,71	0,93	0,98	
0,415	0,74	0,91	0,96	
0,373	0,73	0,91	0,98	
0,312	-	-	-	
0,266	0,75	0,93	0,98	
0,222	0,76	0,96	0,97	
0,209	0,72	0,92	0,98	0,99
0,184	0,77	0,97		
0,161	0,76	0,95	0,99	
0,123	0,76	0,95	0,98	0,99

TABLE 15. Residual intensities of H_{2-16}. λ = 3703,86 A.

cos θ \ Δλ(A)	0	1	2	4
1,000	(0,78)	0,92	0,96	
0,947	(0,74)	0,98	0,94	0,97
0,897	(0,79)	0,90	0,94	0,97
0,849		0,87	0,95	0,97
0,796	(0,72)	0,91	0,97	
0,742	(0,70)	0,86	0,96	0,96
0,692	(0,70)	(0,87)		
0,638	(0,76)	0,90	(0,96)	
0,577	(0,73)	0,98	0,96	
0,537	(0,68)	0,88	(0,95)	
0,464	(0,81)	0,92	0,99	
0,415	(0,80)	0,94	0,99	
0,373	(0,75)	0,84	0,94	
0,312	-	(0,88)	(0,99)	
0,266	-	0,92	0,97	
0,222	(0,97)	0,93	0,99	
0,209	-		-	
0,184	(0,80)	0,94		
0,161	(0,87)	0,94	0,97	
0,123	(0,79)	0,94	0,97	

CHAPTER III

PHOTOGRAPHIC OBSERVATIONS OF THE PROFILES OF THE BALMER LINES AND CHROMOSPHERIC OBSERVATIONS MADE AT MEUDON; COMPARISON OF THE OBSERVATIONS OF THE BALMER LINES WITH THOSE MADE BY OTHER OBSERVERS

§ 1. *Introduction; outline of the investigation.* The problem of the influence of the solar chromospheric regions on the formation of the central parts of the Balmer lines is interesting but difficult. A part of the line centra is probably formed in these regions and a good knowledge of the structure of the low chromosphere is necessary for a successful tackling of this problem.

For that reason the following program of observations was undertaken during a stay at Meudon in 1949.

1. Observations of H_α to H_δ on four places on the solar disc.
2. Photometry of H_α at the extreme limb and in the chromosphere.
3. Photometry of the flocculi on spectroheliograms, made in different wavelengths in the first four Balmer lines; investigation of their variations in the course of time and with heigth.

The second investigation should give information concerning the structure of the chromosphere in layers, higher than can be investigated with observations on the disc. The third investigation should give us data on the detailed structure and the dynamics of the region of transition between the atmosphere and the chromosphere. This latter subject is discussed shortly in Chapter IX; a more extensive discussion will be published elsewhere.

§ 2. *Description of the grating spectroheliograph at Meudon.* An extensive description of the apparatus has already been given elsewhere[38,6]; so we restrict ourselves to some general remarks and to a more detailed description of subjects of photometric interest.

All observations have been made with "combinaison II" of the great spectroheliograph (Cf. [6]). During the time of our observations the spectrograph was equipped with a WOOD grating. The solar image in the plane of the second slit had a diameter of 86,5 mm for 3934 A and of 89,5 mm for 6563 A. All *spectroheliograms* have been made in the second order spectrum; the same is the case with the *chromospheric observations* of H_α. The *spectra* of H_α to H_δ have been made in the third order. The dispersion, as given in D' AZAMBUJA's thesis[6] is 5,9 A/mm in the first order.

For practically all spectra and spectroheliograms the first slit was used at a width of 0,015 mm. For the spectroheliograms the corresponding width of the second slit was chosen at 0,03 mm; this corresponds with a wavelength interval in the second order of 0,09 A. Only for some H_α spectroheliograms the slit widths have been chosen at 0,022 and 0,045 mm respectively. For spectral observations the second slit was widely opened.

Further, some photometric properties of the instrument have been determined; 1) the intensities of the ghosts of the grating; 2) the apparatus function of the instrument and 3) the intensity of the scattered light beside the solar image.

§ 3. *Photometric properties of the apparatus.*

a) The *intensities* of the *Rowland ghosts* of the green ray of mercury produced by a mercury discharge tube were determined photographically with As-de-Trèfle panchro plates. The plates were calibrated with a platinum step weakener, placed between the tube and the first slit. The exposure times ranged between 1 sec. and 30 min. Ghosts were detectable up to a distance of 30 A from the central line (first order); their total intensity, expressed in the intensity of the central line, was 0,00079 in the first order; 0,0053 in the second order and 0,0134 in the third order. It is evident from these results, that the total intensity of the ghosts is practically always negligible in the first and second orders.

b) The *apparatus function* was determined in the same way as is described in Chapter II, section 4. The mean values of the parameters thus found are listed in table 16.

It must, however, be noted that in the red part of the 3^d order spectrum (H_α region) a distinct asymetry was found in the lines, indicating an asymetric apparatus profile, analogous to that of the Mount Wilson spectrograph[19]. Contrary to Mt Wilson, the *violet* wings are stronger here.

TABLE 16. Apparatus function of the spectrograph at Meudon (with WOOD grating).

	β_1	β_2^2	h		
			μλ	mm	A
1st order	16	1421	80	0,088	0,53
2nd order	5,8	336	36	0,080	0,24
3rd order	8,0	96	25	0,110	0,165

Refinements of this kind are not considered, however; they are not important for the Balmer lines.

c) The *intensity* of *scattered light* beside the solar image was measured several times on "normal" days for different wavelengths at points, at different distances to the limb of the sun. This was generally done by opening the second slit to a tenfold width. The results are given in table 17; the data are of the same order of magnitude as those measured at Utrecht (table 4). Hence, corrections for the influence of stray-light can be neglected.

TABLE 17. Mean intensity of light scattered beside the solar disc at Meudon. The intensities are expressed in the intensity of the sun's centre. There is no marked wavelength dependence.

r/R	0,01	0,10	0,30
int.	0,035	0,025	0,011

§ 4. *Observations of H_α in the chromosphere.*

The photometry of H_α in the chromosphere is a task, that should be performed at a high altitude observatory or during eclipses. However, up to now no High dispersion observations of H_α beside the solar disc have been obtained in such conditions (the observations of UNSÖLD[175] and KEENAN[76,77] made at Mount Wilson and Yerkes are not given in a form, suitable for photometric reduction). Hence it was decided, because of the importance of a knowledge of the absolute values of the H_α emission, to undertake the photometry of H_α in the chromosphere at the Observatory of Meudon. Naturally, the errors in the results will be greater than the errors in normal Fraunhofer line photometry but our observations will be of value if the limitations of their precisions are always kept in mind.

The Meudon apparatus possesses some advantages for this kind of work: its grating gives very bright spectra, also in the second order; the exposure time in the second order is about 1 second, while KEENAN, who made similar observations at Yerkes used exposure times, about ten times longer for H_β and still much longer for H_α; UNSÖLD, at Mount Wilson, used still longer exposure times. It is further known, that over the plateau of Meudon only little atmospheric convection occurs. The situation of the coelostat, on a meadow, partially surrounded by a wood, favours the stability of the air. Besides, the apparatus does not possess vertical tubes. They prevent turbulence in the instrument.

On the other hand Paris being near, it will bring dust into the air. However, the town lies to the North East, while our observations have been made with the sun South West.

On September, 2, 1949 in the afternoon it was decided to make some spectra of H_α at the limb. The sky was more transparant than it had been during our three-months stay at Meudon. Small details in the landscape, even North of Paris could be seen without difficulty. It had been raining the days before, and the morning had been cloudy.

The technique was as follows: the spectrograph slit was covered by a metal strip, in which were two circular holes, each 1,0 mm in diameter and at a distance, equal to the diameter of the solar image. The sun's limb intersected these holes at points, near the poles of the sun (fig.3). This procedure garanteed that the stray light in the instrument was faint. In every exposure two limb spectra were thus taken. On each plate four exposures were made; hence,

FIGURE 3

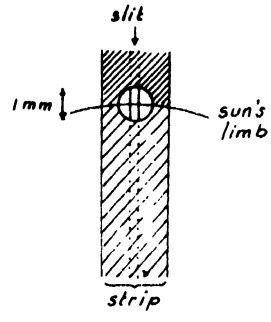

Position of the solar image with respect to the slit and the covering strip.

every plate contained eight limb spectra. Of the four plates which were made, two were photometrically good; on these plates the exposure times ranged between $0^s,2$ and 6^s; the best time being 1^s. The exposures with longer times have been made to measure the intensity of scattered

light. Each plate contained three gradation spectra, taken through a platinum step weakener with exposure times between $0^{s},1$ and $4^{s},0$. The exposures have been made on Hélias, As de Trèfle, panchro plates (backed); they were developed during 4½ minutes, with continuous brushing, in the metol hydrochinon developer "Baldet" [7].

§ 5. *H_α in the chromosphere; results;*
The plates were recorded with a Chalonge microphotometer of the Institut d'Astrophysique of Paris. In order to take the very fast intensity variations on the plates well into account, the dimensions of the microphotometer slit were chosen small: 0,2 x 0,2 mm^2, corresponding with a lightspot on the plate of 25 x 25 μ^2. In each spectrum twelve records have been made in the direction of the dispersion of the spectra, parallel to each other; eight of them at mutual distances of 40 μ, the two first and the two last ones at greater distances, thus covering in total a region with a height of 0,8 mm on the plates (corresponding with about 2% of the solar radius). The small dimensions of the photometer slit caused a greater influence of the graininess of the plate than is usually the case. This could have been avoided by us if the spectrograph slit had been placed tangentially. However, in this latter case many more exposures would have been necessary to give the whole variation of the line profile on and beside the solar disc. As it was necessary to fully utilize the short time of optimal atmospheric conditions, the method, described above, was used.

By combining the 96 records, obtained from the eight limb spectra for each plate, two mean sets of profiles were obtained (one for each plate); each giving the intensity in the spectrum for one value of r/R, expressed in the same intensity scale. Since it was found that all intensity values were for both plates - within the limits of normal errors - the same (there was only a small difference in the intensity of the scattered light at great distances to the limb) the results from both plates were combined to one set of curves.
The following corrections should then be considered:
a) The correction for the apparatus curve has been applied; the greatest value (4%) was reached in the emission line profile at a distance $r = 0,0035\ R$ from the limb.
b) Corrections for scintillation and for scattered light in the atmosphere and in the instrument are by far the most important ones; in many cases they are of the same order as or greater than the intensities to be measured; they will be discussed next.

There exist rather refined methods to find the true intensity profile of an image, blurred by scintillation [189, 196]. They are essentially based on the problem of the solution of an integral equation where the unknown function expresses the influence of scintillation on a luminous point. The difficulty of the method is that the solution is always found with a great relative error.
This method is not followed here, for in the scope of our problem the intensity of the *continuous radiation* near the sun's limb may be regarded as known. Eclipse observations of the intensity distribution at the extreme limb [20 2] agree with calculations made on the base of an isothermal low chromosphere with a temperature of 5000^{o}; cf. [196]. The corrections which must be applied to the continuous spectrum are therefore known and from these the corrections which must be applied to the points in the line profile may be derived. Though perhaps not the most elegant way of solution, it is the surest way. The errors, introduced by this way of reduction will be small, as the true intensity gradient in the continuous spectrum near the limb is great as compared with the observed gradient.

FIGURE 4

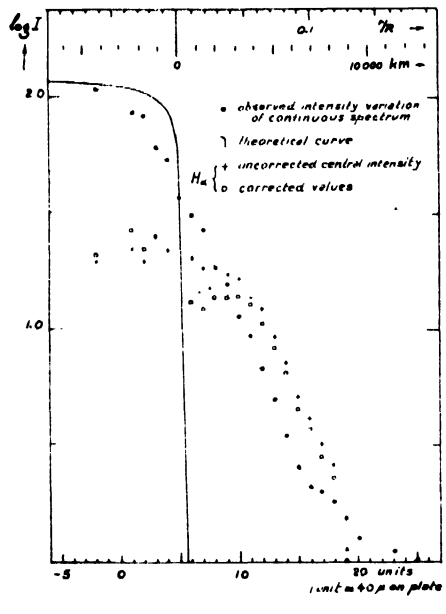

Observed and adopted intensity variation in the continuous spectrum at 6560 A near the limb of the sun. Observed and corrected intensities in the core of H_α.

In figure 4 the observed and the theoretical intensities of the continuous spectrum are com-

pared. The intensity scales are adjusted so, that both curves are equally high on the solar disc; they are shifted in the horizontal direction till the areas enclosed are equal. The *correction curve* $C(r/R;\Delta\lambda)$ which has to be added to the observed curve to yield the "true" intensity variation has the same form for all wavelengths but its absolute value depends on λ; its profile is equal to the profile of H_α, observed in the skylight at some distance to the sun's limb. This profile has been measured between distances of 1,5 and 2,5 % from the limb of the sun; it shows much resemblance with that of H_α on the disc at $\cos\theta = 0,5$.

TABLE 18. The intensity profiles of H_α at the extreme limb of the sun and in the chromosphere. The scale is arbitrary; the data have to be multiplied by $1,17.10^{12}$ to obtain the intensities in ergs/cm^2 sec.

r/R	Δλ (A) / km	-3,0	-2,0	-1,0	-0,8	-0,6	-0,4	-0,2	0,0	+0,2	+0,4	+0,6	+0,8	+1,0	2,0	3,0
0,9938		114	116	100	84			25	21	22			84	99	117	118
0,9965		108'	108'	95'	79'			29'	27'	29'			82'	100'	107	102
0,9975		113"	113"	112"	90"			34'	23'	29'			87"	107"	113"	113"
1,0010	700						12"	13"	13"	14"	14"					
1,0019	1320					14"	12"	11"	12"	11"	14"	15"				
1,0028	1950						13"	13"	14"	14"	15"	15"				
1,0037	2600					10"	11"	14"	14"	14"	16"	16"	12"			
1,0045	3120				8,1"	10"	12"	12'	14	13'	14'	12"	9"			
1,0054	3770				8,1"	9,1"	11'	11'	12	12'	13'	13'	10"			
1,0064	4470				6,4"	7,9"	8,8'	9,7'	10,6	9,8'	9,8'	9,7'	8,0"			
1,0073	5100				5,2"	6,6'	7,5'	7,7	8,3	8,1	8,2'	7,5'	6,2"	4,0"		
1,0082	5720				3,7"	5,0'	6,0'	6,2	6,4	6,2	6,2'	6,4'	4,8"	3,2"		
1,0090	6290			2,0"	3,5"	3,6'	4,9	4,4	4,5	4,8	5,0	4,5'	3,2"			
1,0099	6900				1,6"	3,0"	3,1'	3,6	3,7	3,6	3,7'	3,1"	2,2"			
1,0108	7540				1,5"	1,7"	2,2'	2,8	2,8	2,9'	3,1'	2,5"	1,5"			
1,0117	8150					1,4"	1,8"	2,2	2,3	2,4	2,5'	2,1'				
1,0126	8800							0,6"	0,8'	0,9"	1,0"	0,9"				

The observed and corrected values are given in table 18; the scale is still arbitrary. To have the values expressed in c.g.s. units, they must be multiplied by $1,17.10^{12}$. (This value is obtained, assuming that the intensity of the continuous radiation at r/R = 0,995 near H_α is equal to $1,35.10^{14}$ ergs.cm^{-2} sec^{-1}).
Only those data have been given in the table for which the correction is smaller than 50% of the uncorrected value. Data for which the correction was greater than 30% of the uncorrected value are marked by an " and one ' is used if the correction is smaller than 30% and greater than 20%. In the chromosphere, corrections, smaller than 10% did not occur.

A glance on the table shows among other things, that both emission "peaks" at $\Delta\lambda \approx \pm 1$ A, which existed in the uncorrected observations and which have also been noted by other observers, do not longer manifest themselves in the corrected curves. These peaks are due to the influence of scattered light. This fact has also been noted by KEENAN[76,77] fot the line H_β. His corrected profiles of the chromospheric H_β emission line show nearly always, with an exception in the low chromosphere, where the values are very uncertain, a simple profile.
This result seems to show, that the temperature in the chromosphere does not decrease above the sun's surface. This fact is also in agreement with eclipse observations: REDMAN[145] showed in 1942 that the profiles of H_β, H_γ and H_ζ in the chromosphere, observed during eclipses, are comparable with ordinary Doppler profiles. It is probably reasonable that this is also the case for H_α, the more so, since REDMAN's observations refer to a height of 1500 km; our observations refer to much greater heights.
The only uncertainty in the problem of the central absorption in the emission profiles of the Balmer lines in the chromosphere relates to the very low chromosphere. For KEENAN's corrected observations still show the central absorption in H_ζ at heights lower than 1000 km; while in our H_α observations the same is the case at heights below 1500 km. This latter statement is, however, not very certain. The great influence

of small errors in the assumed intentity of scattered light on the ultimate form of the profile is shown by a discussion of UNSÖLD's data on H_α [175]. If, for instance, his adopted correction curve is multiplied by a factor 1,026, his corrected profile shoudl be - just like our profile - a normal Doppler curve. It seems that the uncertainty in UNSÖLD's data exceeds this precision limit.

§ 6. *Mean profiles of H_α to H_δ on four places on the solar disc.*

The profiles of H_α to H_δ have been determined in the third order spectrum. With a metallic diafragm, pierced by five holes, placed before the slit, we obtained simultaneously one spectrum for $\sin\theta = 0,0$; two for $\sin\theta = 0,61$ and 0,99 respectively. The limb spectra refer to polar regions of the sun; they are made with a radial slit.

One plate has been used for every Balmer line; every plate contained four exposures, giving twenty spectra, and three standardizing exposures. All exposure times ranged between $0^s,2$ and 20^s. The exposures have been made on September 29^{th}, 1949. The following plates have been used

For H_α: Hélias, As de Trèfle, Panchro.
H_β: Guilleminot Radio eclair.
H_γ and H_δ: Guilleminot super fulgur.

The plates were developed $5^{min.}$ with brushing in the metol-hydrochinon developer "Baldet" [7].

Since our exposures have been made with a radial slit, the position of the sun's limb on the limb-spectra was found by comparing it with the well-known limb darkening curve, as in § 5. The mean profiles are determined in the same way as in chapter II; the necessary corrections have been applied; afterwards mean values have been determined. They are given in table 19. Since the total number of spectra, available for reduction was small, the mean errors of the data in table 19 are greater than those of the corresponding tables from chapter II. We estimate that they are of the order of 3% or 4%. On the other hand, these observations are made with an apparatus of a different kind than was used at the Utrecht observatory, so they can be used for comparison.

TABLE 19. Residual intensities of H_α-H_δ observed at Meudon.

	$\Delta\lambda$(A) / sin θ	0	0,2	0,4	0,6	0,8	1,0	1,25	1,5	2	3
H_α	0,00	0,176	0,191	0,269	0,417	0,589	0,651	0,706	0,736	0,782	0,853
	0,61	0,167	0,188	0,296	0,468	0,618	0,691	0,746	0,794	0,843	0,903
	0,990	0,204	0,219	0,286	0,420	0,685	0,818	0,897	0,925	0,956	0,973
	0,995	0,229	0,239	0,301	0,480	0,713	0,848	0,915	0,941	0,975	
H_β	0,00	0,160	0,201	0,388	0,544	0,630	0,681	0,718	0,752	0,803	0,867
	0,61	0,191	0,243	0,418	0,589	0,674	0,712	0,746	0,767	0,808	0,890
	0,993	(0,197)	(0,257)	0,418	0,730	0,867	0,892	0,914	0,929	0,965	0,973
H_γ	0,00	0,191	0,246	0,383	0,474					0,757	
	0,61	0,195	0,277	0,426	0,504					0,813	
H_δ	0,00	0,190	0,266	0,365	0,461	0,513	0,588			0,702	0,784
	0,61	0,242	0,339	0,479	0,577	0,641	0,687				
	0,995	0,348	0,469	0,687	0,829	0,858				0,914	

§ 7. *The limb profile of H_β observed at Mount Wilson.*

At the observatory of Utrecht a plate is available, made at Mount Wilson in the H_β region at two places on the solar disc (centre and limb). The plate was made on January 12, 1923 (plate L22B) with the 75 feet spectrograph of the 150 feet solar tower telescope of Mount Wilson, in the first order (dispersion 0,72 A/mm; diameter of the solar image 425 mm). The plate contains six exposures in the centre of the disc and nine limb exposures, made at $r/R = 0,986$. The plate has not been standardized. Besides, the exposure times of the different exposures were not the same; the ratio between the several centre and limb exposures ranged from 1 to 4. Nevertheless it was decided to record the plate, principally, because the solar diameter exceeds by far the diameters used in other investigations.

The photometry and the reduction have been made by mr. E.W.DENNISON. A transmission curve for the plate was determined with the aid of an *adopted intensity profile* for H_β in the *centre* of the disc. After a comparison of the observations made at Göttingen and Utrecht with the Atlas of the Solar Spectrum[108] the following mean profile of H_β in the centre of the disc was adopted (table 20). The transmission curve for the plate, derived with this profile from the records of the spectra of the centre of the disc was not wholly satisfactory. The scatter of the points is fairly great; the mean error corresponds to $\Delta I/I \approx 0,05$.

TABLE 20. Adopted intensity profile for H_β in the centre of the disc and the deduced profile at $r/R = 0,986$.

$\Delta\lambda$(A)	0	0,2	0,4	0,8	0,8	1,0	1,25	1,5	2,0	3,0	4,0
$\frac{i}{i_{cont}}(r/R=0)$	0,178	0,248	0,429	0,580	0,638	0,674	0,711	0,742	0,790	0,848	0,888
$\frac{i}{i_{cont}}(r/R=0,986)$	0,261	0,304	0,620	0,845	0,894						

It is not necessary to apply the ordinary corrections (apparatus, ghosts) to the line profile, determined with the aid of this transmission curve; an approximate ghost correction has already been applied automatically, when the transmission curve is determined with the aid of an adopted profile for the centre of the disc. The influence of the apparatus function on the line profile is negligible. So the mean profile for H_β at $\sin\theta = 0,986$ has been determined, as it is listed in table 20.

§ 8. *Comparison of our Balmer line observations with those of other observers; the wings.*

A number of other observations of the Balmer line profiles exist; we restrict ourselves to the observations made at four selected values of r/R. The data on the different sets of observations are given in table 21. In figure 5 the observations are compared graphically.

In this section only the line *wings* are discussed.

In general it can be assumed that the *deepest*

TABLE 21. Comparison of observations of Balmer lines; values of $\cos\theta$.

author	observatory	year	ref.	$\cos\theta$	diameter (mm)	disp. (A/mm)	lines
UNSÖLD [I]	Mt. Wilson	1928	175	1,00	425	0,25	H_α H_β H_γ H_δ
MINNAERT	Utrecht	1927	106	1,00	120	4,0	H_α
THACKERAY	Cambridge	1934	170	1,00	16		H_α H_β
ROYDS and NARAYAN [I]	Kodaikanal	1936	151	1,00 0,760 0,312	44	0,75 (1,1 for H_α)	H_α H_β H_γ H_δ
REDMAN	Cambridge	1937	143	1,00	160	0,73	H_γ
EVANS	Oxford	1939	45	1,00 0,741 0,303	186	2,06	H_α
HOUTGAST	Utrecht	1943	69	1,00 0,802 0,312 0,135	31 [II]	4 [II]	H_δ
TEN BRUGGENCATE c.s.	Göttingen	1947	14	1,00 0,80 0,31 0,14	225	0,56	H_α H_β H_γ H_δ
DENNISON	Mt. Wilson	1923		0,167	425	0,72	H_β
DE JAGER	Utrecht	1947	[IV]	1,00 0,796 0,312 0,123	67	2,0 (4,0 for H_α)	H_α H_β H_γ H_δ
DE JAGER	Meudon	1949	[V]	1,00 0,792 0,10-0,14	37 [III]	2,0	H_α H_β H_γ H_δ

I) These data are not represented in figure 5.
II) Enlarged 3,4 times at camera-end of spectrograph, making the effective solar diameter = 105 mm and effective dispersion = 1,3 A/mm.
III) Enlarged with factor 2,4 at camera-end; effective solar diameter = 89 mm.
IV) Chapter II, section 8 of this investigation (tables 6-9).
V) Section 6 of this chapter (table 19).

wings and those with the greatest extension are the most reliable ones. As already noticed before, the continuous spectrum is generally drawn too low; the depth of the line wings are generally underestimated. Practically none of the authors, who up to now have published profiles of the wings of the Balmer lines did estimate these correctly: the height of the continuous spectrum seems generally to be too low. It will be very interesting to secure precise photo-electric observations of the wing profiles of some Balmer lines. We estimate that e.g. in the case of H_α a measurable depression will perhaps be visible up to 40 or 50 A from the line centre.

On the other hand it has to be kept in mind, that there is also a cause, which gives too deep wings: in poorly resolved spectra accumulation of faint lines on the Balmer line wings may cause an additional depression to the wing intensities.

Armed with this knowledge it will be possible to understand at least a part of the differences which are visible in the line wings, as observed by different observers.

When comparing the Utrecht profiles with those, observed at Göttingen, it is obvious, that the H_α and H_β wings, found in Utrecht are deeper than the Göttingen wings. We believe, for the reasons, given above, that the Utrecht wings are better. For the lines H_γ and H_δ there is no systematic difference between both series of observations: here we think, that the influence of the numerous faint lines on the wings becomes visible. But not in the sense described above: we think that the effect of the faint lines (which have a greater influence on the Utrecht measurements than on these made at Göttingen, because of our smaller dispersion) is *overcorrected* in Utrecht; giving agreement between the Utrecht and Göttingen measurements for H_γ and H_δ. We think that the true wing intensity must be lower for these two lines than the communicated intensities.

The case of H_β merits special attention; the Utrecht wings are somewhat lower than the mean, while for the other lines our wings well agree with the mean of the other observations. A repeated inspection of the H_β plates which had been used for the determination of the wing profiles showed that the plates as well as the transmission curves are correct and reliable.

Turning to the other observations we see that in the other Utrecht observations (MINNAERT, HOUTGAST) the wings are placed at the same heights as in our profiles.

EVANS' wing profiles do not deviate systematically from ours; EVANS technique of determining the height of the continuous spectrum with the aid of auxiliary incandescent lamp spectra has wholly eliminated the difficulty of the great variation in the plate sensitivity.

THACKERAY's data agree with ours for H_α; less well for H_β.

§ 9. *Comparison with other observers; the central intensities.*

In table 22 the central intensities as measured by different observers are summarized for four values of r/R. More than any other part of the line profile the central intensity can be influenced by a number of effects as: (1) the Rowland ghosts, (2) light, scattered in the telescope and the atmosphere, (3) light reflected in the spectrograph tube and (4) the apparatus profile. All effects, except the second one have their maximal influence in the centre of the line profile; all errors, also excepting the second, work in the same direction, viz. to increase the central intensity.

On the other hand the breath of the Balmer lines and their rather flat central minima make the *determination* of the central value rather reliable. We may be sure that the communicated values are hardly influenced by systematic personal *measuring errors*.

Table 22 shows that for the central parts of the disc ($\cos\theta = 1{,}0$ and $0{,}75$) the agreement among all authors is fairly good; only in two cases mutual differenced greater than 4% are found. REDMAN's central intensity of H_γ is 4% lower than our Utrecht value. THACKERAY's and MINNAERT's data for H_α and H_β are also lower than ours (the differences are 1,8% and 2,2% for H_α and 2,4% for H_β). Since these observations have been made with great care by experienced scientists, we are inclined to believe that an unknown reason exists, which makes our central intensities somewhat too high.

The Göttingen data are still higher than ours; a possible systematic effect, which may cause these deviations will be discussed further-on in this section.

Notable differences occur in the limb parts of the disc; they cannot be explained by the influence of the Rowland ghosts since this effect influences the centre and the limb spectra in the same way; moreover the differences cannot be so great in that case as is actually observed. It seems better possible to explain them by the influence of scattered light from inside the spectrograph tube. This effect causes a general veil over the spectrum; its intensity is about proportional to the height of the slit. The central measurements at Göttingen ($r/R \leqq 0{,}9$) have been made with a slit with a height of 1 mm, while at the limb ($r/R \geqq 0{,}95$) the slit had a height of 7 mm; hence, the influence of scattered light was greater in this latter case.

FIGURE 5

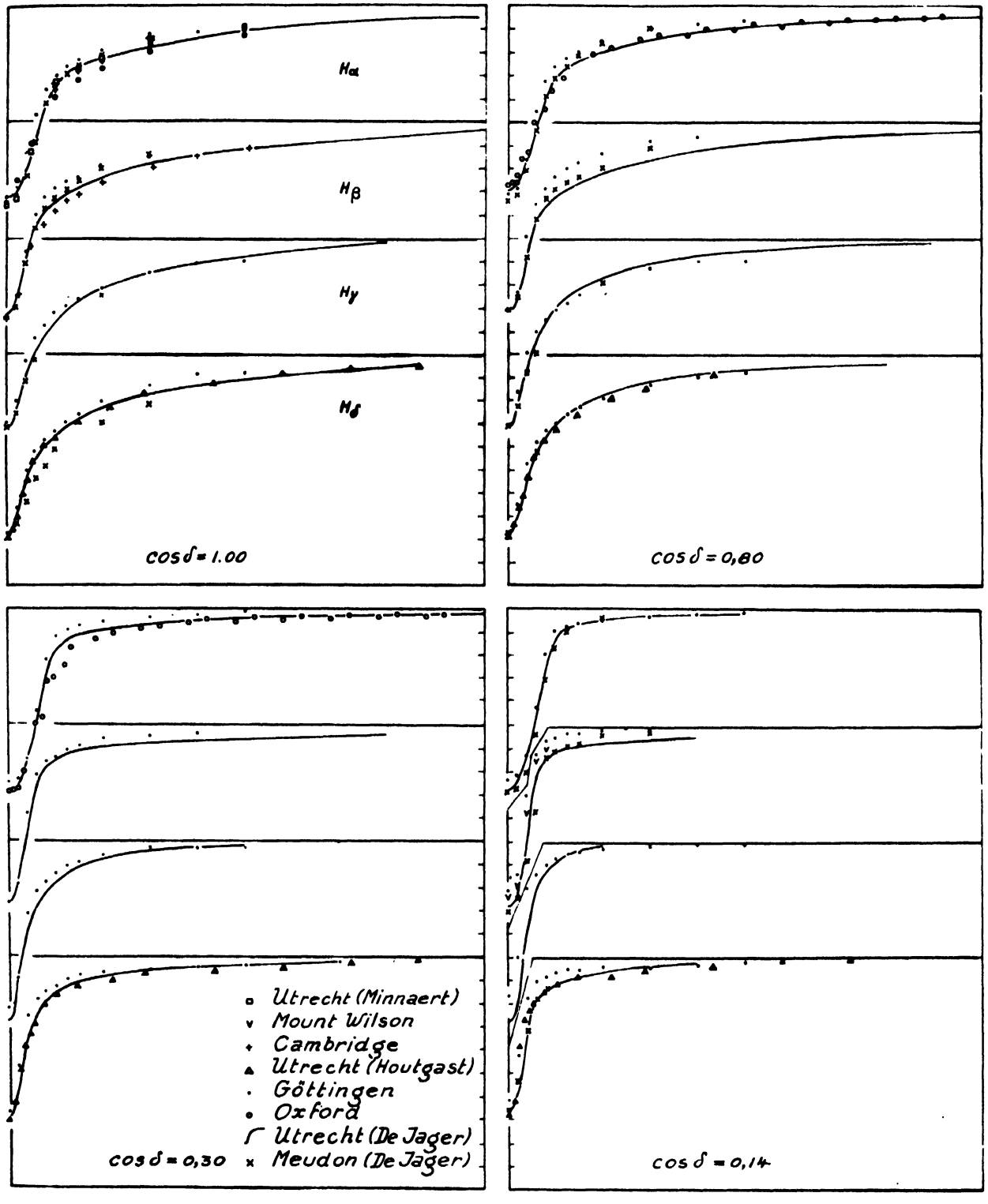

The profiles of H_α to H_δ as observed by various observers for four values of cosθ.

TABLE 22. Central intensities of the Balmer lines (x 1000).

cosθ	1,00				0,8				0,3				0,14			
line	H_α	H_β	H_γ	H_δ	H_α	H_β	H_γ	H_δ	H_α	H_β	H_γ	H_δ	H_α	H_β	H_γ	H_δ
MINNAERT	150															
THACKERAY	154	152														
REDMAN			145													
EVANS	179				230				211							
HOUTGAST				204				216				285				327
GÖTTINGEN	180	180	200	230	190	190	210	230	250	230	270	320	270	290	340	390
DENNISON														261		
DE JAGER (U.)	172	176	185	226	209	193	189	229	193	222	214	293	224	212	224	345
DE JAGER (M.)	176	160	191	190	167	191	195	242					216(197)			348

In fact it was not exactly seven times greater, since not the whole slit was filled with light; the sun's limb appeared also on the spectra. From the data, communicated by the Göttingen observers it may be estimated that about 6 mm of the slit had been filled with sunlight. Moreover, as a consequence of the great intensity variation of the continuous spectrum in the limb region, the influence of scattered light is greatest for spectra, near to the limb.

This can be shown quantitatively: in table 23 the mean residual intensity in the cores of the lines is given, excluding EVANS' data, which show a systematic error (see hereafter, p. 21) and The Göttingen data.

TABLE 23. Mean central intensities of H_α to H_δ (x 1000). The measurements of EVANS and those made at Göttingen are not included.

cosθ	H_α	H_β	H_γ	H_δ
1,00	162	163	174	207
0,80	188	192	192	229
0,13	193	222	214	289
0,14	220	229	224	340

In table 24 the residuals: Göttingen minus mean values, are given. The ratio of the mean differences between limb and centre is 54 : 13 ≈ 4; which is more or less in agreement with the theoretical value which should be 6. Moreover, the mean difference, computed for cosθ = 0,3 is smaller than that at cosθ = 0,14, as it ought to be. We conclude that the influence of light, scattered on the optical parts of the spectrograph is most probably the cause of the systematic differences between the Göttingen measurements and the other data.

In the same way UNSÖLD's measurements at Mount Wilson and the Kodaikanal observations must be considered. UNSÖLD finds for the central intensities of H_α to H_δ the values 0,29; 0,23; 0,24 and 0,32. Since these values are too high it

TABLE 24. Residuals between the central intensities, determined at Gottingen and the mean values given in table 23 (x 1000). The Gottingen observations at cosθ = 0,3 and 0,14 are made with a higher slit than the observations in the central part of the disc.

	H_α	H_β	H_γ	H_δ	mean
cosθ = 1,00	18	17	26	23	
0,8	2	-2	18	1	
mean (1,00 and 0,8)	10	8	22	12	13
cosθ = 0,3	57	8	56	31	38
0,14	50	61	116	50	69
mean (0,3 and 0,14)	53	34	86	40	54

seems very probable, that they are affected by light, scattered and reflected on the optics of the spectrograph. This is easily explained, as the observations have been made in the – less luminous – third order spectrum in order to gain in dispersion. In such a case, however, the relative importance of the scattered and reflected light is strengthened as compared to the first order spectrum.

The Kodaikanal observers notice the centre to limb *variation* very well; the *form* of their centre-to-limb curves agrees with our data. Their *intensities*, however, are all higher by nearly the same amount: the mean differences between their central intensities and ours are for H_α 9,0%; for H_β 7,2%; for H_γ 9,8% and for H_δ 9,2%. Interpretation: the observations have all been made with the same height of the slit but the scattered and reflected light in the spectrograph tube has for the greater part not been eliminated.

Turning next to the other possible sources of errors which have been listed in the first part of this section, we notice that the influence of the *apparatus function* has generally well been taken into account. Only in EVANS's measurements their influence seems to be underestimated, as has been shown already by the Göttingen observers[14]. The maximum influence of the apparatus function is generally not greater than a few percents.

The influence of *straylight* in the *telescope tube* and in the *atmosphere* depends on the intensity of the atmospheric scattering and on the state of the optical parts of the instrument (It does not depend on the seize of the solar image). On the basis of the calculations given in chapter II, section 6 it may be shown that the influence of this effect on the line centra is negligible. To influence the line centra in the limb spectra by about 1%, the intensity of the scattered light at a distance of 0,03 R from the sun's limb should be in the H_α region 15% of the intensity in the centre of the disc and in the H_δ region 12%. Such values have never been measured.

§ 10. *The steepest parts and the "shoulders" of the line profiles.*

In these parts of the profiles the mutual differences between the observers often reach 10% and sometimes more. These differences cannot be ascribed to the four possible sources of errors mentioned in the preceding section since their influence is too small to explain differences as great as these. Obviously they are due to errors in the adopted *widths* of the lines; it may perhaps be assumed that the cause of the differences is the difficulty to draw a mean curve on a record, influenced by graininess, especially in the steep parts.

In order to obtain a more or less objective standard for the line widths, so that the origin of the systematic differences between the authors may be explained, we compare (table 25) the halfwidths of all observers with those derived from the Atlas of the Solar Spectrum. These latter profiles are practically not influenced by the plate graininess and faint Fraunhofer lines may easily be eliminated.

A glance on the data of table 25 shows that for H_α and H_β nearly all observers have drawn their profiles too wide as compared with the Solar Atlas but the reverse is the case for H_γ and H_δ. The data, presented by the Göttingen observers show for the profiles of H_α and H_β the best agreement with the Atlas; but for the lines H_γ and H_δ the Utrecht observations show the best agreement. (This comparison is, of course, only possible for the centre of the disc).

It is difficult to find an explanation; it is certain, that the personal appreciation of a record is of great importance. When judging the dispersions, used in Göttingen and Utrecht respectively (0,56 A/mm and 2,0 A/mm) we should expect that for H_γ and H_δ (many blends!) the

TABLE 25. Half-widths of the Balmer lines (A).

cosθ	1,0				0,8				0,3				0,14			
line	H_α	H_β	H_γ	H_δ	H_α	H_β	H_γ	H_δ	H_α	H_β	H_γ	H_δ	H_α	H_β	H_γ	H_δ
MINNAERT	1,50															
THACKERAY	1,70	1,70														
REDMAN			1,19													
EVANS	1,80				1,80				1,50							
HOUTGAST				1,48				1,35				0,78				0,56
GÖTTINGEN	1,40[1]	1,16[1]	1,35[1]	1,45[1]	1,32	1,03	1,22	1,19	1,28	0,73	0,72	0,61	1,26	0,70	0,58	0,52
DENNISON														0,83		
DE JAGER (U.)	1,66	1,36	1,70	1,60	1,60	1,35	1,33	1,35	1,38	0,96	0,90	0,89	1,32	0,92	0,73	0,75
DE JAGER (M.)	1,56	1,29	1,86	2,10	1,55	1,28	1,48	1,40					1,42	1,12		0,75
Atlas	1,40	1,25	1,65	1,60												

1) Prof. P.TEN BRUGGENCATE communicated the following half-widths as determined by him from his own measurements:

H_α	H_β	H_γ	H_δ
1,42	1,14	1,42	1,50

agreement with the Atlas should be the best for the Göttingen data, just contrary to the actual case. This probably shows, that the different dispersions, used by the several observers do not introduce perceptible systematic differences in the results, though it is also possible that our tendency to overcorrect the influence of the blend lines (already discussed in section 8, when dealing with the wings of the lines) plays a part.

Conclusion: It seems not yet possible to decide between the published profiles for the steep parts and the shoulders of the profiles. For the time being we are obliged to accept the discrepancies in these parts; they are probably caused by personal systematic errors in drawing the line profiles of the records; they may probably be solved after new observations with a high dispersion apparatus.

CHAPTER IV

OBSERVATIONS OF THE PASCHEN AND BRACKETT LINES, MADE AT UTRECHT AND AT THE SCIENTIFIC STATION OF THE JUNGFRAUJOCH

§ 1. *Introduction.*

In this chapter we describe observations of two Paschen lines, made at Utrecht in 1948 and of thirteen Paschen and Brackett lines, observed in June 1950 with the photo-electric infrared spectrograph of the Institut d'Astrophysique of Liège (Belgium), temporarily mounted at the Sphynx observatory at the Jungfraujoch (altitude 3580 meter). These latter observations were made in collaboration with mr. L. NEVEN of the Observatory of Uccle, Belgium and have already been published elsewhere[70]. We will therefore give in the following only a short description of this second series of observations.

§ 2. *Photographic photometry of the infrared Paschen lines.*

Two infrared Paschen lines were put on our photographic program: H_{3-8} at 10938 A and H_{3-7} at 10049 A. We always used the infrared sensitive Kodak Z plates.

Some details are given on the observational technique.

1. The plates were hypersensitized in ammonia, one hour before the exposure.
2. Exposures were always made on two places on the solar disc; centre and limb. In the limb exposures the slit was placed radially; its height was 10 mm.
3. The exposures were made in the first order.
4. A Gevaert infrared filter was used, which cuts off at 7500 A.
5. The plates were standardized with a wedge-shaped slit, 1 cm high; its greatest width was 0,6 mm.
6. To reduce the exposure time the slit was opened till 0,15 mm, two times wider than is prescribed for normal spectrophotometric work. For these broad lines this is, of course, permitted. The exposure times were 20 minutes for H_{3-7} and 30 minutes for H_{3-8}.

Six plates appeared to be of suitable density. They were all taken on the 14th and the 21st of February 1948. When examining the plates, it appeared that they are not wholly satisfactory for critical spectrophotometric work, since the emulsion of the plates seems to be far from homogeneous. A mean profile can nevertheless be determined. It is not necessary to apply the ordinary corrections (ghosts, apparatus) as the lines are very flat and hazy.

In tables 26 and 27 the mean values of the residual intensities of the Paschen lines H_{3-8} and H_{3-7} are given for seven different points on the solar disc. Values between brackets are mean values, determined from two measured points only. The mean error of the communicated values is estimated to be about ± 4%.

§ 3. *The photo-electric observations at the Jungfraujoch.*

A short description of the photometric properties of the apparatus is given; all data are extracted from the paper by DE JAGER and NEVEN[70]. The diameter of the solar image was 15 mm; the monochromator slit of the spectrograph had a height of 7,5 mm, and use was made of a Wood echelette grating with 600 lines per mm. A Cashman PbS cel was used; the light was chopped

TABLE 26. Residual intensities of the Paschen line H_{3-8} (λ = 10938,1 A).

sin C	Δλ(A) / cos θ	0	0,64	1,29	1,93	2,57	3,22	4,83	6,44
0,00	1,000	0,79	0,82	0,87	0,89	0,90	0,93	0,95	(0,97)
0,86	0,510	0,80	0,84	0,90	0,91	0,93	0,94	0,96	
0,90	0,436	0,82	0,85	0,87	(0,91)	0,92	0,92	(0,96)	
0,92	0,391	(0,80)	(0,88)	(0,90)	(0,95)	(0,96)	(0,96)	(0,98)	
0,94	0,341	0,80	(0,87)	(0,87)	(0,88)	(0,92)			
0,96	0,280	0,86	(0,87)	(0,90)	(0,89)	(0,93)			
0,98	0,200	0,85	(0,87)	(0,94)	(0,97)	(0,98)			

TABLE 27. Residual intensities of the Paschen line H_{3-7} (λ = 10049,3 A).

sin θ	$\Delta\lambda$(A) / cos θ	0	0,64	1,29	1,93	2,57	3,22	4,83	6,44	9,65
0,00	1,000	0,82	0,85	0,87	0,90	0,92	0,93	0,95	0,96	(0,97)
0,85	0,526	(0,97)	(0,81)	(0,85)	(0,92)	(0,92)				
0,90	0,436	0,79	0,85	0,89	0,92	0,95	(0,96)			
0,92	0,391	0,81	0,83	0,86	0,88	0,89	(0,97)	(0,98)		
0,94	0,341	(0,84)	(0,82)	0,88	0,93	0,96	0,98	(0,99)		
0,96	0,280		(0,91)	0,92	(0,95)	(0,95)	(0,97)			
0,98	0,200	(0,84)	(0,86)	(0,91)	(0,92)	(0,94)				

1080 times per second, giving an alternating photocurrent which was amplified by a Wilson amplifier[84] and recorded on a Speedomax recorder (Leeds & Northrup).
The dispersion, used by us was 7,7 A/mm on the plane of the second slit of the spectrograph. On the tracings one Angström unit corresponds with 2,5 mm at 1,6 μ.
The apparatus profile was determined, using the atmospheric CO_2 lines at 1,57 μ; since the Doppler width of these lines is very small (a heavy molecule in a cold atmosphere) it may safely be assumed that the whole observed profile is determined by the apparatus. The mean apparatus profile at 1,57 μ is given in table 28.

TABLE 28. Mean apparatus profile of the Liège spectrograph for 1,57 μ.

$\Delta\lambda$(A)	$\Delta\lambda$ (mm)	intensity
0	0	1,00
0,25	0,032	0,85
0,50	0,065	0,52
0,75	0,098	0,25
1,00	0,130	0,10
1,25	0,163	0,03
1,50	0,195	0,01

We compare the half widths of the three instruments, which were used in the investigations, presented in this thesis:

Utrecht (Rowland); 568 lines/mm; h = 0,079 mm
Meudon (Wood) ; ~600 lines/mm; h = 0,101 mm
Liège (Wood) ; ~600 lines/mm; h = 0,13 mm

All half widths are reduced to the same focal length and to a wavelength of 1,57 μ. The greater half width of the Liège apparatus is due to the fact that the resolving power of a slit is smaller than that of the photographic plate.
The intensities of the ghosts are negligible.

FIGURE 6

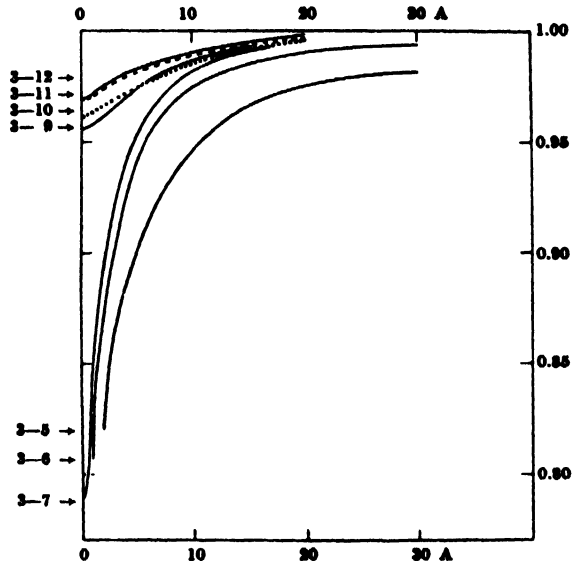

Mean profiles of the solar Paschen lines for the centre of the disc.

The response curve of the apparatus was at the time of the observations only linear in its first part; we practically always worked in that part and corrected, if necessary.
In tables 29 and 30 the profiles of the lines, corresponding with the transitions 3-5; 3-6; 3-7; 3-9; 3-10; 3-11; 3-12 and the transitions 4-7; 4-10; 4-11; 4-12; 4-13 and 4-14 are given. (Figures 6 and 7). The data, contained in the tables are mean values of at least two, and generally four to six individual determinations. The mean error of one determination is 6‰; the mean errors of the data in the tables are consequently smaller. Nevertheless greater *systematic* errors cannot be kept out, especially for the high members, a number of which is consider-

FIGURE 7

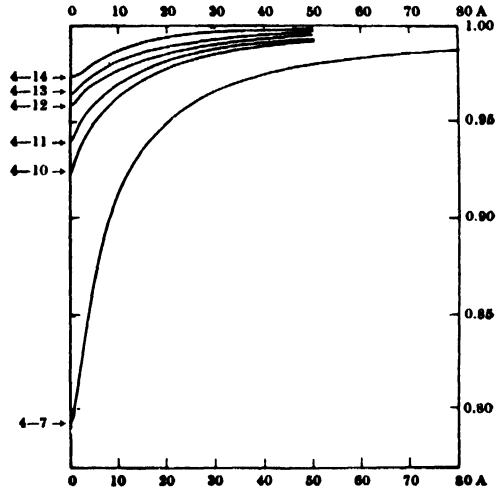

Mean profiles of the solar Brackett lines for the centre of the disc.

TABLE 29. Mean profiles and equivalent widths of Paschen lines in the centre of the solar disc (The table gives the residual intensities multiplied by 1000).

	3 - 5	3 - 6	3 - 7	3 - 9	3 - 10	3 - 11	3 - 12
λ(A)	12818	10938	10049	9292	9015	8863	8750
E.W. (A)	4,388	2,426	1,602	0,748	0,736	0,560	0,486
Δλ(A)							
0	627	742	788	956	961	969	969
0,5	657	768	807				
1,0	739	806	831				
1,5	787	851	874				
2,0	819	864	893	962	967	975	976
4	884	925	935	972	971	980	982
7	925	962	970	979	976	984	986
10	944	976	984	987	986	986	988
15	967	985	991	992	989	992	995
20	976	990		996	995	995	998
30	981	992					

ably blended by water vapour lines, which were still important in some parts of the spectrum even in the favourable conditions at the Sphynx observatory. A comparison with other determinations of the same lines[49,50] shows, however, that it is difficult to find an observing station with conditions as good as on the Jungfraujoch station (see also [70] and [140]).

TABLE 30. Mean profiles and equivalent widths of Brackett lines in the centre of the solar disc.
(The table gives the residual intensities multiplied by 1000).

line	4 - 7	4 - 10	4 - 11	4 - 12	4 - 13	4 - 14
λ(A)	21655	17362	16806	16407	16109	15880
E.W. (A)	7.368	3.182	2.534	1.850	1.334	0.832
Δλ(A)						
0	794	925	940	958	963	972
1	809	930	945	962	967	
2	826	936	952	966	970	975
4	852	944	957	968	974	979
7	885	957	964	973	978	985
10	912	964	968	977	984	986
15	938	970	976	980	986	990
20	950	974	982	984	988	994
30	966	983	987	988	992	997
50	979	992	992	996	996	998
100	990					

TABLE 31. Equivalent widths of the lines of the Balmer, Paschen and Brackett series of hydrogen (Angström units) (centre of disc).

Lowest level (n)		2	3	4
Upper level (m)	3	4,03		
	4	3,80		
	5	2,76	4,39	
	6	3,37	2,43	
	7		1,60	7,37
	8	2,46		
	9		0,75	
	10	3,59	0,74	3,18
	11	2,42	0,56	2,53
	12	1,44	0,49	1,85
	13			1,33
	14			0,83
	15	0,62		
	16	0,48		

§ 4. *The equivalent widths of the hydrogen lines.* Next in table 31 a review of the equivalent widths of the hydrogen lines is given. Attention is drawn to the fact that the Paschen lines show a minimum area as compared with the corresponding areas of the Balmer and Brackett lines. This is *not* due to superexcitation of the Brackett lines; the explanation will be discussed in Chapter XI.

CHAPTER V

A PRELIMINARY DETERMINATION OF THE TEMPERATURE DISTRIBUTION IN THE SOLAR ATMOSPHERE, USING THE OBSERVED LIMB DARKENING AND THE ENERGY-WAVELENGTH CURVE OF THE CONTINUOUS SPECTRUM BETWEEN 4000 AND 6000 A.

§ 1. *Introduction.*

In order to be able to compare the observed profiles of the hydrogen lines with the results of theoretical calculations, we need a model of the solar atmosphere.

This model must be an *observational* model; the theoretical models, which exist at present do not confirm by sufficient exactness the observed values of $I(\lambda;0)$. (I is the emergent radiation of the sun; θ is the angle of emergence). The observational models, on the other hand, are derived, by using some observed fundamental properties of the solar radiation, such as the limb darkening of the continuous spectrum; these data are interpreted with the very simple assumption of local thermodynamic equilibrium, which assumption seems to be justified in that part of the solar atmosphere from which the radiation mainly originates.

An observational model which is often used, is that of BARBIER[8], derived primarily from the limb darkening of the continuous spectrum of the sun; it is valid for optical depths, smaller than about $\tau_{5000} = 2$. Later, it was extended by the present writer to greater depths by a semitheoretical reasoning[68]. The latter model is in agreement with the observed *relative* limb darkening at 5000 A but by integration we find that the *absolute* values of $I(\lambda;0)$ are too great by some percents. This shows, that this model, which will be called *model III*, in accordance with the quoted paper (see also table 34, first column), is not a correct one and that a better model is desired, which should be in agreement with $I(\lambda;0)$ in absolute values.

In this chapter attempts will be made to find such a model; we use the available observations of the limb darkening of the sun, as published in the last decades by various authors and the energy-wavelength curve of the sun, derived by ABBOT and corrected by MULDERS and later by CHALONGE and coworkers. Only the observations in the wavelength region between 4000 and 6000 Angstrom are used.

§ 2. *The relation between the temperature in the sun and the emergent radiation.*

The relation between the emission $B(\lambda;\tau_\lambda)$ per unit of volume, time, wavelength and solid angle in the solar atmosphere, and the temperature is given by PLANCK's law (assumption of local thermodynamic equilibrium). It is related to the emergent radiation $I(\lambda;\theta)$ by

$$I(\lambda;\cos\theta) = \int_0^\infty B(\lambda;\tau_\lambda)\, e^{-\tau_\lambda \cos\theta} \sec\theta\, d\tau_\lambda \quad (V,1)$$

The solution of this integral equation of the first kind may be found in many ways. BARBIER[8] assumed, following LUNDBLAD[92] that

$$B(\lambda;\tau_\lambda) = \sum_1^N A_n\, \tau_\lambda^n$$

then

$$I(\lambda;\cos\theta) = \sum_1^N A_n\, \cos^n\theta/n!$$

However, the result of such a solution is not always reliable. From the mathematical point of view $B(\lambda;\tau_\lambda)$ can be solved exactly if $I(\lambda;\theta)$ is known with (a) mathematical exactness in (b) an infinite number of points. Since both requirements are not fulfilled, $B(\lambda;\tau_\lambda)$ is uncertain, especially for $\tau_\lambda > 1,0$ since $I(\lambda;\theta)$ is of course not known for $\cos\theta > 1,0$.

This was also shown with an example by EVANS[46]: two $I(\lambda;0)$ curves, which are identical but for $\cos\theta < 0,25$ yield with the method of the polynomia two $B(\lambda;\tau_\lambda)$ curves, which show great differences, especially for $\tau_\lambda < 0,25$ and for $\tau_\lambda > 1,0$. Partly this is also caused by the unappropriate form of the polynomia for the deep layers, which may sometimes yield negative values for the temperature for great values of τ_λ. The proposal of KOURGANOFF (see e.g.[138]) to put

$$B(\lambda;\tau_\lambda) = A + B\tau_\lambda + \Sigma\, \alpha_n\, e^{-\beta n \tau_\lambda} \quad (V,2)$$

or to suppose[81]

$$B(\lambda;\tau_\lambda) = \Sigma^n\, A_n\, K_n\, (\tau_\lambda)$$

should already give better results since these formulae give a more reasonable $B(\lambda;\tau)$ relation. We will use in the following an equation resembling (V,2).

§ 3. *Program of the calculations.*
In this section we give only the program with no details on the performance. The derivation of the new model will proceed in several steps. See also table 32.

1. Our first approximation is model III. We calculate by numerical integration $I(\lambda;\cos\theta)_{calc}$ for this model.
2. From the observed relative limb darkening and the observed energy-wavelength curve we derive $I(\lambda;\cos\theta)_{obs.}$.
3. We determine $\Delta I = I(\lambda;\cos\theta)_{obs} - I(\lambda;\cos\theta)_{calc}$ We intend to apply to model III some temperature corrections by which these ΔI values are explained.

TABLE 32. Successive steps in the determination of the new model of the solar atmosphere. N.B. The suffix $_0$ always means: reduced to 5000 A. If a variable, such as $\cos\theta$ or λ is placed as an index (and not between brackets) this means that it is kept constant in that step.

step no.	basis	intermediary step	result
1	model III	numerical integration	$I(\lambda;\cos\theta)_{III}$
2	$\left[\frac{I(\lambda;\cos\theta)}{I(\lambda;1,00)}\right]_{obs.} \times (I(\lambda;1,00))_{obs.}$		$I(\lambda;\cos\theta)_{obs.}$
3	$I(\lambda;\cos\theta)_{obs.} - I(\lambda;\cos\theta)_{III}$		$\Delta I(\lambda;\cos\theta)$
4 a	$\Delta I(\lambda;\cos\theta)$	PLANCK	$\Delta\Omega(\lambda;\cos\theta)$
4 b	$(\cos\theta)_\lambda$	$\left[\frac{(\cos\theta)_\lambda = \tau_\lambda^*}{\tau_0(\tau_\lambda)}\right]$	$\cos\theta_0$
5	$\Delta\Omega(\lambda)_{\cos\theta_0}$	interpolation	$\Delta\Omega_0(\cos\theta_0)$
6	$\Delta\Omega_0(\cos\theta_0)$	PLANCK	$\Delta I_0(\cos\theta_0)$
7	$\Delta I_0(\cos\theta_0)$	LAPLACE transformation	$\Delta B_0(\tau_0)$
8	$\Delta B_0(\tau_0)$	PLANCK	$\Delta\Omega_0(\tau_0)$
9	model III + $\Delta\Omega_0(\tau_0)$		model V

4. For the sake of clear explanation it is *provisionally* assumed that the radiation $I(\lambda;\cos\theta)$ has been emitted at an effective depth $\tau(\lambda;\cos\theta)$ and that each ΔI is due to a $\Delta\Omega$ in this representative layer.
Two $\Delta I(\cos\theta)$ values for different wavelengths are not directly comparable since their relation to the temperature variation differs according to PLANCK's law. In order to make them comparable we first transform ΔI into $\Delta\Omega$.
Let us refer for comparison to the radiation at λ_0 = 5000 A, and to $\Delta\Omega(\cos\theta;\lambda_0)$ issued from the corresponding standard layer at an optical depth $\tau_0 (= \tau_{5000})$. A value of $\Delta\Omega(\cos\theta;\lambda)$ at an other wavelength is not yet comparable since the radiation, observed at the same value of cos θ, but at two different wavelengths does not emerge from exactly the same layer, the absorption coefficient being different according to λ. But this same $\Delta\Omega$ will apply to the standard layer if $\cos\theta$ is slightly changed into $\cos\theta_0$ (figure 8). With a simple relation we determine for each value of $\cos\theta$ at the wavelength λ the corresponding $\cos\theta_0$ which reduces the $\Delta\omega$ to the standard layer.

FIGURE 8

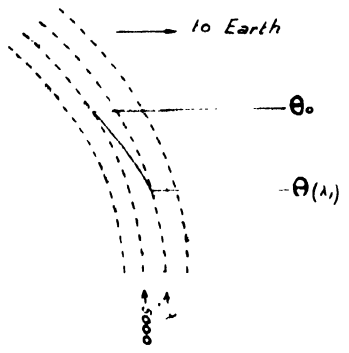

The reduction of $\cos\theta(\lambda_1)$ to $\cos\theta_0$. The dotted lines are lines of equal height and, hence, of equal temperature and ergiebigkeit. The dashed-dotted lines represent the "effective depths" from where the radiation, observed at the wavelength λ emerges.

(N.B. The index $_0$ always denotes: reduced to λ = 5000 A).

5. Now, all values of $\Delta\omega(\lambda)_{\cos\theta_0}$ which belong to the same $\cos\theta_0$ should be equal. (If a variable such as $\cos\theta$ or λ is placed as an index – and not between brackets – this means that it is kept constant). However, it will be found that they still depend on λ; this can be explained only by assuming that the observed energy-wavelength curve of the sun is in error for the small wavelengths. For the time being we base our model on the wavelength 5000 A. We plot $\Delta\omega(\lambda)_{\cos\theta_0}$ as a function of the wavelength for which it has been derived; we draw a mean curve and find the best value for λ_0 = 5000 Angström, which will be called $\Delta\omega_0(\cos\theta_0)$; being determined from the mean of the measurements, this is a better value than the original $\Delta\omega(\cos\theta;\lambda_0)$.

6. The preceding program points 4 and 5 have been explained in terms of an "effective layer", but actually they refer to the photosphere as a whole. The $\Delta\omega_0(\cos\theta_0)$ found has only a formal meaning and describes a $\Delta I_0(\cos\theta_0)$. By PLANCK's law we transform $\Delta\omega_0(\cos\theta_0)$ into $\Delta I_0(\cos\theta_0)$.

7. The function $\Delta B_0(\tau_0)$ is solved from the function $\Delta I_0(\cos\theta_0)$ with a Laplace transformation.

8. This function is transformed with PLANCK's law into values of $\Delta\omega_0(\tau_0)$. These are now real temperatures; ω has no formal value, as in steps 4, 5 and 6.

9. The new model is derived as the sum of model III and these new $\Delta\omega_0(\tau_0)$-values, found in step no. 8. This model is called *model V*.

Separately we shall discuss the variation of $\Delta\omega(\lambda)_{\cos\theta_0}$ with λ found in step no. 5.
After this short review we shall turn to a detailed description of each step.

§ 4. *Determination of* $I(\lambda;\cos\theta)_{calc}$. *(Step I of table 32).*

The integration, according to (V,1) was performed for all values of $\cos\theta$ and of λ (restricted to the interval between 4000 and 6000 A), corresponding with the observations of
ABBOT[1,2] (1908 - 1913; bolometric)
RAUDENBUSCH[141] (1937; photo-electric)
MOLL, BURGER and Van der BILT[116] (1925; thermo-electric)
CHALONGE and CANAVAGGIA[21] (1946; photographic)
MINNAERT, Van den HOVEN van GENDEREN and Van DIGGELEN[110] (1946; photographic)
The observations of KRAT[82] and of Ten BRUGGENCATE *et al.*[15] could not be included since our calculations were already finished when their data reached us.

To perform the integrations with the aid of model III, we need for other wavelengths than 5000 A the relation between τ_0 and τ_λ. This is found by numerical integration of

$$\tau_\lambda = \int \frac{\kappa_{\bar{\lambda}} + \kappa_\lambda}{\kappa_{\bar{0}} + \kappa_0} d\tau_0 \qquad (V,3)$$

in which formula $(\kappa_{\bar{\lambda}} + \kappa_\lambda)$ is the sum of the continuous absorption coefficient due to the negative hydrogen ion as calculated by CHANDRASEKHAR and BREEN[25] and that, due to the absorption of the neutral hydrogen atom. (see e.g. UNSÖLD[177]).

The integrations according to (V,1) were performed with the method of NEWTON-GAUSS, in which the summation was made over 8 terms. In this case our computing error, being smaller than 0,05%, is smaller than the error in the observations, this being for most observers of the order of 0,5%. For the measurements of MINNAERT, near the limb of the sun, the six term approximation was used (computing error = 0,05%). The summation interval was chosen for all observers, except for MINNAERT *et al.* from $\tau_\lambda = 0$ to τ_λ = 5,0. Since the part of the integral beyond τ_λ = 5 cannot be neglected – its contribution being of the order of 3%, we approximate $B_\lambda(\tau_\lambda)$ for greater values by a linear function, the gradient being chosen equal to the gradient over the interval $0 \leqq \tau_\lambda \leqq 5$. This value is not the best one, but a small error in B has a negligible influence on the emergent radiation. For comparison with the observations of MINNAERT *et al*, which refer to the extreme limb of the sun, the summation interval was chosen from τ_λ = 0 to τ_λ = 1,0; for greater depths the correction term, described above, was applied *mutatis mutandis*.

In total, 305 integrations have been performed. The detailed results are not communicated in

TABLE 33. Example of the course of the computations for two wavelengths (All intensities are to be multiplied by 10^{14} (c.g.s.).

I λ = 4030 A (Chalonge and Canavaggia).

cosΘ	1,00	0,954	0,866	0,800	0,714	0,609	0,436	0,312	0,221
$[I(\cos\Theta)/I(1,00)]_{obs.}$	1,000	0,959	0,877	0,859	0,767	0,664	0,533	0,423	0,346
$[I(\cos\Theta)]_{obs.}$	4,38	4,20	3,84	3,76	3,36	2,91	2,24	1,85	1,52
$[I(\cos\Theta)]_{calc.mod.III}$	5,627	5,392	5,046	4,697	4,254	3,677	2,845	2,275	1,842
$\Delta\Theta_0$	0,030	0,031	0,035	0,029	0,029	0,030	0,026	0,025	0,025
$\cos\Theta_0$	1,240	1,185	1,070	0,985	0,875	0,750	0,550	0,405	0,285

II λ = 5010 A (Abbot).

cosΘ	1,00	0,980	0,916	0,835	0,760	0,661	0,565	0,484	0,392	0,312
$[I(\cos\Theta)/I(1,00)]_{obs.}$	1,000	0,985	0,945	0,894	0,845	0,777	0,711	0,650	0,583	0,517
$[I(\cos\Theta)]_{obs.}$	4,15	4,09	3,92	3,71	3,51	3,22	2,95	2,70	2,42	2,15
$[I(\cos\Theta)]_{calc.mod.III}$	4,476	4,405	4,211	3,999	3,725	3,450	3,128	2,846	2,525	2,260
$\Delta\Theta_0$	0,014	0,013	0,012	0,012	0,010	0,011	0,010	0,009	0,008	0,009
$\cos\Theta_0$	0,998	0,980	0,914	0,833	0,757	0,658	0,563	0,483	0,391	0,312

this investigation, but in table 33 an example of the calculations is given for two sets of observations.

§ 5. *"Observed" values of $I(\lambda;\cos\Theta)$; calculation of $\Delta I(\lambda;\cos\Theta)$.*

In the calculations, according to steps 2 and 3 of table 32 we used the energy wavelength curve of MULDERS[118] corrected for wavelengths, smaller than 5000 A by CHALONGE and CANAVAGGIA[22]. The recent further corrections to this curve by CANAVAGGIA, CHALONGE, EGGER-MOREAU and OZIOL-PELTEY[20] reached us too late to be used in the calculations. Nevertheless they will be compared further on with the results of the present calculations (section 10).
The differences $\Delta I(\lambda;\cos\Theta)$ are then determined without difficulties.

§ 6. *Reduction of $\Delta I(\lambda;\cos\Theta)$ to 5000 A.*

Next we describe step 4 of table 32. The $\Delta I(\lambda)$ values, now derived, are mutually comparable, if they are expressed with PLANCK's law into $\Delta\Theta$-values. (This conversion is purely formal; primarily it has nothing to do with the temperature correction which will finally be applied to model III).

But still, when the conversion is performed, two $\Delta\Theta$-values, observed at the same value of cosΘ but at other wavelengths are not completely comparable. Because the transmission of the solar atmosphere varies with λ, these two observations do not correspond exactly with the same layers of the atmosphere. This can be corrected in first approximation by "reducing" the cosΘ value for the wavelength λ to that for the wavelength 5000 A, as has already been explained qualitatively in section 3. The reduction is made in two steps (See also figure 8).
First step: The relation between $\Delta I_\lambda(\Theta)$ and $\Delta B_\lambda(\tau)$ is

$$\Delta I_\lambda(\cos\Theta) = \int_0^\infty \Delta B_\lambda(\tau_\lambda)\, e^{-\tau_\lambda \sec\Theta} \sec\Theta \, d\tau_\lambda \qquad (V,4)$$

We next develop $\Delta B_\lambda(\tau_\lambda)$ around the point $\tau_\lambda^* = \cos\Theta$ and suppose (approximatingly) that $\Delta B_\lambda(\tau_\lambda - \tau_\lambda^*)$ can be represented by a second degrees polynomium in $(\tau_\lambda - \tau_\lambda^*)$.

$$\Delta B_\lambda(\tau_\lambda - \tau_\lambda^*) = a_\lambda + b_\lambda(\tau_\lambda - \tau_\lambda^*) + c_\lambda(\tau_\lambda - \tau_\lambda^*)^2$$

In that case, as has already been shown by BARBIER[8] and by UNSÖLD[181]:

$$\Delta I_\lambda(\cos\theta) = a_\lambda + b_\lambda(\cos\theta - \tau^*_\lambda)$$

$$\Delta I_\lambda(\cos\theta = \tau^*_\lambda) = \Delta B_\lambda(\tau^*_\lambda) \qquad (V,5)$$

which relation is valid in good (second!) approximation.

Second step: Since the relation between τ_λ and τ_0 is known, we also know that between $\cos\theta$ and $\cos\theta_0$.
The approximation which has been applied here, would certainly not be permitted in solving the equation (V,4), but it is sufficiently correct for the reduction of $\cos\theta$ to $\cos\theta_0$. An example of the reduction if given in table 33.

§ 7. *The derivation of* $\Delta I_0(\cos\theta_0)$ *(Steps 5 and 6 of table 32).*
We now meet an interesting fact. It would be expected, that the values of $\Delta\omega(\lambda;\cos\theta_0)$, which are found in the preceding step, are now only a function of $\cos\theta_0$ and no longer of the wavelength λ to which the $\Delta I(\lambda;\theta)$ values originally belonged. But this is not correct; if the $\Delta\omega(\lambda)_{\cos\theta_0}$ values, belonging to one value of $\cos\theta_0$ are selected, we observe, that they depend very markedly on the initial wavelength of the observations. An example is given in figure 9, where $\Delta\omega(\lambda;\cos\theta_0)$, corresponding with the observations of CHALONGE and CANAVAGGIA is given for three wavelengths. It would be expected that the points, belonging to different wavelengths would define all the same mean curve (but for the scatter of the points, due to unevitable measuring errors), but this is not so. This fact does not only exist for the observations of CHALONGE and CANAVAGGIA but also, in the same form, for *all observers*. We note further that these deviations occur only in the wavelength interval between 4000 and 5000 A and not for greater wavelengths. This means, that it is in this wavelength region not possible to find *one unique* function for the temperature variation in the solar atmosphere from the whole of the observed $I(\lambda;\theta)$.
We decided to restrict ourselves for the time being to the calculation of a model of the solar armosphere, using the $\Delta I(\cos\theta_0)$ values for one wavelength only (5000 A). These values will be derived *by interpolation* from the values for the other wavelengths, which belong to the same value of $\cos\theta_0$. The systematic dependence on the wavelength will be investigated in detail in section 10, where also a possible explanation will be given.

FIGURE 9

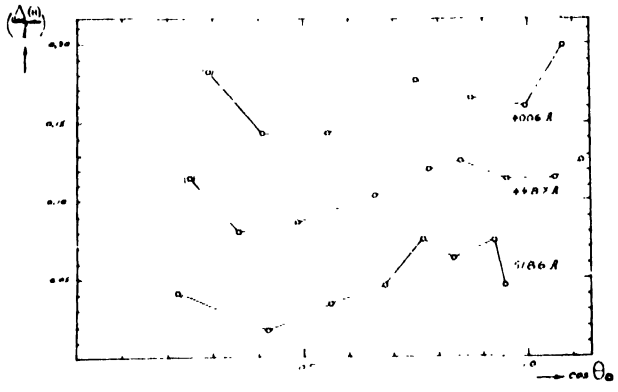

The reduced values of $\Delta\omega(\lambda;\cos\theta_0)$ should be the same for each wavelength, but this is not so, in fact, as is shown for three sets of observations of CHALONGE and CANAVAGGIA. This wavelength-dependent effect will be investigated in § 10.

FIGURE 10

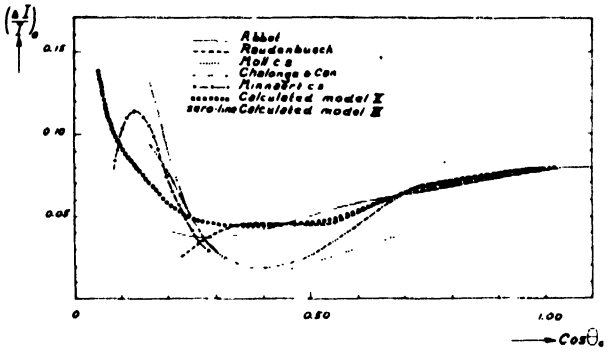

The interpolated values of $(\Delta I/I)_0$ for the various groups of observers.

The (interpolated) values of $\Delta\omega_0(\cos\theta_0)$, transformed into $\Delta I_0(\cos\theta_0)$ values (step 6 of table 32) are given for the five sets of observers in figure 10. It is obvious, that the observations fall distinctly into two groups: one containing the measurements of ABBOT and these of RAUDENBUSCH and another, containing the other three groups of observers. These differences could perhaps be due to real variations in the solar temperature curve; there is, however, no correlation with the solar cycle. But on the other hand the differences between the groups may not be caused by measuring errors; at $\cos\theta = 0,40$ they amount to a value, corresponding with $\Delta I/I = 2,5\%$, which is much greater than the individual scatter of the $\Delta I/I$ values around the mean curve.
However, in one sense the observations are incomplete, since all refer to the *same* energy-wavelength curve for the centre of the disc.

For that reason there only *seems* to be agreement among all groups of observers near $\cos\vartheta = 1,0$. In order to test, whether the solar temperature curve changes indeed with time, a *complete* set of observations should be obtained. Such a set ought to include a simultaneous determination of the limb darkening for at least one wavelength and of the energy-wavelength curve for the centre of the disc. Only the observations of ABBOT and partly those of CHALONGE and CANAVAGGIA fulfill this demand. *For that reason we must restrict ourselves to the determination of one mean $\Delta\Theta(\tau_0)$ curve for the solar atmosphere, neglecting the differences which exist between the several observers.*

§ 8. *The solution of equation (V,4) (Steps 7 - 9).*

The shape of the ΔI-curve, now obtained is fairly regular for $\cos\vartheta_0 > 0,4$ but it is more irregular for small values of $\cos\vartheta_0$. For $\cos\vartheta_0 > 0,4$ it can well be approximated by a linear function; we hence adopt the following function for $\Delta B_0(\tau_0)$:

$$\Delta B_0(\tau_0) = \alpha + \beta\tau_0 + (\gamma + \delta\tau_0)\, e^{\varepsilon\tau_0} \qquad (V,6)$$

The solution, according to (V,1) is

$$\Delta I(\cos\vartheta_0) = \alpha + \beta\cos\vartheta_0 + \frac{\sec\vartheta}{\sec\vartheta-\varepsilon}\left[\gamma + \frac{\delta}{\sec\vartheta-\varepsilon}\right] \qquad (V;7)$$

For α and β we found directly

$\alpha = -\ 0,108.10^{14}$ c.g.s.
$\beta = +\ 0,439.10^{14}$ c.g.s.

Satisfactory values for the three other parameters could be found after some trials:

$\gamma = +\ 0,064.10^{14}$ c.g.s.
$\delta = -\ 0,20\ .10^{14}$ c.g.s.
$\varepsilon = -\ 1,5$

TABLE 34. The derivation of model V.

τ_0	Θ model III	$\Delta\Theta$ linear part of (V,7)	$\Delta\Theta$ exp. part of (V,7)	$\Delta\Theta$ total	Θ_{new} (=model V)	log P	log P_e
0,01	1,019	-0,019	+0,052	+0,033	1,052	4,13	0,27
0,02	1,013	-0,017	+0,048	+0,031	1,044	4,28	0,42
0,03	1,008	-0,016	+0,044	+0,028	1,036	4,38	0,50
0,04	1,003	-0,014	+0,041	+0,027	1,030	4,44	0,56
0,06	0,993	-0,012	+0,034	+0,022	1,015	4,54	0,65
0,08	0,981	-0,010	+0,029	+0,019	1,000	4,60	0,72
0,10	0,973	-0,009	+0,024	+0,015	0,988	4,65	0,78
0,15	0,949	-0,005	+0,016	+0,011	0,960	4,75	0,90
0,20	0,933	-0,002	+0,009	+0,007	0,940	4,81	1,00
0,30	0,900	+0,002	+0,001	+0,003	0,903	4,91	1,14
0,40	0,873	+0,005	-0,001	+0,004	0,877	4,97	1,28
0,50	0,850	+0,007	-0,001	+0,006	0,856	5,04	1,43
0,60	0,830	+0,009	-0,001	+0,008	0,838	5,06	1,54
0,80	0,798	+0,012	-0,001	+0,011	0,809	5,11	1,75
1,00	0,772	+0,014	-0,001	+0,013	0,785	5,14	1,94
1,20	0,750	+0,016	-0,001	+0,015	0,765	5,16	2,08
1,40	0,733	+0,017	-0,001	+0,016	0,749	5,18	2,24
1,60	0,716	+0,018	-0,001	+0,017	0,733	5,19	2,34
1,80	0,702	+0,019		+0,019	0,721	5,20	2,46
2,00	0,690	+0,020		+0.020	0.710	5,21	2,56
2,50	0,664	+0,020		+0,020	0,684	5,23	2,76
3,00	0,634	+0,020		+0,020	0,654	5,24	2,99
4,00	0,614	+0,020		+0,020	0,634	5,26	3,14
5,00	0,602	+0,020		+0,020	0,622	5,28	3,25
7,00	0,588	+0,020		+0,020	0.608	5,31	3,35
9,00	0,581	+0,020		+0,020	0,601	5,33	3,14

The $\Delta I_0/I$ curve, corresponding with this solution is also given in figure 10.

The solution (V,7) will be fairly good in the regions where τ_0 is smaller than – say – 1,5 or 2. It becomes less and less reliable when progressing towards greater depths in the solar atmosphere, and the linear function $\alpha + \beta\tau_0$, which determines the solution in regions deeper than $\tau_0 = 0,5$ would lead to improbable low temperatures – and even to an inversion ! – in the deep layers ($\tau_0 > 6$). Beyond a certain depth the temperature curve, determined theoretically must be more reliable than the empirical correction curve. We place this limit, rather arbitrarily at $\tau_0 = 2,0$, where, in model III we have the upper limit of the convection zone. In model III, from that point onwards the temperature curve had been calculated theoretically; here, we roughly use the results of that calculation and assume provisionally, that for $\tau_0 > 2,0$ the correction $\Delta\Theta_0(\tau_0)$ is constant and equal to its value at $\tau_0 = 2,0$.
Model V, which is derived in this way, as a correction to model III, is given in table 34 (this is the final step, no. 9, of our program). The parts for $\tau_0 < 0,08$ and $\tau_0 > 1,2$ are based on extrapolations and are, hence, less certain than the parts between these limits.

§ 9. *The accuracy of the new model.*
The residuals

$$(I_{obs.} - I_{calc.V})/I_{obs.} \qquad (V,8)$$

where $I_{calc.V}$ is the intensity of the solar radiation, calculated with model V for the wavelength 5000 A, are represented in figure 10. It is clear, that *systematic differences* occur only for $\cos\theta_0 < 0,2$; there, (V,8) becomes in some points as great as 4%; it reaches more than that for a part of the observations of MOLL *et al.*
The *internal agreement* between the observations of *one* observer may be judged from figure 11, which will be discussed in § 10. In anticipation, we observe, that the mean error of one determination (with reference to "its" mean curve) is about the same for all observers; it is about ± 0,5% with no clear difference between photo-electric, thermo-electric, bolometric and photographic observations. Obviously, all observers have produced sets of observations which are in good internal agreement, but apparently, systematic errors have not been entirely avoided (The alternative possibility, that real temperature changes occur in the solar atmosphere, has already been discussed in section 7).
Our solution does not show, as is clear from figure 10, the characteristic depression which occurs in the observations of CHALONGE and CANAVAGGIA and in those of MOLL, BURGER and Van der BILT. In fact, we shall find further-on (chapter IX) that this depression is very probably related to a kind of "hump" in the $\Theta(\tau)$ curve, as was e.g. found by PLASKETT[139,140].
Finally, it will be very interesting to see, whether further investigations of the energy distribution close to the sun's limb will show the same character as the measurements of MINNAERT *et al.*, because their curve seems to require an interesting temperature curve in the highest parts of the solar atmosphere.

§ 10. *Discussion of the wavelength dependent residuals.*
We have already observed in § 7 that the values of

$$[\Delta\Theta(\lambda) - \Delta\Theta(5000)]_{\cos\theta_0} \qquad (V,9)$$

depend on the wavelength. This means that either all observers have made the same errors, which seems improbable, or that the effect must be ascribed to other causes. Essentially, this means that it is not possible to find with the present data a temperature distribution in the solar atmosphere using at the same time the limb darkening observations and the energy-wavelength curve in the region between 4000 and 5000 A. In that wavelength region for every wavelength another temperature distribution would be found.
Details are shown in figure 11. There, we have plotted the values of (V,9) grouped according to $\cos\theta_0$; the value of $\Delta\Theta(5000)_{\cos\theta_0}$ being the interpolated value from figure 10.
The most important fact, shown by figure 11 is, that there is no dependance of the form of the function (V,9) on $\cos\theta_0$. In the whole region between $\cos\theta_0 = 0,2$ and 1,2 the *form* of the function is the same and a mean curve may be obtained, which curve is drawn in figure 11 and listed in table 35.
This property of the residuals leads immediately to their explanation:
They cannot be explained as errors in the adopted continuous absorption coefficients since in that case the residuals would tend to zero for $\cos\theta_0 \to 0$.
They can neither be ascribed to errors in the adopted temperature function in the deep layers (which function has been found in a more or less tentative way – cf. § 8 – since also in that case the residuals would tend to zero near the sun's limb.
But since for each value of λ, $\Delta\Theta$ is proportional to $\Delta I/I$, according to PLANCK's law, the figure 11 means, that for any fixed wavelength

FIGURE 11

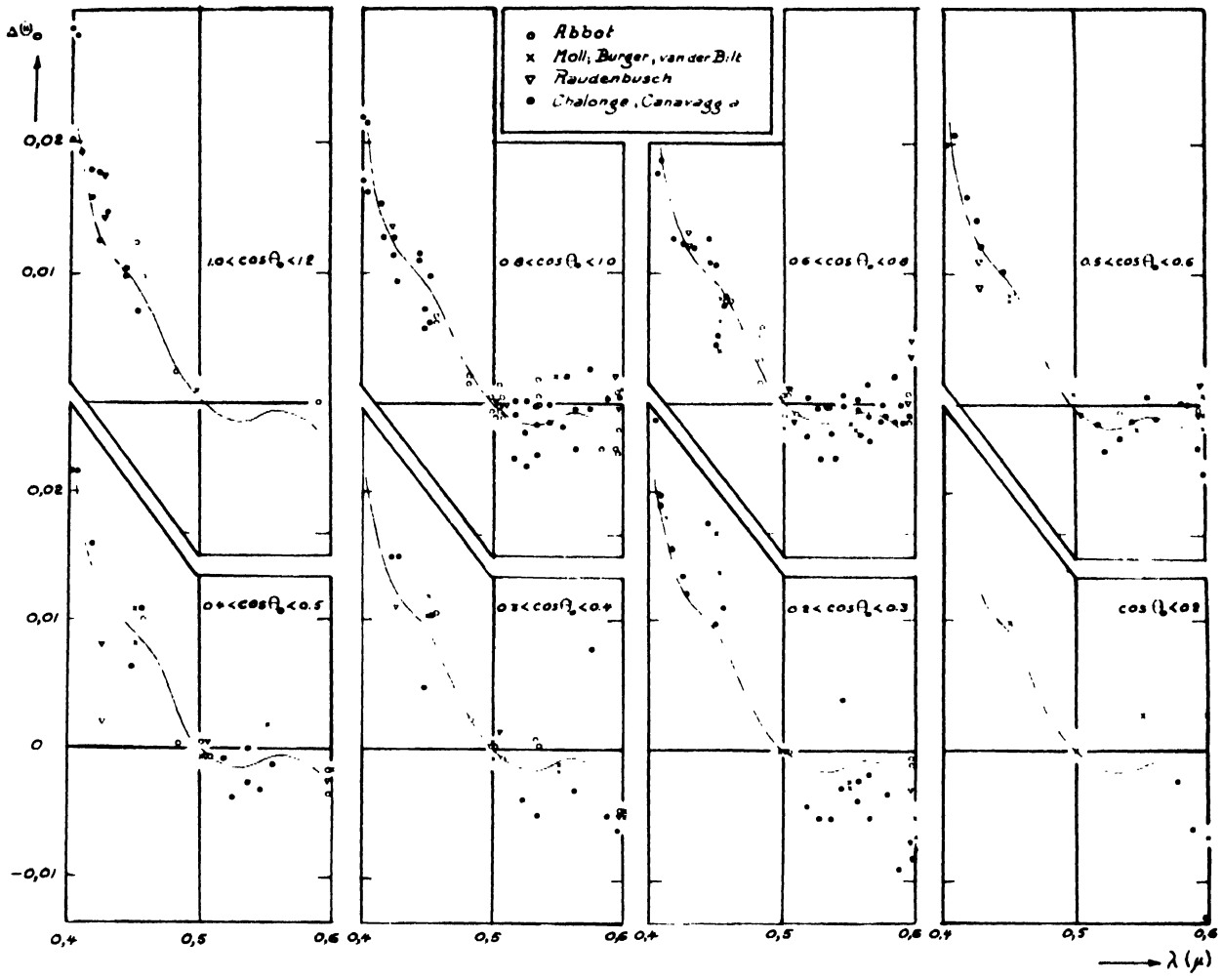

The wavelength-dependent effect. The points are grouped according to their $\cos\theta_0$ values. The full drawn curve is the mean curve which is assumed to be the same for all points on the disc.

all observed intensities are over the whole disc too great or too small, as compared with the computed intensity; the ratio between them being the same for all values of cos θ. This can only be explained by assuming that the energy-wavelength curve for the centre of the disc, which has been used in our calculations, is not correct. *This is indeed the case*, since we have used the energy-wavelength curve, deduced by CHALONGE and CANAVAGGIA in 1946[22], while in 1950 a correction to this curve has been published by CANAVAGGIA, CHALONGE, EGGER-MOREAU and OZIOL-PELTEY[20]. But although this correction reduces the differences found by us to about the half, they do not disappear entirely. See figure 12. As the latter result of CANAVAGGIA *et al.* was found after a careful reduction, it does not seem probable, that these should still need further corrections to an amount, as great as 6% at 4000 A. (For the greater wavelengths the necessary correction would be smaller). Nevertheless, it seems difficult to find another solution for this problem; a new investigation of the energy distribution is this wavelength region seems to be worth wile.

Model V, presented in this chapter, seems at present the best model, deduced from the continuous spectrum of the sun; in fact it is only valid for λ = 5000 A. *For each other wavelength another model applies*, which can be obtained from model V by adding of the small quantities, listed in table 35. Since, however, these corrections are for $\lambda > 5000$ A only of the order of

TABLE 35. Mean systematic differences between the solar temperature functions, derived observationally for different wavelengths.
N.B. The temperature differences are all very small: if $\Theta = 1,0$. the greatest value, $\Delta\Theta = +0,02$ corresponds with $\Delta T = 100^{o}$. In the wavelength region $\lambda > 5000$ A the differences do not exceed 20^{o} in that case.

λ (A)	4050	4150	4250	4520	4820	5050	5150	5300	5500	5700	5920
$\Delta\Theta$	+0,0212	+0,0151	+0,0124	+0,0092	+0,0026	0,0000	-0,0009	-0,0017	-0,0006	-0,0006	-0,0021

FIGURE 12

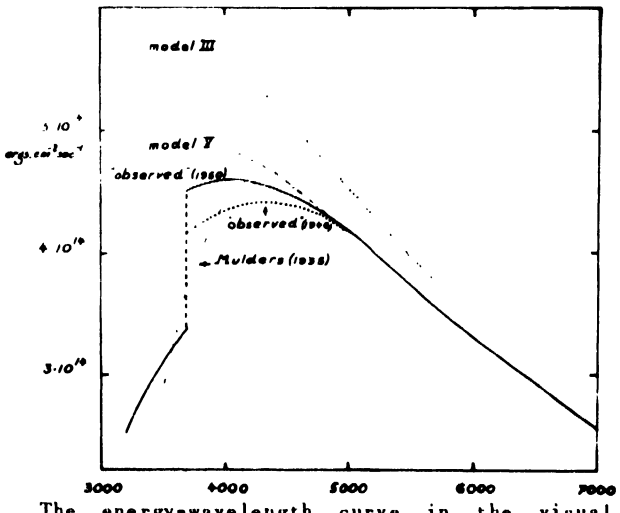

The energy-wavelength curve in the visual spectral region. Both the observed curves and the computed ones are given (models III and V). The differences between model V and the observed curve near 4000 A may be due to an error in the latter curve.

some tenths of degrees, it may be assumed in very good approximation, that the model is valid for all wavelengths from 5000 to 6000 A.

§ 11. *An alternative model of the atmosphere.* There is some arbitrariness in the way, according to which the solution found in section 8 is obtained: our new model is in the central parts of the disc in agreement with ABBOT and with RAUDENBUSCH, while it is in the limb parts more in agreement with the other observers. This arbitrariness is obviously due to the uncertainty in the observational material, which manifests itself in step no. 7: in this step some assumption is made about the form of the function $B(\tau)$; then the coefficients are determined so, that they give agreement with the observations; in how far this agreement is satisfactory depends on the set of observational material which is chosen.
In this section we derive an alternative model. The calculations are approximative and not as detailed as the preceding ones, which lead to model V, but they serve to show the relative uncertainty in the derivation of a model of the atmosphere.
A sharp gradient is observed in the $\Delta\Theta_0(\cos\theta_0)$ curve for $0,15 < \cos\theta_0 < 0,25$, especially in the observations of MOLL *et al.*, CHALONGE and CANAVAGGIA and MINNAERT *et al.* This might indicate, that there exists a corresponding steeper gradient in the $\Delta B(\tau_0)$ curve at a depth of about $\tau_0 = 0,2$. The more is this probable since the emergent intensity is found by an integration over the depth of the atmosphere, so that abrupt changes in the gradient are smoothed out. We consider especially the observations of MINNAERT *et al.*, since they come nearer to the limb than the other ones. We take again model III as a first approximation and assume that the corrections to the ergiebigkeit have the form (see also figure 13):

$$\Delta B(\tau_0) = \alpha + \beta\tau_0 \qquad (V,10)$$

with $\alpha = 0$; $\beta = -p$ for $0 < \tau_0 < 0,19$
$\alpha = q$; $\beta = -q/(\tau_0)_2$ for $0,19 < \tau_0 < (\tau_0)_2$
$\alpha = \beta = 0$ for $\tau_0 > (\tau_0)_2$.

FIGURE 13

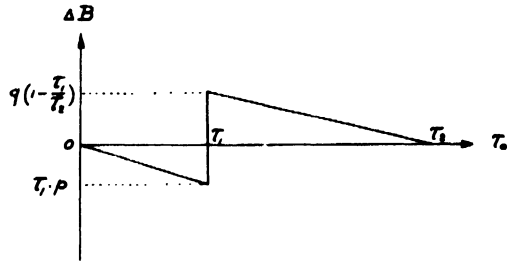

The value $\tau_0 = 0,19$ is the optical depth where the gradient of $\Delta B(\tau_0)$ is tentatively assumed to have its maximum value.
The parameters p, q and $(\tau_0)_2$ are to be determined from the two sets of observations of MINNAERT *et al.* (wavelengths 5593 and 6425 A).

If (V, 10) is substituted in (V, 4) we obtain

$$\Delta I = -p[\cos\theta - e^{-\tau_1 \sec\theta}(\tau_1 + \cos\theta)] +$$

$$+ q[e^{-\tau_1 \sec\theta}(1 - \frac{\cos\theta}{\tau_2} - \frac{\tau_1}{\tau_2}) + e^{-\tau_2 \sec\theta}\frac{\cos\theta}{\tau_2}]$$

In this formula, τ_1 is the value of τ_λ corresponding with $\tau_0 = 0,19$ while τ_2 corresponds with the unknown value of $(\tau_0)_2$.

Several values for $(\tau_0)_2$ have been adopted, then p and q have been solved from the two equations. It turned out that both $|p_{5593} - p_{6245}|$ and $|q_{5593} - q_{6245}|$ were minimum for $(\tau_0)_2 = 0,6$, while $\sum\mu^2$ showed its minimum for $(\tau_0)_2 = 0,7$. (μ is the deviation (obs - calc)). So, the value $(\tau_0)_2 = 0,6$ was adopted. This gives the temperature curve listed in table 36. (*Model VI*).

TABLE 36. Model VI of the atmosphere.

τ	0,05	0,10	0,15	0,19	0,20	0,25	0,30	0,35	0,40	0,45	0,50	0,55
T	1,036	1,035	1,029	1,020	0,872	0,863	0,858	0,852	0,846	0,844	0,842	0,838

The fundamental difference between this model and model V is obvious. The residuals of model VI are about twice those of model V, which is still of the same order of magnitude (Table 37).

TABLE 37. Comparison of model VI with the observations.

$\sin^2\theta$	$\Delta I \cdot 10^{14}$		$\Delta I/I$	
	λ 6245	λ 5593	λ 6245	λ 5593
0,995	-0,013	+0,011	-0,010	+0,008
0,990	-0,014	+0,013	-0,010	+0,009
0,980	-0,007	+0,024	+0,005	+0,015
0,960	-0,008	-0,017	-0,004	-0,009

We have made this small computation to show how uncertain the solar model in fact is, if it is derived only from the limb darkening and the energy-wavelength curve. This fact becomes still more striking when we consider that other empirical models have residuals which are of the same order of magnitude: in PLASKETT's model the residuals between the computed and the observed limb darkening are smaller than 0,5%, if expressed in the intensity of the centre of the disc. The same is the case in miss BUSBRIDGE's model, where the residuals are of the order of 0,3%. BARBIER's residuals are of the same order of magnitude.

In conclusion we note that *a satisfactory model must in any case not only explain the energy distribution in the continuous spectrum of the sun but also the line spectrum and its variation over the disc.* It is expected that such a model will in any case be more reliable than a model, derived from the continuous spectrum only.

It is the aim of the present investigation to derive such a model.

CHAPTER VI

THE WINGS OF THE BALMER LINES. THE TEMPERATURE DISTRIBUTION IN THE SOLAR ATMOSPHERE BETWEEN $\tau_0 = 0{,}4$ AND 2,8. PRELIMINARY DISCUSSION OF THE WIDENING MECHANISM OF THE BALMER LINES

§ 1. *Introduction and survey.*

The profiles of the Balmer lines in the solar and in stellar spectra cannot be described like the normal Fraunhofer lines by classical mechanisms as collisional damping and Döppler effect only. In 1930, STRUVE and ELVEY could demonstrate that the Balmer lines in stellar spectra are widened by the Stark effect, due to the surrouding electrically charged particles[168].

The profiles of the line excitation coefficient*) are calculated according to HOLTSMARK[60,61], as a function of T and P_e, where T and P_e are always expressed in one other function F_0, the „normal field strength": $F_0 = 46{,}8\ (P_e/T)^{2/3}$.

This was done for the first time in a systematic way by VERWEY[183]. A small neglect in the current theories was noted by MROWKA[117]; this has been taken into account afterwards by SCHMALJOHANN[156], but these latter calculations may not be entirely correct either. They will be corrected in this chapter, § 2. In § 3 the calculations are extended to the higher Balmer lines with a more approximative method, according to PANNEKOEK.

In his textbook, UNSÖLD[177] showed that the absorption coefficient at great distances from the line centre can be represented by a formula of the form $C_n . F_0^{3/2} \Delta\lambda^{-5/2}$; values of C_n are given for Hα to Hδ. These values are once more computed in section 4; the results differ somewhat from those of UNSÖLD.

Still later UNSÖLD[178] argued that in fact only the protons (or, in general the ions) have a broadening influence; the encounters with electrons, moving very fast, should be described by „collisional broadening", but their influence is negligible as compared with that of statistical widening by the Stark effect of the ions. In the calculations which are described in this chapter, this point of view is provisionally accepted. It if for that reason that the above defined normal field strength F_0 contains the factor (P_e/T) and not $(2P_e/T)$. Afterwards, § 11 and 12, this assumption will be further investigated when the results of the calculations are compared with the observations.

Program of this chapter: First a survey is given of the parameters which describe the widening of the line excitation coefficients. Then we compute the profiles of the line *wings* with model V. It will be found that small differences between the calculated and the observed profiles occur. This enables us, firstly to correct our model of the atmosphere in the layers between $\tau_0 = 0{,}4$ and 2,8, and secondly to obtain corrected values for the constants C_n, defined above.

§ 2. *Profiles of the excitation coefficients in the Stark widened Balmer lines Hα to Hδ.*

The profile of the excitation coefficient, widened by the Stark effect is found[183] by:

$$S(\alpha) = \sum \frac{I}{c} . W\left(\frac{\alpha}{c}\right) + \text{central component}$$

I is the intensity of the Stark coefficients of the line; the σ components obtain double weight (MROWKA[117]);

c is the displacement of the component in Angström units, with respect to the central, unshifted, component and for a field of unit strength in electrostatic c.g.s. units;

$\alpha = \Delta\lambda/F_0 = c.F/F_0$;

W is the probability distribution of the field strength, calculated by VERWEY.

According to more recent calculations[161,162,83] the function $W(F)$ should deviate in the solar atmosphere from the function, originally calculated by VERWEY; the deviations should be due to the influence of colissional broadening. Since, however, the statistical approximation can always be applied to the *wings* of the lines (which are discussed in this chapter) the classical HOLTSMARK-VERWEY distribution is maintained.

*) It is confusing that the word „absorption" is often used in two entirely different meanings. It means firstly the process of *excitation* of an atom by a lightquant and secondly it is used as one of the possible mechanisms of *re-emission*, the other being the scattering mechanism. Accordingly, „absorption coefficient" sometimes means $(\varkappa_\nu + \sigma_\nu)$ (first meaning) or only $\varkappa_\nu$.

To avoid confusion we shall call $(\varkappa_\nu + \sigma_\nu)$ the *excitation coefficient*. It is true, that this name can also be criticized; it avoids, however, the danger of one name for two different things. We call $\varkappa_\nu$ and σ_ν the absorption- and scattering-coefficient, as usual.

The function $S(\alpha)$ is normalized so that

$$\int_{-\infty}^{+\infty} S(\alpha)d\alpha + \text{central component} = 1$$

The Stark profiles for H_α to H_δ were calculated for small values of α (inner part of the profiles) by VERWEY and corrected afterwards by SCHMALJOHANN. The latter's curves are given graphically in UNSÖLD, Sternatmosphären, figure 65. Since, however, a normalizing error seems to occur in one of SCHMALJOHANN's curves - the area of his H_β curve is 0,55, while it should be 0,50 - we calculated all curves anew, using the data on the Stark splitting, summarized by VERWEY with double weight for the σ-terms.
The new profiles are given in table 38. When comparing them to the profiles, computed by SCHMALJOHANN, it is found that there are some minor differences.

Apart from computing errors, a possible cause for the differences between SCHMALJOHANN's calculations and ours may be the fact that SCHMALJOHANN used for his calculations not exactly the same data as are used by the present author.
For H_α to H_δ we used the data, given by VERWEY, where the distances of the splitted components from the central component are those, measured by STARK; the intensities have been calculated by SCHRÖDINGER[157]. The data, used by UNSÖLD and SCHMALJOHANN were the *theoretical* data[87]. The differences are small. With regard to the exactness of the data, communicated by STARK it must be noted that though his intensities, which were derived in the period of childhood of photographic photometry may be criticized, this is not the case with his distances of the components. It must be further remarked that the theory is not yet complete either, as is e.g. shown by the occurrence of „forbidden" components in the splitting pattern. For these reasons we do not think to have made great errors by using the data of STARK and SCHRÖDINGER, and we consider the curve of table 38 als reliable.

§ 3. *Profiles of the excitation coefficients in the high Balmer lines.*

For the high Balmer lines things are more difficult than for the low series members since no experimental values of the Stark splitting are known for these lines. Besides, although SCHRÖDINGER's and GORDON's[52] formulae may be applied, their application still requires a rather large amount of work and grows more and more difficult for the high quantum numbers. So the profile was calculated with a more approximate method based on work of PANNEKOEK[126]. The same calculations have also been performed by Mrs. Van ALBADA-van DIEN, and have been published already earlier[40].
In reality the lines are split into a great number of terms with intensities, varying from one component to the other. The mutual distances of the components also vary. Now, it is supposed that the splitting of the lines can be ascribed approximately as if at a certain field strength F the line was broadened into a band

TABLE 38. Stark profiles for H_α ... H_δ (central part of the lines).

$\alpha = \frac{\Delta\lambda}{F_0}$	H_α	H_β	H_γ	H_δ
0,001	0,15	0,04	0,03	0,04
0,0025	0,84	0,19	0,16	0,20
0,005	2,98	0,66	0,59	0,64
0,0075	5,35	1,58	1,14	1,21
0,010	7,00	2,18	1,72	1,65
0,0125	7,55	3,07	2,14	1,90
0,015	7,37	3,86	2,45	2,10
0,020	5,65	5,13	2,65	2,31
0,0225	4,81	5,53	2,63	2,46
0,025	4,22	5,77	2,57	2,59
0,0275	3,82	6,02	2,48	2,73
0,030	3,60	6,27	2,41	2,84
0,035	3,23	6,35	2,31	3,04
0,040	2,86	6,20	2,32	3,12
0,045	2,72	5,87	2,39	3,07
0,050	2,42	5,42	2,45	2,98
0,060	1,94	4,44	2,54	2,68
0,070	1,51	3,67	2,60	2,44
0,080	1,14	2,82	2,66	2,26
0,090	0,84	2,39	2,40	2,06
0,100	0,55	1,95	2,25	1,90
0,120	0,40	1,27	1,80	1,66
0,140	0,26	0,81	1,30	1,45
0,160	0,15	0,58	1,04	1,25
0,180	0,11	0,44	0,81	1,05
0,200	0,07	0,29	0,61	0,87
0,250		0,17	0,33	0,54
0,300		0,10	0,19	0,33
0,350		0,06	0,12	0,22
0,400		0,02	0,08	0,15
0,500			0,04	0,08
0,600			0,03	0,04
0,700			0,02	0,02
0,800			0,01	0,01
1,000			0,01	0,01

with a half width $\Delta\lambda^*$, equal to the distance of the most shifted component. Here, according to PANNEKOEK:

$$\Delta\lambda^* = +0,00256\left[\frac{n^2}{n^2-4}\right]^2 . (n(n-1)+2)F - s_n F \quad \text{(VI,1)}$$

n in the principal quantum number.

In the solar atmosphere the values of the field strength F are distributed according to a frequency curve $W(\beta)$, with $\beta = F/F_0$.
$W(\beta)$ is calculated by HOLTSMARK and VERWEY.

In order to determine the STARK profile $S(\alpha)$ the function (VI,1) should be combined with $W(\beta)$. This gives the profile:

$$s_n\, S(\beta)\, d\beta = \tfrac{1}{2}\left(\int_{\beta}^{\infty} W(x)\frac{dx}{x}\right) d\beta \qquad \text{(VI,2)}$$

$$\beta = \alpha / s_n$$

The result of a numerical integration of (VI,2) is given in table 39. The table gives the Stark profile for all lines, the splitting of which can be represented by the formula (VI,1). It is satisfactory to notice that the values from the table are practically identical with those computed by Mrs. Van ALBADA-van DIEN (l.c. table 1).

TABLE 39. The approximate from of the Stark profile for the high Balmer lines.

β	$s_n S(\beta)$	β	$s_n S(\beta)$	β	$s_n S(\beta)$
0	0,287			3,25	0,0258
0,1	0,286	1,6	0,125	3,75	0,0172
0,2	0,283	1,7	0,113	4,00	0,0144
0,3	0,278	1,8	0,103	5,00	0,0074
0,4	0,271	1,9	0,0936	6,00	0,0044
0,5	0,262	2,0	0,0847	7,00	0,0028
0,6	0,252	2,1	0,0766	8,00	0,0020
0,7	0,241	2,2	0,0692	9,00	0,00145
0,8	0,228	2,3	0,0626	10	0,00111
0,9	0,215	2,4	0,0566	12	0,000689
1,0	0,202	2,5	0,0511	15	0,000382
1,1	0,118	2,6	0,0462	17	0,000280
1,2	0,175	2,7	0,0420	20	0,000187
1,3	0,162	2,8	0,0382	25	0,000108
1,4	0,149	2,9	0,0348	30	0,000070
1,5	0,136	3,0	0,0318	35	0,000050
				40	0,000037
				50	0,000022

§ 4. *Some parameters, describing the Stark-widened hydrogen lines profiles.*

The function (VI,2) is extremely useful and will practically always be used in this investugation. The more exact functions, given in table 38 will not be used. That this is fully permitted will be shown in this section.

We first show that the curves given in table 38 for H_α ... H_δ can be approximated very well by the curve $s_n.S(\alpha/s_n)$ from table 39. Of course, PANNEKOEK's approximation, based of the assumption of homogeneous widening into a rectangular profile is not valid for the cores of these lines; the paramater s_n cannot be calculated *a priori* for them with the formula (VI,1), but new, *empirical* s_n values must be introduced. This is done by adapting the wings of the exact curves – which can be represented, as is known, by the asymptotic law

$$S_n(\alpha) = K_n.\alpha^{-5/2} \qquad \text{(VI,3)}$$

to the wing of the curve (VI,2), which can be approximated by the same law. The process of adaptation determines the value of the constant s_n for the lines H_α ... H_δ. The results are given in table 40, first four values of column 5. Of course, the agreement between the adapted Stark curves and the true profiles is good in the wings only; discrepancies occur in the central parts. Their amount may be judged with the aid of figure 14. There we have drawn (*a*) the curve (VI,2) and (*b*) the curves $s_n S(\alpha/s_n)$ which are obtained by combining the exact curve $S(\alpha)$ for H_α ... H_δ (table 38) with the empirical s_n values, given in table 40, column 5.

FIGURE 14

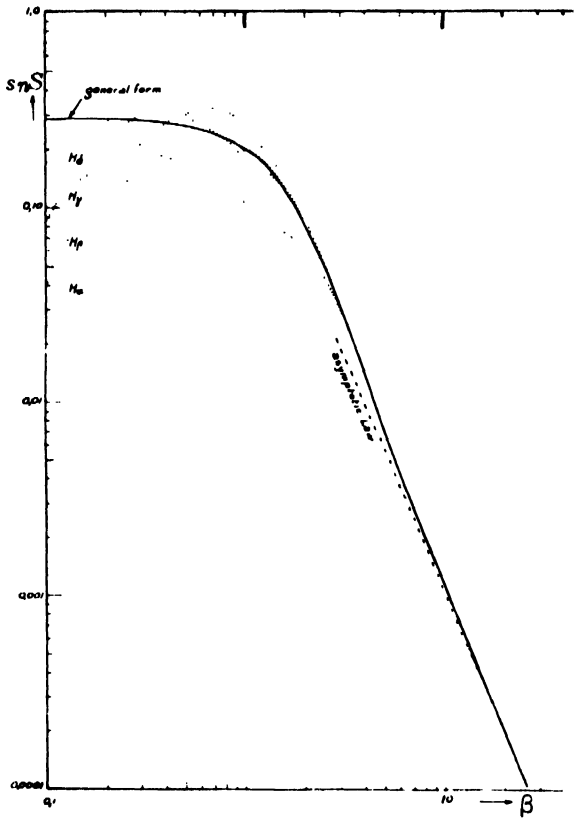

Full drawn: the $s_n S(\beta)$ curve computed with PANNEKOEK's approximation for the high series members.
Dotted: the adapted curves for H_α ... H_δ.

TABLE 40. Parameters of the Stark widening of the Balmer lines.

n		λ (A)	fn2	s_n (empirical)	s_n (with (VI,1))	K_n	$C_n \cdot 10^{16}$	$C_n \cdot 10^{16}$ (UNSÖLD)
3	H_α	6562,82	0,641	0,0264	0,0662	0,001415	3,43	3,13
4	H_β	4861,33	0,119	0,0512	0,0638	0,00382	0,951	0,885
5	H_γ	4340,47	0,0447	0,0746	0,0800	0,00670	0,493	0,442
6	H_δ	4101,74	0,0221	0,1023	0,1008	0,01080	0,340	0,309
7	H_ε	3970,07	0,0127		0,1332	0,0157	0,277	
8		3889,05	0,00804		0,1688	0,0222	0,230	
9		3835,37	0,00543		0,2100	0,0309	0,199	
10		3797,90	0,00385		0,2506	0,0400	0,187	
11		3770,63	0,00284		0,3062	0,0575	0,181	
12		3750,15	0,00215		0,3645	0,0706	0,179	
13		3734,37	0,00167		0,4255	0,0900	0,176	
14		3721,94	0,00133		0,503	0,114	0,175	
15		3711,97	0,00107		0,564	0,136	0,174	
16		3703,86	0,000877		0,640	0,164	0,173	
17		3697,15	0,000727		0,721	0,201	0,172	
18		3691,56	0,000610		0,808	0,238	0,172	

Agreement between both curves occurs for all lines for $\alpha/s_n > 3$; for H_γ and H_δ practically already for $\alpha/s_n > 1$. The great differences in the cores of H_α and H_γ are due to the neglected central components of these lines, which cannot be drawn as they have no width.
Still the remaining deviations would not be negligible if the lines were not obliterated by the Doppler effect which obliteration causes a further reduction of the differences shown in figure 14.
The influence of the Doppler effect on the profiles is quantitatively shown as follows.
For a temperature of 5000° the half half-width $\Delta\lambda'$ of the doppler core of the Balmer lines is about 0,2 A for H_α and 0,1 A for the high Balmer lines near the Balmer limit. As the cores of these lines are mainly formed in the high parts of the solar atmosphere where F_0 varies between 0,1 and 0,3 and as for the first four Balmer lines s_n varies between 0,02 and 0,1, it is found that $F_0 . s_n$ ranges between 0,002 and 0,03. Hence, from

$$\beta = \alpha/s_n = \Delta\lambda/F_0 s_n$$

we find that the limiting value $\beta' = \Delta\lambda'/F_0 s_n$ varies between 30 and 100 for H_α and between 3 and 10 for H_δ. Hence the Doppler width is practically always greater than the width of the region where the exact $s_n S(\alpha)$ curve disagrees from the approximated curve; it is consequently *permitted to use the approximate curve for all lines, inclusive H_α to H_δ.*

In some cases, – e.g. when dealing with the far wings of the lines – it is permitted to use only the wing approximation (VI,3). We now determine the value of the constant K_n, occurring in (VI,3) for the different lines.
From table 39 we deduce the asymptotic relation

$$s_n S(\beta) = 0,330 . \beta^{-5/2}$$

Hence

$$K_n = 0,330 . s_n^{3/2} \qquad (VI,4)$$

K_n is computed for H_α to H_δ with the empirical s_n-values and for the other lines with formula (VI,1); see columns 6 and 7 of table 40.

Besides s_n and K_n there is a third parameter, which is of interest for our purpose, it is the parameter C_n, already defined in § 1. It will be computed anew for the Balmer lines, also for H_α to H_δ; the latter is done since our starting data differ somewhat from those of UNSÖLD.
The excitation coefficient per hydrogen atom in the state n-2 is:

$$k(\alpha) = \frac{\pi e^2}{mc^2} . \lambda^2 f . \frac{S(\alpha)}{F_0} \qquad (VI,5)$$

This is approximated in the wings by

$$k(\Delta\lambda) = C_n . F_0^{3/2} . (\Delta\lambda)^{-5/2} \qquad (VI,6)$$

A comparison of (VI,5) and (VI,6), using the asymptotic relation (VI,4) gives

$$C_n = \frac{\pi e^2}{mc^2} . \lambda^2 f . 0,330 . s_n^{3/2} \qquad (VI,7)$$

In columns 8 and 9 of table 40 our values of C_n and those of UNSÖLD are given; the differences are generally small - of the order of 10%. We use in the following calculations always our values.

Finally we must observe that in the *preliminary* calculations which are given in this chapter, *other* values of C_n have been used, owing to an error of computation. *These* values are listed in table 41; they are about 50% greater than the right ones but this fact has no consequences.

TABLE 41. Values of C_n used in the preliminary calculations of this chapter.

n	$C_n^1.10^{16}$
3	3,81
4	1,245
5	0,757
6	0,521

For - as will be shown at the end of this chapter - we shall find that the C_n values used in our calculations can not explain the observed line profiles, even after a correction of the temperature distribution in the atmosphere. It will be found necessary to derive new C_n values which give a better representation of the observed profiles. These "observed" C_n values are much greater than the values given in table 41 and *a fortiori* than the right values from table 40.

§ 5. *Calculation of the profiles of the wings of the Balmer lines; theory.*

When dealing with the wings of the lines, which are formed mainly in deep layers, it may be assumed, that the source function is equal to the Planck function. So the emergent radiation is:

$$I_\lambda(\theta) = \int_0^\infty B_\lambda(\tau)\, e^{-\tau \sec\theta} \sec\theta \, d\tau \qquad \text{(VI,8)}$$

We have defined $d\tau = (\kappa_\lambda + \kappa_\nu + \sigma_\nu)\rho dh = d\tau_\lambda + d\tau_\nu$

κ_λ = continuous absorption coefficient at the wavelength λ.

κ_ν and σ_ν are the selective absorption and scattering coefficients at the same wavelength.

The relation between τ and τ_0 is found according to

$$\frac{d\tau}{d\tau_0} = \frac{\kappa_\lambda + \kappa_\nu + \sigma_\nu}{\kappa_0} =$$

$$= \frac{\kappa_\lambda}{\kappa_0} + \frac{C_n\, F\delta^{3/2}\, \Delta\lambda^{-5/2}.4.10^{-10,15\theta}}{\kappa_0} =$$

$$= \frac{\kappa_\lambda}{\kappa_0} + \frac{1,281.10^3.10^{-10,15\theta}}{\kappa_0}.C_n\Delta\lambda^{-5/2}$$

In this formula κ_λ is the sum of the absorption coefficients of the negative hydrogen ions and of the neutral hydrogen atoms. If the contribution of the neutral atoms is neglected, which is permitted in layers above $\tau_0 = 2,5$, we may write

$$\kappa_0 = k_0.P_e$$

and hence

$$\frac{d\tau}{d\tau_0} = \frac{\kappa_\lambda}{\kappa_0} + \frac{1,281.10^3.10^{-10,15\theta}}{k_0\, T}.C_n.\Delta\lambda^{-5/2} \qquad \text{(VI,9)}$$

We arrive thus at the important conclusion that the excitation coefficient in the *wings* of the Balmer lines *does not depend on the pressure* but *only on the temperature*. This is only exact if the neutral hydrogen absorption can be neglected. As this is not entirely the case, a correction factor has to be introduced in the denominator of (VI,9) which factor is small in the region, important for us; it is given in table 42 for 5000 A. It is nearly the same for other wavelengths. We call k_0^1 the corrected value of k_0, and maintain the simple formula (VI,9), which is thus approximately valid in the deep layers.

TABLE 42. Influence of the neutral H absorption on the continuous absorption coefficient in the solar atmosphere (computed for model V for 5000 Å).

θ	$\frac{\kappa_{H^-} + \kappa_H}{\kappa_{H^-}}$
0,75	1,00
0,70	1,01
0,65	1,06
0,60	1,18
0,55	1,42
0,50	1,82

The integration, according to (VI,9) can now easily be performed. This is only done for $H\alpha$ to $H\varepsilon$, since the application of the asymptotic relation (VI,6) is dangerous for the high lines. This is shown with the aid of figure 14, from which it is obvious that the wing approximation is valid with some reability only for $\alpha/s_n > 3$. The wavelength distances, corresponding to this limit are given for several depths in the atmosphere in table 43; this table shows that the asymptotic relation is still permitted for $H\alpha$ to $H\delta$ but not in the deepest layers and that it is certainly dangerous to apply it to the high Balmer lines.

TABLE 43. Limiting wavelengths for the wing approximation (expressed in Angström units; computed with $\Delta\lambda_l = 3.Fosn$).

τ_o	F_o	H_α	H_γ	H_β	H_{15}
0,01	0,260	0,10	0,13	0,26	0,87
0,08	0,501	0,20	0,24	0,51	1,7
0,30	0,898	0,36	0,42	0,91	3,0
0,80	1,72	0,69	0,81	1,7	5,8
1,60	5,08	2,0	2,4	5,2	17
3,00	12,5	5,0	6,0	12,6	42
9,00	21,7	8,7	10,4	22	74

§ 6. *The integrations; comparison with observations.*

The value of (VI,8) has been computed for H_α to H_δ for the combinations of the following values of $\cos\theta$ and $\Delta\lambda$:

$\cos\theta$ = 1,000; 0,755; 0,484; 0,142.

$\Delta\lambda$(A) = 1,0; 2,0; 4,0; 8,0 and continuous spectrum.

Besides, for H_α the integration was performed for $\Delta\lambda$ = 12,0 A. All integrations were made with GAUSS' method (eight term approximation with rest term – see chapter V).

The results are given in table 44; for the sake of comparison the observed values are also given.

Comparison. The agreement is best for H_γ; less for H_δ, H_β and H_α. Near the limb the observed depressions are stronger than the calculated ones.

This relatively great limb intensity of the lines cannot be due to the influence of the neglected contribution of scattering since this has no influence on the lines wings. Others[149,14] have ascribed this phenomenon, which is already well known, to superexcitation in the outer layers in the sun. It may, however, be more fruitful, to try to explain the observations in the classical way, with the usual equilibrium formulae but with another solar temperature. We mention in this respect the great uncertainties in the limb temperature of the sun, as found in chapter V. Moreover, the excitation of the Balmer lines is greatly dependent on the temperature and small deviations in the model will have a great influence on the computed line excitation coefficients. Since, moreover, the Balmer line wings depend *only* on the temperature we have here a new and very sensitive method to determine the solar temperature, even in the relatively deep layers.

TABLE 44. Computed and observed line depressions and the mean optical depths $\bar{\tau}_0$ for H_γ...H_β for four places on the solar disc. The profiles have been computed with model V of the atmosphere and with the C_n values of table 41.

	$\Delta\lambda$	computed depressions (x 1000)					observed depressions (x 1000)					$\bar{\tau}_0$				
	$\cos\theta$	1	2	4	8	12	1	2	4	8	12	1	2	4	8	12
H_α	1,000	241	139	72	34	19	343	232	138	59	31	0,63	1,02	1,40	1,96	2,29
	0,755	194	102	48	22	11	301	180	97	54	29	0,60	0,92	1,29	1,71	1,97
	0,484	129	56	20	9	3	225	121	65	35	23	0,51	0,76	1,07	1,40	1,60
	0,142	18	3				130	50	30	10		0,32	0,47	0,65	0,90	1,03
H_β	1,000	319	206	107	41		353	235	136	63		0,86	1,30	1,90	2,51	
	0,755	260	160	73	27		300	227	134	58		0,80	1,20	1,77	2,26	
	0,484	171	92	31	10		287	157	120	57		0,67	1,02	1,47	1,83	
	0,142	19	12				120	80				0,38	0,60	0,92		
H_γ	1,000	370	234	133	51		373	220	103	11		1,01	1,49	2,11	2,71	
	0,755	300	180	86	32		339	174	72	18		0,94	1,39	2,02	1,54	
	0,484	195	105	37	13		220	79	40			0,80	1,20	1,67	2,06	
	0,142	29	12				100	20				0,43	0,72	1,03	1,35	
H_δ	1,000	350	228	113	41		346	227	129	50		1,10	1,61	2,26	2,83	
	0,755	290	178	83	29		312	196	83	41		1,01	1,48	2,07	2,59	
	0,484	192	104	40	13		217	101	48	15		0,88	1,23	1,71	2,10	
	0,142	31	12	3			110	60	20			0,48	0,70	0,98	1,30	

§ 7. *Description of the method to correct the approximately known solar temperature with the aid of the hydrogen line observations.*

The depressions of the lines, as given in table 44, were calculated as follows

$$1 - \frac{I(\lambda;\theta)}{I_{cont.}(\theta)} = 1 - \frac{\int_0^\infty B(\lambda;\tau) e^{-\tau \sec\theta} \sec\theta \, d\tau}{\int_0^\infty B(\lambda;\tau_\lambda) \, e^{-\tau_\lambda \sec\theta} \sec\theta \, d\tau_\lambda} \qquad \text{(VI,10)}$$

For a given wavelength the main contribution to (VI,10) generally originates only from a relatively *thin* layer of the atmosphere. This is caused by the fact that the line excitation coefficient is greatly dependent on the temperature; so it is always possible to compute a mean optical depth for the origin of the line depression, calculated with (VI,10). This mean optical depth will be computed in § 8, it will be called $\bar{\tau}_0$.

The way to correct the adopted temperature curve will be shown by an *example*.

For H_β, $\cos\theta = 1{,}00$ and $\Delta\lambda = 4{,}0$ we will find $\bar{\tau}_0 = 1{,}90$. In table 44 the computed depression 0,107 is found and the observed value is 0,136. This discrepancy may be explained by assuming that the temperature at $\tau_0 = 1{,}90$ is higher than was assumed in our model.

Now in the temperature region with which we are concerned $d \log(\kappa + \sigma)_\nu / d\omega = -11{,}1$; we assume further that also $d(\log \textit{depression})/d\omega = -11{,}1$ (thin layer approximation). This gives

$$\Delta\omega = -0{,}009.$$

A rather great difference between the observed and the computed line depressions (the relative difference is of the order of 25%) is in this case caused by a very small temperature difference. The value $\Delta\omega = -0{,}009$ corresponds with a temperature difference of no more than 90^0!

Before applying this method, we discuss its limitations:

a. A basic assumption is that the temperature correction is small and does not vary much with depth. The method could be applied exactly – apart from other criticisms – if the temperature correction would be constant with depth. Since – as will be shown in section 8 – this correction does indeed not change much with depth, this criticism is not too serious.

b. A further limitation is disclosed when we compare *this* method for computing the temperature distribution in the sun with the method, which is usually followed, e.g. in discussions of the continuous radiation of the sun (Cf. chapter V).

Here we have taken the mean optical depth over the region where the depression originates; in chapter V we took the mean optical depth over the *emergent radiation*.

What method should be followed depends actually on the extension of the region over which the mean is taken; this region should always be chosen so, that it is as small as possible, as is demonstrated in figure 15. In both parts of this figure we have drawn the function

$$B(\tau_\lambda) \; e^{\tau_\lambda}$$

for the continuous spectrum near $H\beta$. Moreover, the reduction of this radiation by the line absorption in the way, as indicated by formula (VI,10) is shown in the figure (shaded regions).

FIGURE 15

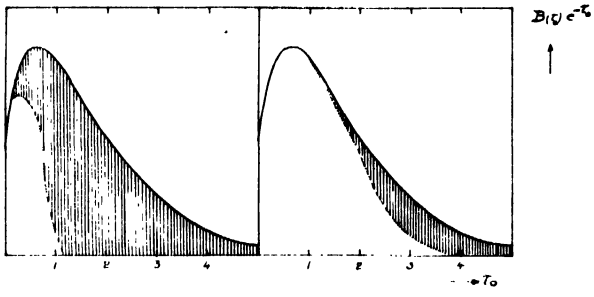

Schematic representation of the selective excitation in the Hβ line; left: near the core and right: in the far wing.

In general our new method is advisable for the *wings* of the lines and the *deep* layers, while for the study of the *high* solar layers and especially for the *cores* of the lines the old method of the ergiebigkeit is the best one.

c. Essentially, the method, discussed in this § is a *thin layer method*. It can only used without danger if the absorption takes place in a thin atmospheric layer so that the line depression is proportional to the excitation coefficient. Since this is not the case, our method is only approximately valid. We shall discuss its value by studying another expreme case, – that of *sudden complete absorption*.

Compare figure 16, which is analoge to figure 15. The true selective line depression which originates in a certain, more or less extended region of depth, may be drawn approximately in two ways: firstly – the dashed curve – as a constant depression over the whole region of depth, and secondly – the dotted curve – by a sudden complete absorption model. The position of the two curves, which are valid for $H\beta$, $\cos\theta = 1{,}0$; $\Delta\lambda = 4{,}0$ and $\tau_0 = 1{,}90$, is easily computed.

FIGURE 16

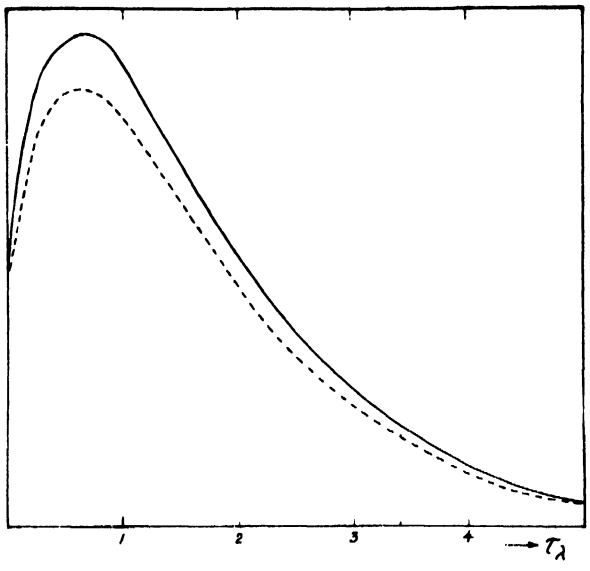

Schematic representation of two extreme possibilities for the process of line formation in the solar hydrogen lines. Dashed: thin layer model and dotted: complete absorption.

Now, *this* case is compared with the case of a somewhat higher temperature. The question is: what temperature variation - constant with depth is necessary to explain a certain observed difference in the line depressions?
For the thin layer model this has already been discussed in the first half of this section; we found the value $\Delta\omega = -0{,}009$.
For *the same example* the influence may be computed for the complete absorption model (the discussion of the *general case* is difficult).
To yield the depression 0,107 complete absorption has to begin at $\tau_0 = 3{,}44$. To yield the observed depression 0,136 it has to begin at a depth 3,04. Hence $\Delta \log \tau_0 = -0{,}116$.
We suppose that

$$\frac{d \log \tau_0}{d\omega} = \frac{d \log \tau}{d\omega} = \frac{d \log \kappa}{d\omega} \; (= 11{,}1)$$

which seems the most plausible supposition. This gives the temperature correction

$$\Delta\omega = \frac{d \log \tau_0}{11{,}1} = -0{,}010$$

This is practically the same value as the one obtained in the thin layer model. Naturally, this is no proof, that the way followed by us, gives in all cases a reliable temperature correction but it seems to make acceptable that the method might be applicable in many cases.

§ 8. *The mean optical depths and the preliminary temperature corrections.*
The mean optical depths are computed with

$$\bar{\tau} = \frac{\int_0^\infty x\{B(\tau=x) - B(\tau_\lambda = x)\} e^{-x \sec\theta} dx \sec\theta}{\int_0^\infty B(\tau_\lambda) e^{-\tau_\lambda \sec\theta} d\tau_\lambda \sec\theta}$$

Next, $\bar{\tau}$ is converted into $\bar{\tau}_0$. The results are given in table 44.
In figure 17 the values of ($\log D_{obs} - \log D_{th}$) for H_α to H_δ are plotted against $\bar{\tau}_0$. We did not plot the dots corresponding with observed D-values, smaller than 4%. For, if e.g. the measuring error is ± 2% of the continuum, then already the mean relative error in a point with depression 4% is as great as 50%.
In the figures we notice the following features: The general relation $(\omega; \bar{\tau}_0)$ is not quite the same for the several lines. This does certainly not indicate different temperatures for the different wavelengths at the same depths. Most probably another effect is interfering; this may be found by considering the systematic deviations of the points. It is obvious that the spread of the points shows a minimum for H_γ and a maximum for H_α and H_β. In the figures, some points, corresponding with the same value of $\Delta\lambda$ (but with different values of $\cos\theta$) are connected by lines. It is seen that the great spread for H_α and H_β is due to a systematic effect: the dots, corresponding with the small values of $\cos\theta$ - but with the same value of $\Delta\lambda$ generally lie higher with respect to the H_γ - curve that the points with greater values of $\cos\theta$. This is caused by the fact that the points for which $\cos\theta$ is small are also the points for which the depression D is small.
Clearly, the H_α, H_β and H_δ curves are affected by a systematic effect, which has the greatest relative influence on the small D values. It seems that the H_γ observations are free of this effect.
Provisionally we assume, that the H_γ curve, given here, shows the correct temperature corrections and that the other curves are affected by a systematic effect, the cause of which has still to be investigated.
In the following § it will be shown that such a cause can be found, thus justifying this provisional assumption.

§ 9. *Explanation of the systematic differences found in H_α, H_β and H_δ.*
In turn we try several possibilities.
1. We think that *observational errors* cannot be held responsable. This may already be shown by the fact that the measurements of Ten BRUGGENCATE *et al.*, which show the greatest differen-

FIGURE 17

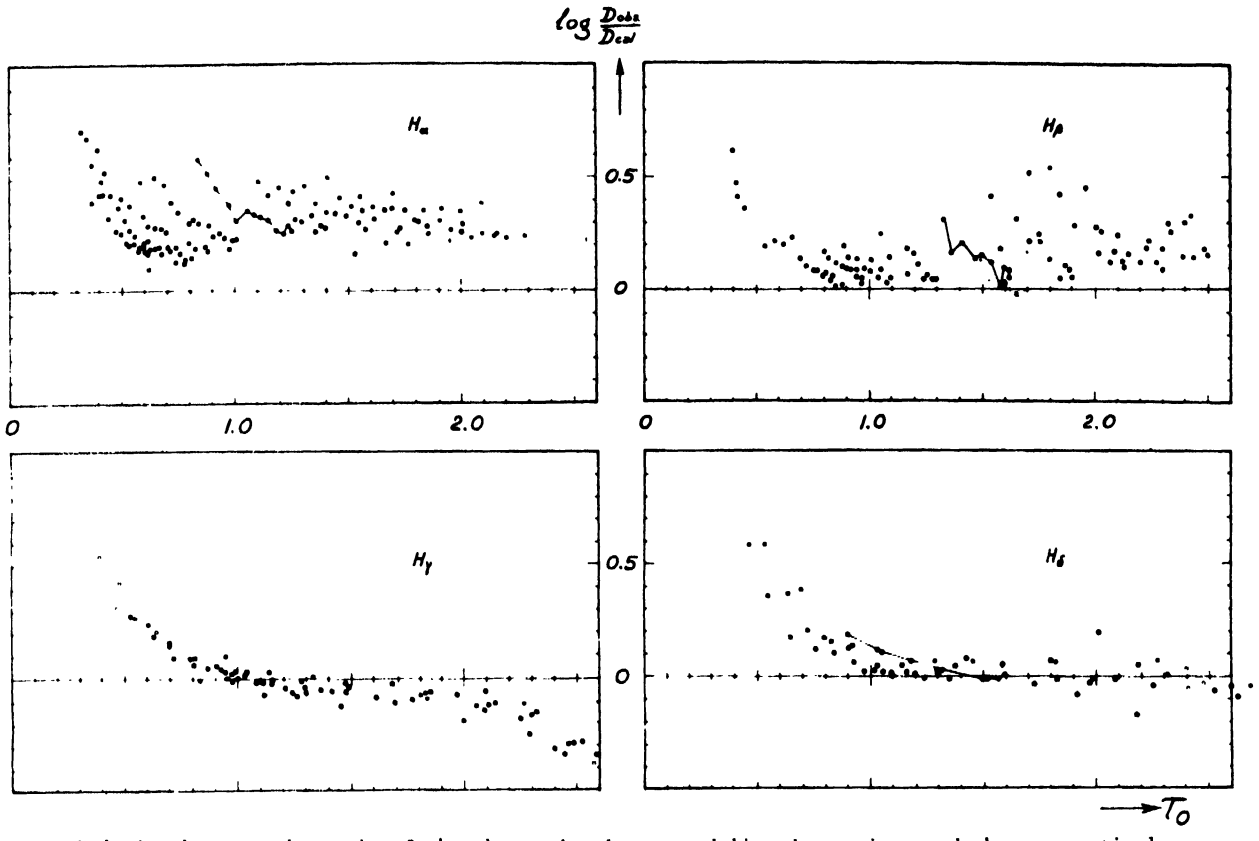

Relation between the ratio of the observed and computed line depressions and the mean optical depth where the depression originates. The best internal agreement occurs for Hγ. It is supposed that the differences between the various curves are due to deviations between the true line excitation coefficients and the assumed values.

ces with our measurements give practically the same results as ours if they are plotted in a figure, similar to figure 17.

2. Another reasonable error could be a wrong assumption of the height of the continuous background in constructing the line profiles. It might be suggested that such an error would indeed explain the observed effect. But this is not true: suppose that the continuous background is for all profiles of a given line too high or too low, then this means that all values of tables 6 to 9 included should be multiplied by a factor of the order unity. For in chapters II and III the mean line profiles have been determined on a *logarithmic scale*. An error, thus made in the height of the continuous background should be corrected logarithmically, thus leading to a vertical shift of the whole figure and not to a reduction of the spread of the points in figure 17.

3. It can be shown that is is possible to explain the deviations by a new C_n value for each of the lines. This new value is not computed: Suppose that $(C_n)_{new} = P(C_n)_{old}$. (With $(C_n)_{old}$ we mean the values from table 41).

In that case the new value of the depression $D(\Delta\lambda;\cos\theta)$ is the same as the value which corresponds with another $\Delta\lambda$ value, so that

$$(\Delta\lambda)_{new}/(\Delta\lambda)_{old} = P^{2/5}.$$

The values of P have been derived for the three lines; it was found that they were in good internal agreement, which is obvious from the following table 45.

The mean value $\overline{P}$ is only fixed in a relatively narrow wavelength interval, as is seen in the table. To the side of the long wavelengths the observed depressions are too small and too uncertain, to the side of the small wavelength distances the temperature curve, derived from H_γ becomes too uncertain.

In any case we think that we may draw from this discussion the *conclusion*, that we were justified

TABLE 45. Determination of P for Hα, Hβ, Hδ.

$\Delta\lambda$ (A)	cosθ	$p^{2/5}$	$\overline{P}$
4	1,00	2,3	
4	0,85	2,4	
4	0,69	2,3	8,6 ± 0,5
6	1,00	1,8	
6	0,58	2,3	
8	1,00	2,5	
3	1,00	1,3	
3	0,80	1,6	
3	0,64	1,8	
5	1,00	1,4	3,4 ± 0,4
5	0,80	1,5	
5	0,69	1,9	
6	1,00	1,5	
6	0,80	1,6	
2	1,00	1,1	
2	0,80	1,2	
3	1,00	1,1	1,5 + 0,2
3	0,80	1,1	
5	1,00	1,3	
5	0,80	1,3	

in assuming that *the temperature curve from H_γ was right*. Further it seems that our assumption that *the C_n values needed correction* was correct.

Now, these C_n values *do* need corrections, as we used the erronous values from table 41. But it is found here, that the observed values are much greater than the values from table 41 and *a fortiori* than the correct values from table 40. Since the correction factor is known, the true „observed" C_n values may be computed; they are given in table 46.

TABLE 46. „Observed" deviations in the line excitation coefficients of Hα ... Hδ. All C_n values have been multiplied by 10^{16}.

line	C_n (correct)	C_n^1 (table 41)	C_n (observed)	$\frac{C_n(\text{"obs."})}{C_n(\text{theory})}$
H_α	3,43	3,81	33	9,3
H_β	0,951	1,245	4,24	4,4
H_γ	0,493	0,757	0,757	1,5
H_δ	0,340	0,521	0,781	2,3

§ 10. *Model VII of the atmosphere.*

Before starting the interpretation and the discussion of the observed new C_n values, we give in table 47 the new model, which is called *model VII;* it is derived from H_γ and it is supported by Hα, Hβ and Hδ. We do not yet compare it with other models, this is postponed till chapter IX.

TABLE 47. Temperatures in model VII.

τ_0	θ
0,40	0,839
0,50	0,829
0,60	0,819
0,80	0,803
1,00	0,785
1,20	0,769
1,40	0,754
1,60	0,739
1,80	0,728
2,00	0,718
2,20	0,712
2,40	0,704
2,60	0,697
2,80	(0,689)

§ 11. *The line broadening of the strong Balmer lines.*

We have found in table 46 the ratio of the „observed" excitation coefficients in the wings of the lines H_{2-3} .. H_{2-6} and the theoretical values. It is not known whether these ratios are valid in the whole line wing or only in the small part for which they are derived. This can not be deduced from the present observations, which have certainly their limits.

Next we will investigate whether they can be reconciled with the existing theories on the widening of these lines. In particular we want to know whether the line wings must be explained by collisional widening or by statistical Stark widening or by a combination of both possibilities. - A review of the possible mechanisms of line broadening has been given by UNSÖLD[178].

In the case of *collisional widening* LINDHOLM's general theory shows that the intensity profile of an emission line, produced by an optically thin layer is

$$I(\omega) = \frac{\alpha}{\pi} \frac{1}{(\omega - \omega_0 + \beta)^2 + \alpha^2} \qquad \text{(VI,11)}$$

where α and β are constants. Since β = 0 in the case of the Stark effect we find in that case a normal damping profile with a half width $\gamma = 2\alpha$. For $n = 2$ (Stark widening) the theory yields

$$\gamma = \frac{8\pi^5 C^2 N}{\nu} \left(0{,}923 - \ln\eta_m + \frac{\eta_m^2}{24} \ldots\right) \qquad \text{(VI,12)}$$

with $\eta_m = \frac{2\pi^2 C}{\nu \rho_m}$.

The constant C was computed by UNSÖLD for the first four Balmer lines.

N is the number of particles per unit of volume;

v is the velocity of the colliding particle;

ρ_m is the distance of closest approach.

In the case of *statistical widening* the profile may be approximated, if we adopt *one disturbing particle*, by[203]

$$I(\Delta\omega)\,d\omega = \frac{3}{2}\left(\frac{\Delta\omega_0}{\Delta\omega}\right)^{5/2} e^{-\left(\frac{\Delta\omega_0}{\Delta\omega}\right)^{3/2}} \frac{d\omega}{\Delta\omega_0} \qquad \text{(VI,13)}$$

with $\Delta\omega_0 = \frac{2\pi C F_0}{e}$

Of course there must be a continuous transition between both extreme theories but in the approximate theory used by us, we assume a sharp limit between both regions. This limiting wavelength $\Delta\lambda_g$ may be found if we equalize formulae (VI,11) and (VI,13) and solve for $\Delta\omega$. This gives

$$\Delta\omega_g = \frac{v^2}{2\pi^3 C}$$

In this formula v represents the relative velocity of the ions or the electrons (dependent on the particular case which is studied). With UNSÖLD's values for C, we find

$$\Delta\lambda_g = \frac{\lambda^2}{2\pi c}\cdot\frac{v^2}{2\pi^2 C} = 1,19.10^{-6}\,\frac{\lambda^4 v^2}{s\eta} \qquad \text{(VI,14)}$$

The transition wavelengths computed for $T = 5000^0$ are given in table 48 (given by UNSÖLD).

TABLE 48. Limits between the regions of collisional and statistical widening for the Balmer lines at $T = 5000^0$, calculated by UNSÖLD. The values are expressed in Angström units.

n	3	4	5	6
$\Delta\lambda_g$ (ions)	0,12	0,03	0,01	0,007
$\Delta\lambda_g$ (electrons)	110	24	9	6

We now want to represent the observed discrepancies between the observed broadening of the hydrogen lines and the theoretical results and to compare these with the theory, developed in this section.

In figure 18 we have drawn:

a) the excitation coefficient in the line as it ought to be according to the theory of statistical widening by ions only (dotted);

b) the coefficient corresponding with widening by ions *and* electrons (dashed);

c) the coefficient corresponding with collisional widening by ions and by electrons (both fulldrawn).

The open circles represent the result of our reduction, presented in table 46. As the theoretical values of C_n refer to statistical widening by ions only (dotted line), the open circles are plotted higher than that line over the amounts given in table 46.

FIGURE 18

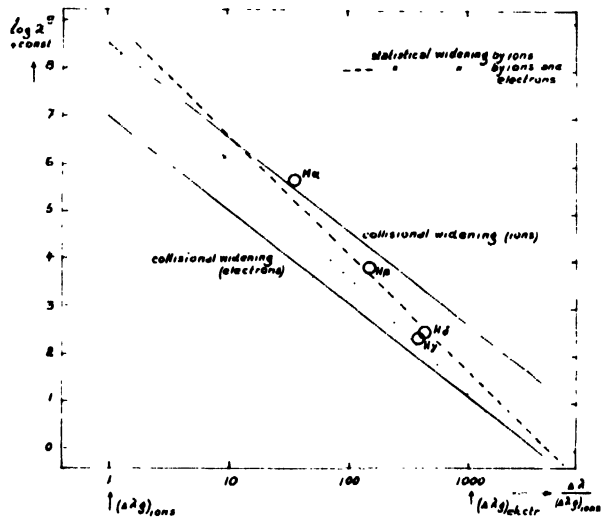

Excitation coefficients in the wings of the hydrogen lines. The wings of the Balmer lines seem to be widened statistically by ions and electrons rather than by ions alone.

From an inspection of figure 18 it seems to be permitted to draw the *preliminary conclusion* that *the lines* H_α ... H_δ *seem to be widened statistically, by ions and electrons, rather than by ions alone.* A verification of this working hypothesis is, however, necessary. This will be done in chapters VIII and X.

§ 12. *Comparison with more exact theoretical studies.*

It is worth while to compare this result with the theoretical results, obtained by SPITZER[161,162] and KROGDAHL[83]. The HOLTSMARK distribution describes only a static configuration of perturbers, neglecting the effect of any relative motion between the perturbing and the perturbed particles. Both SPITZER and KROGDAHL examined in what way the HOLTSMARK distribution is modified by the relative motion of the particles. SPITZER based himself on the mechanism of impact broadening and investigated its influence in the case of moving particles interacting by

means of the Stark effect. For slow collisions and in any case for great distances to the line centre he finds the same results as are already found in the statistical case, but for the central parts of the lines and great velocities he finds the well known impact broadening formula of LORENZ, WEISZKOPF, LENZ and LINDHOLM.
Both SPITZER and KROGDAHL introduced the usual approximations: the relative trajectory of the perturbing particle is a straight line; miss KROGDAHL assumed that for the relative velocity of the perturbing particle the mean value v could be taken while SPITZER assumed a Maxwellian velocity distribution.
The total phase shift, produced by the encounters is calculated by a fairly simple integration; its influence on the form of the HOLTSMARK distribution is examined by integration over all values of ρ (distance of closest approach) and v (this latter is only done by SPITZER).
Their results are given in SPITZER's figure 2 (l.c. pag. 45) and KROGDAHL's figure 2 (l.c. pag. 370). It is obvious that the differences are great. To show this, we compare in one diagram SPITZER's and KROGDAHL's results with our observational results.
Figure 19 shows the line excitation coefficient computed according to SPITZER's and KROGDAHL's results for H_α, $\omega = 1,0$ and $N_e = 5,7.10^{12}$; together with the HOLTSMARK-VERWEIJ curve for statistical widening. We have further plotted our observed excitation coefficients which are higher in the figure than the wing of the statistical curve.
From the examination of the figure we conclude that there exists no agreement between the theoretical results; moreover, none of these agrees with the observations. These results seem to indicate that a complete theory of the widening of the hydrogen lines, including the collosional theory and its transition into the statistical theory in necessary; the present situation is not satisfactory.

FIGURE 19

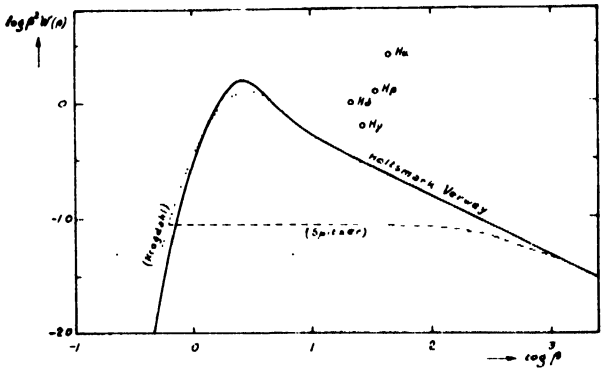

Comparison of the theoretical excitation coefficients in the Balmer lines with our observed values.

CHAPTER VII

INDUCTIVE DETERMINATION OF THE SOURCE FUNCTIONS FOR THE NEAR WINGS AND THE CORES OF $H\alpha$ TO $H\gamma$. OBSERVATIONAL DETERMINATION OF THE TEMPERATURE IN THE OUTER SOLAR LAYERS ($\tau_0 < 0{,}4$).

§ 1. *Introduction.*

In the preceding chapter we have principally dealt with the deep layers and the wings of the lines. In this one we shall investigate the *cores;* they are formed in the highest layers and give information on the temperature distribution near the surface of the sun. In fact, by means of these lines it is possible to investigate layers, which can be studied hardly, or not at all by means the limb darkening of the continuous spectrum.

Our method will be the inductive one: guided by a minimum of theory we shall use only the results of observations. This seems a difficult task: the problem of the line formation is generally thought to be complicated but actually (as it will be shown in chapter VIII) the line profiles may be fairly simply explained; the differences between the source functions and the black body radiation are generally small – not greater than 10%. This will enable us to derive the complementary part of model VII, which model has already been found for layers deeper than $\tau_0 = 0{,}40$.

§ 2. *Determination of the source functions* $S(\tau)$ *for* $H\alpha$ - $H\gamma$.

The radiation emerging at the surface is

$$I(\lambda;\theta) = \int_0^\infty S(\lambda;\tau)\ e^{-\tau\sec\theta}\ \sec\theta\ d\tau \qquad \text{(VII, 1)}$$

Our object is to find $S(\tau)$ directly from the observations *for the lines* $H\alpha \ldots H\gamma$. It may be made plausible that $S(\tau)$ is of the form

$$S(\tau) = a - b.e^{-c\tau} \qquad \text{(VII, 2)}$$

The absorption coefficient in the Balmer lines depends greatly on the temperature, as has already been shown in the preceding chapter. So $S(\tau)$ consists (schematically!) of two parts:

a) a "linear" part where the line excitation coefficient is still negligible as compared with the continuous absorption coefficient;

b) a "constant" part, where $dS/d\tau = 0$.

There is a continuous transition between (*a*) and (*b*), thus making formula (VII, 2) plausible. Naturally, it would still be possible to find other functions with more parameters, which better represent the true situation, but it would be very difficult – with regard to the relative inexactness of the data – to find reliable solutions in that case. The function (VII, 2) is so simple that it never leads to unreasonable source functions.

The solution of (VII, 1) and (VII, 2) is:

$$I(\theta) = a - \frac{b\sec\theta}{c + \sec\theta} \qquad \text{(VII, 3)}$$

The values of a, b and c are found as follows:

1. $I(\lambda;\theta)$ is obtained in c.g.s.-units, multiplying the residual intensities $\frac{I(\lambda;\theta)_{line}}{I(\lambda;\theta)_{cont}}$ given in chapter II with the intensity of the radiation in the continuous spectrum $I(\lambda;\theta)_{cont}$. This latter quantity has already been measured by different authors. These measurements do not refer, however, to exactly the same wavelengths and places on the solar disc for which our profiles are given. Therefore, they have been derived by us in two steps.

By interpolation the relative limb darkening of the continuous radiation of the sun has been derived for the wavelengths of $H\alpha \ldots H\gamma$. After these values have been transformed into absolute values with the aid of the energy wavelength curve for the centre of the disc given by CANAVAGGIA, CHALONGE, EGGER-MOREAU and OZIOL-PELTEY[20]. For the few points near the extreme limb of the sun, the data have been obtained by extrapolation, taking into account the expected temperature variation in the highest parts of the atmosphere, according to model V. (There was no other way of finding these data). Table 49 summarized these values.

2. Secondly $I(\lambda;\theta)_{line}$ is represented by a function of the type (VII, 3). This has been done graphically, plotting $I(\lambda;\theta)$ against $\frac{\sec\theta}{c + \sec\theta}$ for different values of c. It was always possible to find a c-value for which the representation gave a straight line; this value has been chosen. It gives the values of a and b, but a small change in c even within the limits determined by its mean errors, appeared to give

TABLE 49. Values of $I(\lambda;\Theta)$ for the wavelengths of $H\alpha$ ... $H\delta$ (in c.g.s. units x 10^{-14}).

cosΘ	Hα	Hβ	Hγ	Hδ	Hε
1,000	2,92	4,17	4,56	4,60	4,50
0,947	2,86	4,03	4,40	4,40	4,28
0,897	2,79	3,89	4,25	4,24	4,12
0,849	2,72	3,80	4,09	4,08	4,06
0,796	2,65	3,61	3,93	3,92	3,87
0,742	2,58	3,46	3,73	3,68	3,65
0,692	2,50	3,34	3,54	3,49	3,46
0,638	2,40	3,20	3,34	3,26	3,23
0,577	2,32	3,00	3,14	3,02	2,96
0,537	2,25	2,90	2,98	2,86	2,81
0,464	2,14	2,64	2,71	2,58	2,50
0,415	2,05	2,50	2,54	2,40	2,26
0,374	1,95	2,37	2,38	2,24	2,12
0,312	1,83	2,18	2,14	2,00	1,89
0,266	1,72	2,02	1,92	1,80	1,70
0,222	1,54	1,78	1,69	1,61	1,51
0,209	1,50	1,72	1,62	1,53	1,41
0,184	1,45	1,54	1,50	1,42	1,33
0,161	1,40	1,48	1,40	1,30	1,20
0,123	1,32	1,26	1,24	1,11	1,00

relatively great errors in a and b. We have therefore first determined approximate values of c; afterwards all c-values for each line were plotted against $\Delta\lambda$ and a smooth curve was drawn. The ultimate c-values were derived by interpolation from this smooth curve. Next a and b were determined. In table 50 the values of a, $(a-b)$ and both the unsmoothed and the smoothed values of c are given. The differences between both c-values are great in some cases. Nevertheless, with these new, smoothed, c-values, the relation (VII,3) in practically all cases still yielded solutions which were, to within the limits of errors, straight lines.

§ 3. *The region of validity of these source functions.*

The observations of $I(\Theta)$ are given for the interval $0,123 < \cos\Theta < 1,000$. The τ-region, corresponding with this region is found by solving the equation

$$a - b\, e^{-c\tau} = a - b\, \frac{\sec\theta}{c + \sec\theta}$$

for $\cos\theta = 0,123$ and $1,000$ respectively. The solution is given in table 51 for different values of c.

Only inside the intervals, given in the table,

TABLE 50. Values of a, $(a-b)$ and c for the Balmer lines $H\alpha$ ... $H\varepsilon$. a and b are expressed in c.g.s. units x 10^{-14}.

	Δλ	0	0,2	0,4	0,6	0,8	1,0	1,25	1,5	2	3	4
$H\alpha$	c	4,0	3,5	3	2,75	3,5	4,0	2,0	4,0	2,5	2,0	1,75
	c (smooth)	4,0	3,75	3,5	3,4	3,2	3,0	2,85	2,7	2,45	2,0	1,70
	a	0,68	0,81	1,09	1,63	2,05	2,34	2,52	2,65	2,87	3,22	3,51
	a-b	0,01	-0,01	0,16	0,26	0,49	0,64	0,78	0,77	0,72	0,73	0,84
$H\beta$	c	1,0	1,0	1,75	0,3	1,5	1,5	1,0	1,0	1,0	0,75	0,67
	c (smooth)	1,65	1,55	1,45	1,35	1,3	1,2	1,5	1,08	0,95	0,78	0,65
	a	1,13	1,50	2,64	3,69	3,98	4,25	4,69	5,10	5,76	6,85	7,80
	a-b	0,09	0,11	0,30	0,69	0,70	0,80	0,76	0,74	0,75	0,76	0,80
$H\gamma$	c	4,0	2,5	6,0	4,0	3,3	3,0	2,0	2,0	1,8	1,25	1,0
	c (smooth)	5,0	4,4	3,9	3,5	3,1	2,7	2,32	2,0	1,65	1,20	0,9
	a	1,01	1,48	2,30	2,96	3,40	3,75	4,60	4,80	5,48	6,72	7,99
	a-b	-0,20	-0,09	0,19	0,23	0,23	0,31	0,28	0,39	0,41	0,51	0,66
$H\delta$	c	2,5	3,0	2	1,8	1,75	1,5	1,5	2,0	1,6	0,9	1,0
	c (smooth)	2,9	2,6	2,3	2,1	1,9	1,8	1,65	1,52	1,3	1,0	0,75
	a	1,35	1,80	2,88	3,27	3,57	4,47	5,00	5,35	6,05	7,50	8,77
	a-b	0,08	0,25	0,36	0,38	0,59	0,54	0,44	0,48	0,45	0,44	0,69
$H\varepsilon$	c	0,5	2	2	1,3	1,5	1,4	1,0	1,0	0,75	1,0	0,75
	c (smooth)	2,0	1,8	1,68	1,55	1,42	1,3	1,21	1,12	1,0	0,8	0,65
	a	1,72	2,29	3,07	3,57	4,26	4,19	4,94	5,65	6,56	8,44	9,87
	a-b	0,27	0,35	0,79	0,81	0,46	0,47	0,46	0,40	0,37	0,33	0,50

TABLE 51. A. The region of validity of the source functions as a function of c. The table gives the limiting τ-values.

c	0,00	0,25	0,60	1,00	2,00	4,00	6,00
$\cos\theta$ = 0,123	0,123	0,122	0,118	0,114	0,110	0,099	0,090
$\cos\theta$ = 1,000	1,000	0,895	0,782	0,695	0,550	0,404	0,324

B. $S(\tau).10^{-14}$ in H_α for two different expressions.
upper part: solution with polynomial; lower part: solution with exponential.

$\Delta\lambda$ \ τ	0,33	0,5	0,8	1,0
0,2	0,45	0,56	0,72	0,81
0,6	0,97	1,20	1,52	1,72
1,0	1,50	1,71	1,93	2,27
0,2	0,58	0,68	0,77	0,79
0,6	1,19	1,38	1,54	1,59
1,0	1,71	1,96	2,19	2,25

the S functions found with the method, described in this chapter, may be reliable; outside this interval S is based on an extrapolation and loses much of its significance.

But also *in* the regions given in the table the S functions are rather uncertain. This may be illustrated by adopting another mathematical expression for the function $S(\tau)$. As a trial the function

$$S(\tau) = A_0 + A_1\tau + 2A_2\tau^2$$

has been adopted and the parameters A_0, A_1 and A_2 have been derived for three wavelengths inside the line H_{2-3} ($\Delta\lambda$ = 0,2; 0,6 and 1,0 A). After $S(\tau)$ has been computed for some optical depths, both with this function and with the exponential formula (see table 51 B).
It appeared, that for some depths the relative differences are rather great; they range between + 20% and - 8% for τ-values between 0,33 and 1,00. This fact shows clearly how uncertain the observational s-values may be. It is obvious that many conclusions drawn from these data may have only a small value.

§ 4. *The relations between the source functions and the black body radiation.*
In order to be able to find the temperature distribution in the high layers with the aid of the source functions found in this chapter, the relation between the functions $S(\tau)$ and $B(\tau)$ must be known. This relation will be examined in detail in chapter VIII; there it will be shown after numerical calculations that the function

$$\frac{\sigma_\nu + \kappa_\nu + \kappa_\lambda}{\sigma_\nu}(S_\nu(\tau) - B_\lambda(\tau))/B_\lambda(\tau)$$

is not greater than about 0,1; moreover, the greatest values occur near the surface of the sun. Since further $(\sigma_\nu + \kappa_\nu + \kappa_\lambda)/\sigma_\nu$ approaches unity only in the very centre of the lines and grows quickly greater at greater distances from the line centre, it is permitted to assume that the differences between S and B are negligible for all wavelengths in the region of the line except for $\Delta\lambda$ = 0.
Accepting this assumption the temperature will be derived in first approximation.
We shall not use the values for $\Delta\lambda$ = 0, since these may differ by too great an amount from the true values; the data from the other wavelengths will be more reliable.

§ 5. *The relations between the optical depths; model VII.*
The distribution of temperature with depth may be found if the relations between τ and τ_0 are known, because the relation between the temperature and τ is already known. However, the first relation depends on the solar model and on the widening mechanism; so it has to be deduced from the observations. The same problem has already been discussed by CHALONGE and KOURGANOFF[23] and by BARBIER[8] for the continuous radiation of the sun; our way of solving will be the same in principle as theirs.
The relations $S(\tau)$ for the different parts of

the line profile have been plotted on a graph with a logarithmic τ-scale. As it was found, that the different curves have about the same gradients in the region with equal $S(\tau)$ values, it was assumed that in that region $\tau(\lambda_1)/\tau(\lambda_2)$ may be considered as constant. In this way the different curves have been reduced by a horizontal shift to *one mean curve*.
This yields four different $S(\tau^*)$ functions, with $\tau^* = \tau_0 f(\lambda)$, one for each of the lines H_α to H_ε (the line H_ν has not been used). In order to compare these results mutually, the S functions (which have been supposed to be identical with the B functions) are transformed into Θ-functions by PLACKS's law; after that the four curves have each been connected to the temperature curve, already found for model VII in the deep atmosphere. Thus the final temperature curves in the high atmosphere have been derived.

TABLE 52. Θ-values in the high atmosphere.

τ_0	H_α	H_δ	H_γ	H_ε	mean
0,01	1,195	1,168	-	-	1,18
0,02	1,148	1,126	1,134	-	1,136
0,04	1,072	1,074	1,097	-	1,075
0,08	1,014	1,012	1,016	-	1,014
0,15	0,960	0,968	0,956	0,972	0,964
0,20	0,952	0,958	0,926	0,929	0,941
0,30	0,893	0,895	0,865	0,878	0,883

The results have been given in table 52 for the four lines; it is obvious that for some depths fairly great differences occur between the four sets of temperatures. They are probably caused by the method of deriving these results, which method may easily introduce deviations from the true curve. The general aspect of the curves seems, however, to be about the same; so it has been decided to adopt the mean values (table 52, last column) as our *model VII*. In order to have a smooth transition between the parts for the high and the deep layers, the original value of Θ at $\tau_0 = 0,40$ has been slightly modified. We adopt henceforth $\Theta(0,40) = 0,843$ in the place of 0,839. Model VII is given in table 53. The values of *log P* and *log* P_e have been computed according to BARBIER's method in two approximations, with the abundance ratio hydrogen to metals = $10^{3,8}$. Better values, calculated with CLAAS's new value $10^{3,95}$ will be given in chapter IX.

§ 6. *Discussion.*
In this chapter and in the preceding one it has been proved possible to find the distribution of the temperature in the solar atmosphere by using only the profiles of the hydrogen lines.

TABLE 53. Model VII of the atmosphere. Values between brackets are extrapolated. (log P and log P_e have been computed, assuming log A = 3,80).

τ_0	θ	logP	logP_e
0,01	1,180	4,16	-0,12
0,02	1,136	4,32	0,06
0,03	1,098	4,42	0,20
0,04	1,075	4,50	0,31
0,06	1,043	4,60	0,49
0,08	1,020	4,67	0,58
0,10	1,003	4,72	0,68
0,15	0,972	4,82	0,87
0,20	0,941	4,89	1,03
0,30	0,883	4,98	1,29
0,40	0,843	5,01	1,48
0,50	0,829	5,04	1,54
0,60	0,819	5,06	1,61
0,80	0,803	5,12	1,74
1,00	0,785	5,15	1,85
1,20	0,769	5,17	1,96
1,40	0,754	5,19	2,08
1,60	0,739	5,20	2,19
1,80	0,728	5,21	2,28
2,00	0,718	5,22	2,36
2,5	0,700	5,24	2,50
3,0	(0,690)	5,26	2,60
4,0	(0,670)		
5,0	(0,658)		
7,0	(0,644)		
9,0	(0,637)		

The method which has been used is fairly simple both for the deep and the high layers and it looks like it that this method could also be applied, though with somewhat greater difficulty perhaps, to the stars in order to find the models of stellar atmospheres *).
It may be that model VII is not yet entirely reliable since both the part in the deep layers (chapter VI) and the part in the high layers are found in approximative ways. Model VII should be considered as a first approximation; it will now be necessary to calculate the profiles of the Balmer lines with it and – if necessary – to correct the model.
In the following chapters the profiles of the Balmer lines and the intensity of the continuous radiation of the sun will be calculated deductively with model VII; it will be found that no further corrections of the model are necessary and that this first approximation is sufficiently correct.

*) Such an investigation has been started by Mr. NEVEN (Uccle, Belgium) and by the author.

CHAPTER VIII

CALCULATION OF THE PROFILES OF THE BALMER LINES AND OF THE BALMER DISCONTINUITY WITH MODEL VII. A DISCUSSION OF THE "LIMB" TEMPERATURE OF THE SUN. AN ESSAY TO DETERMINE OBSERVATIONALLY THE ELECTRON PRESSURE IN THE SOLAR ATMOSPHERE

§ 1. *Introduction.*

In this chapter the profiles of the Balmer lines will be computed with model VII. An uncertain point in this calculation is the widening of the excitation coefficients of the hydrogen lines. It is clear from chapter VI, that the observations do not confirm the assumption of statistical widening by ions alone; they rather suggest statistical widening by ions *and* electrons, though this statement is not conclusive. Tentatively, the calculations will be made for the latter case.

§ 2. *Excitation coefficients in the cores of the lines.*

The excitation coefficients in the line H_{2-n} are primarily broadened by the Stark effect and are described by

$$\frac{\kappa_n(\alpha)}{\kappa_0} = \frac{\pi e^2}{mc^2}\lambda^2 f.\frac{4.10^{-10},150}{\kappa_0}.\frac{S_n(\alpha)}{F_0} \qquad \text{(VIII,1)}$$

All quantities, occuring in this formula have already been defined earlier. For $S_n(\alpha)$ we take the general form, given numerically in table 39 and figure 14. The use of the more exact curves given in table 38 is not necessary, since the profiles of the central parts of the lines, where the differences between the curves from table 38 and table 39 are important are exclusiverly determined by the Doppler effect:

$$\kappa = \frac{1}{\sqrt{\pi}}.e^{-(\Delta\lambda/\Delta\lambda_D)^2} \qquad \text{(VIII,2)}$$

with

$$\Delta\lambda_D = \frac{\lambda}{c}\sqrt{\frac{2RT}{\mu} + \xi_t^2}$$

μ = the molecular weight = 1,0;
R = the gas constant;

$$\xi_t = \sqrt{2/3}.v_{turb}$$

With a mean turbulent velocity of 1,3 km/sec[143,197, 64,5,34,29] the influence of ξ_t on the value of $\Delta\lambda_D$ is smaller than 1% and can be neglected. The more so as it is possible that the „observed" turbulent velocity does not originate in the highest layers, which layers may be assumed to be in radiative equilibrium, but in deeper layers, where the atmosphere shows convective motions. The observed values might be a mean between these of the two layers[71].

Next the widening of the Stark profile (VIII,1) with the Doppler profile (VIII,2) is described.

The profile obtained after the obliteration is

$$\frac{\kappa_n\left(\frac{\alpha}{s_n}\right)}{\kappa_0} =$$

$$= \frac{\sqrt{\pi}e^2}{mc^2}.\lambda^2 f.\frac{4.10^{-10},150}{\kappa_0\ s_n F_0}\int_{-\infty}^{+\infty} s_n S\left(\frac{\alpha}{s_n}+\frac{\alpha_D}{s_n}v\right)e^{-v^2}\,dv \qquad \text{(VIII,3)}$$

with $\alpha_D = \Delta\lambda_D/F_0$

v is the integration variable.

This integral can only be solved numerically; we shall follow an approximative method:

1. The *exact obliteration* has been carried out *only* for the central parts of the lines ($\alpha/s_n=0$) for twenty different values of α_D/s_n.

The resulting central values are given in table 54.

TABLE 54. Central intensities of the normal Stark profile $s_n\,S(\alpha/s_n)$, obliterated by a Doppler curve with parameter α_D/s_n.

$$\alpha_D = \frac{1}{F_0}\frac{\lambda}{c}\left(\frac{2RT}{\mu}\right)^{1/2}$$

α_D/s_n		α_D/s_n	
0	0,287	1,0	0,237
0,01	0,287	2,0	0,181
0,03	0,287	3,0	0,145
0,05	0,287	5,0	0,102
0,07	0,286	7,0	0,0786
0,10	0,285	10	0,0581
0,20	0,282	20	0,0322
0,30	0,276	30	0,0220
0,50	0,268	50	0,0136
0,70	0,257		

2. In a double logarithmic graph we draw the non-obliterated Stark profile $s_n S(\beta)$.

In this same graph we draw also the non-obliterated Doppler profiles with half widths α_D/s_n and with their tops at the heights given in table 54; cf. figure 20. In the central parts of the curve the Doppler profile is predominant while in the wings the Stark curve is the most important one.

3. In the region of transition the obliteration is performed, *in an approximative way*, by adding up both values. The same method has already been used by PANNEKOEK[124] and by MINNAERT and MULDERS[107] for the description of a profile, widened by Doppler effect and by damping. This method works well and quickly and is sufficiently exact because the slope of the Doppler profile is so steep.
The resulting obliterated profiles are given in figure 20.

FIGURE 20

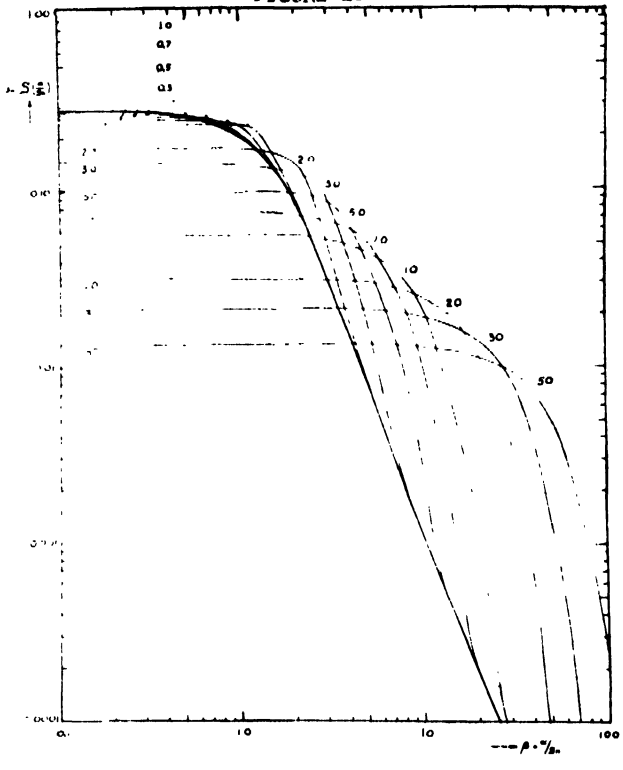

The figure gives the profiles, obtained after obliteration of the Stark function $s_n S(\alpha/s_n)$ with a Doppler curve. Parameter is $\Delta'\lambda_D/s_n F_0$; $\Delta'\lambda_D$ is the half Doppler half-width.

After this obliteration the line excitation coefficients have been calculated for model VII according to formula (VIII, 3) in which the integral parts has been approximated in the way described above. This has been done for the Balmer lines H_{2-3}, H_{2-4}, H_{2-5}, H_{2-6}, H_{2-8}, H_{2-10}, H_{2-11} and H_{2-12}. Since at H_{2-15} the mutual overlapping of the lines is already very important, we have also computed the profile of the whole wavelength region between the centres of H_{2-14} and H_{2-16} and in the same way the value of the Balmer discontinuity. The calculations have been performed for the wavelength distances $\Delta\lambda$ = 0; 0,2; 0,4; 0,6; 1,0; 2; 4; 10 Angström units from the line centre.
After that the optical depths in the lines have been derived by integration, from the line excitation coefficients thus calculated.

§ 3. *The re-emission mechanism in the lines.*
Before we are able to use these optical depths for determining the profiles of the Balmer lines, the re-emission mechanism must be known.
The differential equation:

$$\cos\theta \frac{dI}{d\tau} = I - \frac{\sigma_\nu}{\kappa_\lambda+\kappa_\nu+\sigma_\nu}\int I \frac{d\omega}{4\pi} - \frac{\kappa_\lambda+\kappa_\nu}{\kappa_\lambda+\kappa_\nu+\sigma_\nu} B \qquad \text{(VIII, 4)}$$

suffices generally for the description of the radiative transfer and the line formation in the greatest part of the solar atmosphere. In this equation EDDINGTON[41] introduced κ next to σ, to account for the influence of collisions of the second kind in the re-emission. Still later, PANNEKOEK[124] showed that collisions do not play an important part in the solar atmosphere and that consequently the lines are mainly formed by scattering. Recently, however, GIOVANELLI[54], basing himself on new calculations on the collisional cross-sections, again advocated the importance of collisions, even in the high chromosphere. But GIOVANELLI's calculations are made for a chromospheric model with a constant kinetic temperature of 25000°, even in the low chromosphere. Now, – because of the high excitation potentials of the hydrogen levens – collisional excitation becomes highly improbable, as can be shown by a brief calculation, when the temperature falls to 10000° so that in our solar model the influence of collisions is negligible. *In this case all hydrogen lines would be pure scattering lines.*

But an important way is left by which the exchange between line excitation energy and thermic energy may occur. In every atomic level scheme the electrons do not simply jump to and fro between two atomic levels, but they may follow complicated ways and cyclical quantum jumps may occur. If the solar atmosphere is in thermodynamic equilibrium, we are dealing with the case of detailed balancing and the cyclical transitions which may exist have no influence on the radiation transfer. However, in a diluted radiation field, which exists e.g. near the surface of the sun, transition cycles involving a small number of upward transitions are favoured as compared with the opposite cycles involving a greater number of upward transitions (ROSSELAND, 1926[150]). If the continuous state is involved in the cycle, this causes a transfer of thermic energy towards the wave-

length of the line considered. This increases the emission in the core of the line and as this emission has the radiative properties of the thermic radiation of the solar matter, this process of fluorescence may formally be described by the adoption of a non-zero value of κ_ν/σ_ν in formula (VIII,4). This was shown for the first time by STRÖMGREN[165], who considered a simplified case in which the atomic level scheme consists only of a ground level, an excited level k and the continuous state; fluorescence coupling with other states that the continuous state being neglected. The transfer of energy depends on the ratio between (a) the number of spontaneous transitions from the level k to the ground state and (b) the sum of the transitions from k to the ground state by collisions of the second kind and from k upward to the continuous state by photo-ionisation.
Then, according to STRÖMGREN:

$$\frac{\sigma_\nu}{\kappa_\nu} = \frac{a_{k1}}{c_{k1} + C_{kf}} \qquad \text{(VIII, 5)}$$

with a_{k1} = total number of spontaneous transitions from k to 1;
c_{k1} = number of transitions from k to 1, due to collisions of the second kind;
C_{kf} = number of photo-ionisations;
1 refers to the ground state;
k refers to the excited state;
f refers to the continuous state.

Since collisions play no part, formula (VIII, 5) reduces to

$$\sigma_\nu/\kappa_\nu = a_{k1}/C_{kf} \qquad \text{(VIII, 6)}$$

This formula, deduced for the simplified case discussed by STRÖMGREN, is extended without theoretical difficulties to the more general case of many discrete levels, following considerations of UNSÖLD[176] and PANNEKOEK[125]. We replace STRÖMGREN's a_{k1} by a more generalized quantity, which involves also the transitions to other lower levels, while at the same time C_{kf} is generalized so that it involves the higher levels. But this latter must be done in a special way. Consider figure 21; an atomic level scheme is considered in which the third atomic level is excited from the second. Transitions are possible in four different directions, characterized by suffices a to d. The process a can be identified with true absorption; for d we use the term scattering. For b and c absorption may be said to occur, only if after these steps a photo-ionisation follows. If immediately after these steps the electron returns to the second level, we are certain to deal with scattering. UNSÖLD[176] made the acceptable proposal that re-excitation of high atomic levels, like b should be considered mainly as "absorption".
An exact solution of the problem has not yet been given; neither is it given here, as the

FIGURE 21

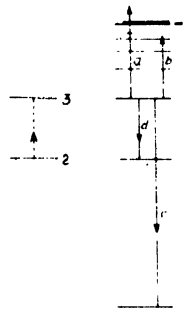

approximate solution is sufficient for us. We shall consider two extreme possibilities.
We assume, as was done also by STRÖMGREN, the validity of the equilibrium equations of BOLTZMANN and SAHA. We further put $S(\tau) = B(\tau)$; this approximation is *for the present purpose* - the computation of a value for κ_ν/σ_ν - fully permissible.
First assumption: The ratio κ_ν/σ_ν is equal to the ratio between (a) the total number of all transitions from the n^{th} excited level to the levels with $n > 20$ and (b) the total number of all other transitions. It is clear that this is a lower limit, since the transitions to levels with $n \geq 20$, which are subsequently "absorbed" (e.g. by photo-ionisation) have been considered here as "scattering". It may safely be assumed that the transitions to $n > 20$ are to be ranged under the head "absorption", the merging of these states into the continuum being practically complete.
Second assumption: All transitions, other than $n \rightarrow 2$ are considered as absorption, only $n \rightarrow 2$ is called scattering. This is the upper limit for κ_ν/σ_ν.

The results of the calculations according to these two assumptions are given in table 55. It is clear that the differences between the upper and the lower limit are not very great and that the lines may all in good approximation be considered as formed by "*scattering*". In the following calculations, however, account will be taken of the small contribution of "absorption"; we shall take the *mean* of the upper and the lower limit for κ_ν/σ_ν.

UNSÖLD has computed this same ratio[177] and has found for H_α a value, somewhat greater than our values (6% - 8%). It seems that this difference is due to the approximations introduced by UNSÖLD is his calculations and - partly - to the fact that in our computations also the lowest level has been taken into account.

TABLE 55. Ratio $(\kappa/\sigma)_\nu$ for the Balmer lines in the solar atmosphere (*in percents*).

	n = 3	4	5	6	7	8	9	10	11	12	13
UPPER LIMIT											
0,581	5,6	14,1	10,6	6,9	4,6	3,1	2,4	1,6	1,5	1,3	1,3
0,716	4,2	12,9	9,8	6,6	4,4	3,0	2,3	1,5	1,1	0,9	0,7
0,900	2,9	11,6	9,2	6,2	4,2	2,9	2,2	1,4	1,1	0,8	0,6
1,019	2,2	10,8	8,7	6,0	4,0	2,8	2,1	1,4	1,1	0,8	0,6
LOWER LIMIT											
0,581	1,0	0,9	0,6	0,4	0,3	0,2	0,2	0,1	0,1		
0,716	0,6	0,7	0,6	0,4	0,2	0,2	0,1	0,1	0,1		
0,900	0,3	0,5	0,4	0,3	0,2	0,1	0,1	0,1			
1,019	0,2	0,4	0,3	0,3	0,2	0,1	0,1	0,1			

These results are derived for the case of thermodynamic equilibrium and for $S = B$, but they will in good approximation also be correct if these conditions are not wholly fulfilled, as is e.g. the case in the low chromosphere.

We finally want to notice, that a more refined discussion of the fluorescence problem is also possible, as was done by WOOLLEY[193], who considered for the lines H_{2-3} and H_{2-4} the three possible transition cycles between the levels $n = 1$, 2 and 3 and the continuous state, taking into account the *multiplet splitting* of the second and the third levels. He calculated the ratio α of downward to upward transitions between the levels 2 and 3, respectively 2 and 4. With a dilution factor $W = 1/3$ and $T = 6500^{\circ}$, $\alpha = 1,03$ for H_{2-3} and 1,17 for H_{2-4}; these results lead to lower limits for the central intensities of the two lines which might be of the right order of magnitude; but precise values were not yet computed, however. Quantitatively, his results are not correct since a dilution of radiation was used much too great to be right. So the minimum central intensities, computed with WOOLLEY's method will still be smaller than the values, already found. Though it is difficult to estimate the influence of the multiplet splitting on the values of κ_ν/σ_ν translated into STRÖMGREN's nomenclature, this influence does not seem to be very important.

§ 4. *The influence of redistribution on the re-emission coefficients.*

The possibility that non-coherent scattering might be important for the formation of Fraunhofer lines has been pur forward for the first time by EDDINGTON[42]. In later years several theoretical treatments of the problem have been published[160,198,199,158,85] but observational evidence has been given for the first time by HOUTGAST[63].

Criticisms of HOUTGAST's treatment was published afterwards by UNSÖLD[178] who drew attention to the important influence of the *model* of the solar atmosphere on the profiles of Fraunhofer lines and who suggested that HOUTGAST's observations might be explained partly or wholly by another atmospheric model (HOUTGAST used the linear approximations for B).

Another criticism has been published still later by SUEMOTO[169] who doubted whether redistribution has any observable influence on the wings of the lines, because the effect is only important in the cores and in the outer layers of the atmosphere. But apart from all doubts as to the interpretation of the observations the theoretical evidence for redistribution is very strong, especially after the investigation of SPITZER[163], who showed that there is hardly any reason why scattered quanta should *not* be redistributed.

In the case of the hydrogen lines an atomic substate may be excited at a moment, when a perturbing ion is close to the atom. Then the absorbed energy will differ from the energy which would be absorbed if the lines were not split. But at the time, that the atomic state is de-excited, the perturbing ion may have gone far away and the re-emitted energy will be about equal to the energy difference between the levels in the non-disturbed case. So the re-emitted frequency generally differs from the exciting frequency. The excess energy contributed to, or has been taken from the kinetic energy of the surrounding matter. The completeness of the distribution depends on the ratio between the time of the disturbance ($\approx 10^{-13}$sec) and the life time of the excited state, this being generally of the order of 10^{-11} to 10^{-8} sec. Hence *the distribution is complete* in these layers of the solar atmosphere where the Stark

effect is the predominant cause of the line widening, that means: in the levels with $\tau_0 \gtrsim 0{,}05$ and at wavelength distances greater than 0,3 A from the centre of the lines.

In the higher levels, Doppler broadening is the main cause of the widening; this case has been discussed by HENYEY[59]. He showed that in the Doppler *wings* the scattering may approximately be assumed to be for two thirds redistributed and for one third non-distributed; in the Doppler *cores* the excitation energy will be completely redistributed. Since for the Doppler broadening of the Balmer lines we are only concerned with the most central parts of the lines - see figure 20 - it may be permitted to assume complete redistribution in the whole line profile.

There is a strong analogy between redistribution and fluorescence. The mechanisms of cyclical quantum jumps and of redistribution may both occur everywhere in the solar atmosphere, but both mechanisms have only influence on the emergent radiation in a diluted radiation field and manifest themselves in the form of non-compensated cycles (cf. figure 22); they cause a transfer of energy from the continuous state towards the wavelengths with greater excitation coefficients. In a diluted radiation field a transition like (a) in figure 22 occurs more often than a transition like (b); the transition (α) occurs more often than the transition (β). A difference between fluorescence and redistribution is that in the latter case the small energy shifts within each energy level are caused either by radiation or - as in our case of the hydrogen lines - by collisions, whereas in the case of fluorescence we are dealing with transitions between discrete atomic levels with great energy differences; the transitions being always caused by radiation. Fluorescence is a macro-effect and redistribution is a micro-effect. In the case of fluorescence the detailed structure of the atomic levels is not considered; kinetic energy is transferred to the line as a whole. In the case of redistribution we are also dealing primarily with a transfer of energy from the continuous state towards the atomic level, but in this case it is practically only the cores of the lines which receive extra energy. The statement that redistribution may be described as a transfer of radiation from the line wings to the line centre is not correct for the hydrogen lines, from this point of view.

FIGURE 22

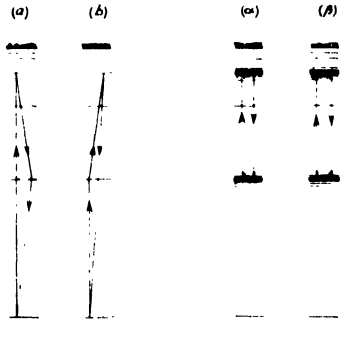

Cyclical quantum jumps on a macro-scale may cause fluorescence; those on a micro-scale may cause redistribution. Both effects occur only in a diluted radiation field.

Final remark: "Dilution of radiation" has always to be interpreted in a formal way. Not always does $S \neq B$ also mean that $S < B$. If $S > B$, which may occur e.g. in the chromosphere, the effects of fluorescence and redistribution cause an extra depression of the line centres.

§ 5. *The source functions in the wavelengths of the Balmer lines.*

In the equation of transfer both the effects of scattering with redistribution and absorption have to be included. HOUTGAST[62] already wrote down the equation of transfer for the case of scattering with complete redistribution. His formula (32) was, with some minor alterations taken over by MÜNCH[119]. In our case, with scattering *and* absorption, the equation for the transfer of radiation becomes

$$\cos\theta \frac{dI_\nu(\tau,\theta)}{d\tau} = I_\nu(\tau) - \frac{\sigma_\nu}{\sigma_\nu+\kappa_\nu+\kappa_\lambda}\overline{\int J_\nu \frac{d\omega}{4\pi}} - \frac{\kappa_\nu+\kappa_\lambda}{\sigma_\nu+\kappa_\nu+\kappa_\lambda} B_\lambda(\tau) \qquad \text{(VIII,7)}$$

In this equation the mean value $\overline{\int I_\nu \frac{d\omega}{4\pi}} = \overline{J_\lambda}$ must be taken according to HOUTGAST as follows:

$$\overline{J_\lambda} = \frac{\int J_\nu \sigma_\nu d\nu}{\int \sigma_\nu d\nu}; \quad J_\nu = \int I_\nu \frac{d\omega}{4\pi}$$

We now introduce into (VIII,7) the source function $S_\nu(\tau)$:

$$S_\nu(\tau) = \frac{\sigma_\nu}{\sigma_\nu+\kappa_\nu+\kappa_\lambda}\overline{J_\lambda(\tau)} - \frac{\kappa_\nu+\kappa_\lambda}{\sigma_\nu+\kappa_\nu+\kappa_\lambda} B_\lambda(\tau) \qquad \text{(VIII,8)}$$

Since

$$J(\tau) = \tfrac{1}{2}\int_0^\infty S(x)\, K(|\tau-x|)\, dx,$$

formula (VIII,8) becomes:

$$\frac{\sigma_\nu+\kappa_\nu+\kappa_\lambda}{\sigma_\nu}\,(S_\nu(\tau) - B_\lambda(\tau)) =$$

$$= \tfrac{1}{2}\int_0^\infty S_\nu(x)\; K(|\tau-x|)\; dx - B_\lambda(\tau) \qquad \text{(VIII,9)}$$

Solution. The equation (VIII,9) will be solved in successive approximations. We first put, neglecting the suffices $_\nu$ and $_\lambda$:

$$S_1(\tau) = B(\tau)$$

The n^{th} approximation for $S(\tau)$ is found by

$$\frac{\sigma_\nu+\kappa_\nu+\kappa_\lambda}{\sigma_\nu}\,(S_n - B)(\tau) =$$

$$= \tfrac{1}{2}\int_0^\infty S_{n-1}(x)\; K(|\tau-x|)\; dx - B(\tau) \qquad \text{(VIII,10)}$$

Obviously it is necessary to compute for each line the function $\int_0^\infty S\; K(|\tau-x|)\,dx$, which is only a function of depth; not of ν.
In the successive approximations, according to (VIII,9) the integration has been performed with GAUSS method with six terms; this has been done for the lines H_{2-3}, H_{2-4}, H_{2-5} and H_{2-6} and for the depths τ_0 = 0,01; 0,03; 0,10 and 0,30.

TABLE 56. Values of $(S - B)$ calculated in third approximation for $H\alpha$ ... $H\delta$, assuming complete redistribution. (c.g.s. units x 10^{-14}).

τ_0	0,01	0,03	0,10	0,30
$H\alpha$	-0,07	-0,06	-	-
$H\beta$	-0,06	-0,07	-0,08	-
$H\gamma$	-0,06	-0,07	-0,12	-0,01
$H\delta$	-0,06	-0,06	-0,10	-0,05

The values of $\int_0^\infty S_n\; K(|\tau-x|)\,dx$ have been calculated for $\Delta\lambda$ = 0,0; 0,2 and 0,6; after that the mean values were taken over this wavelength interval. The resulting values of $S_3 - B$, found after three succesive approximations are tabulated in table 56 (expressed in c.g.s. units).
As for H_{2-3} at the limb of the sun the value of B is about $1,3.10^{14}$, we conclude that compared with the case of pure absorption thr maximum correction for redistribution, to be applied to B is for H_{2-3} of the order of 6% at τ_0 = 0,01; it is for H_{2-6} of the order of 10% at $\tau_0 \geq 0,10$. The correction is therefore of some importanc in the high layers; it has no influence at all on the wings of the lines, for $\Delta\lambda$ > 0,6 A.

§ 6. *Computed profiles of the Balmer lines.* The profiles of the Balmer lines were computed in the same way as described already earlier. The profiles have been derived for the wavelength distances, given in § 2 of this chapter and for cos θ = 1,000; 0,755; 0,484 and 0,142. In table 57 and figure 23 the resulting profiles of the lines H_{2-3} ... H_{2-6} are given and compared with the observations.

TABLE 57. Profiles of H_{2-3} ....H_{2-6}, calculated with model VII. All residual intensities are multiplied by 1000.

$\Delta\lambda$	cos θ = 1,000	0,755	0,484	0,142
0,0	211	216	238	363
0,2	258	267	283	468
0,4	407	431	470	617
0,6	589	615	662	871
$H\alpha$				
1,0	698	727	774	942
2,0	826	857	898	976
4,0	910	934	964	996
10,0	973	985	992	1000
0,0	198	203	220	318
0,2	262	284	326	502
0,4	478	508	562	818
0,6	597	635	696	904
$H\beta$				
1,0	690	735	802	952
2,0	802	841	899	985
4,0	906	930	961	996
10,0	979	986	993	1000
0,0	201	213	235	329
0,2	266	286	329	534
0,4	470	504	561	814
0,6	570	613	684	901
$H\gamma$				
1,0	665	717	799	959
2,0	797	837	898	988
4,0	893	916	951	997
10,0	980	986	994	1000
0,0	254	265	292	423
0,2	304	326	264	591
0,4	406	501	564	817
0,6	555	602	680	908
$H\delta$				
1,0	657	712	798	962
2,0	787	829	893	986
4,0	901	926	960	998
10,0	978	984	992	1000

FIGURE 23

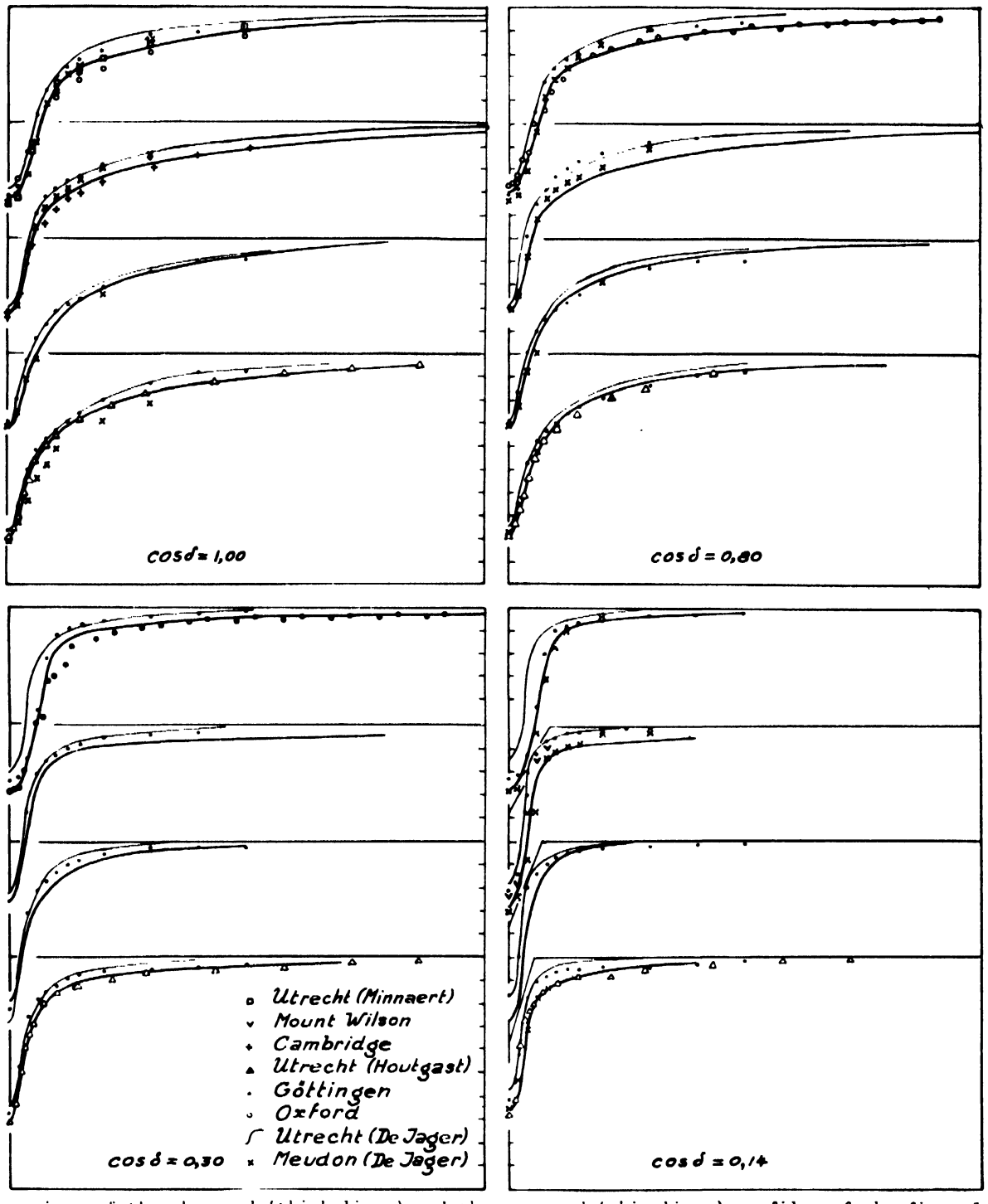

Comparison of the observed (thick lines) and the computed (thin lines) profiles of the first four Balmer lines. The computed intensities are all greater than our observed values, though the differences are in most cases not so great that the calculations disagree with the other observations. The systematic differences near the sun's limb and in H_α might indicate a slightly lower limb temperature than is defined by model VII.

Discussion. The agreement between the observed and the computed profiles is generally satisfactory. In practically all cases the calculated profiles do not deviate more from the observed ones than is permitted by the scatter of the observed points. The only exceptions are: (*a*) H_{2-3} at the limb of the sun, which profile is not in agreement with the observations; and (*b*) the central intensities of the other lines at the limb, which are all too high by some percents.

Summarizing, we conclude that *the profiles of Hα - Hδ calculated with model VII, assuming statistical widening by ions and electrons and scattering with complete redistribution as the main process, practically all agree with the observations.*

The small remaining differences will be discussed in § 7.

§ 7. *A further correction to the limb temperature?*

The calculated limb values differ systematically from *our* observations, though, for the greater part they are within the area occupied by the dots of all observers together. We tentatively neglect the observations of the other observers and investigate whether the differences between the calculations and our observations may be interpreted as due to an erroneous model of the outer atmosphere. This is done in an approximate way as follows.

a. Determination of the quotients.

$$\frac{I(\Delta\lambda;\cos\theta)_{obs}}{I(\Delta\lambda;\cos\theta)_{calc}}$$

b. Tranformation of these quotients into $\Delta\Theta$-values with the aid of PLANCK's law.

TABLE 58. Tentative temperature correction to model VII in the high atmosphere of the sun.

		$\overline{\tau_0}$				$\Delta\Theta$			
	cos θ →	1,000	0,755	0,484	0,142	1,000	0,755	0,484	0,142
H_α	Δλ = 0,0	0,015	0,011	0,009	0,004	0,019	0,006	0,011	0,049
	0,2	0,02	0,02	0,015	0,01	0,022	0,012	0,015	0,034
	0,4	0,07	0,07	0,06	0,03	0,039	0,028	0,014	0,058
	0,6	0,16	0,14	0,13	0,10	0,030	0,026	0,027	0,045
	1,0	0,24	0,22	0,20	0,11	0,005	0,032	0,001	0,010
H_β	0,0	0,05	0,04	0,04	0,02	0,004	0,010	0,017	0,037
	0,2	0,09	0,08	0,07	0,04	0,003	0,018	0,023	0,045
	0,4	0,22	0,21	0,18	0,10	0,008	0,009	0,023	0,046
	0,6	0,32	0,29	0,24	0,12	0,000	0,003	0,012	0,017
	1,0	0,41	0,38	0,31	0,13	0,000	0,004	0,012	0,012
H_γ	0,0	0,07	0,06	0,06	0,03	0,002	0,008	-0,001	0,019
	0,2	0,12	0,11	0,10	0,06	-0,002	-0,002	0,000	0,034
	0,4	0,23	0,21	0,19	0,10	0,009	0,004	0,004	0,017
	0,6	0,30	0,28	0,24	0,12	0,005	0,002	0,002	0,009
	1,0	0,40	0,36	0,31	0,13	0,001	0,002	0,001	0,007
H_δ	0,0	0,11	0,11	0,09	0,05	0,006	0,016	0,002	0,017
	0,2	0,15	0,13	0,12	0,09	-0,002	0,004	-0,005	0,017
	0,4	0,27	0,25	0,22	0,11	0,001	0,003	-0,003	0,015
	0,6	0,34	0,32	0,28	0,13	-0,003	-0,001	-0.002	0,009
	1,0	0,46	0,42	0,38	0,14	-0,002	0,000	0,000	0,009

c. Determination of the mean optical depth $\overline{\tau_0}$, corresponding with the emergent radiations $I(\Delta\lambda;\cos\theta)$. First step: determination of $\overline{\tau_{\nu+\lambda}}$ with the formula

$$\overline{\tau_{\nu+\lambda}} = \frac{\int_0^\infty \tau\, S(\tau)\, e^{-\tau \sec\theta} \sec\theta\, d\tau}{\int_0^\infty S(\tau)\, e^{-\tau \sec\theta} \sec\theta\, d\tau}$$

Second step: Determination of the corresponding values of $\overline{\tau_0}$.

The values of $\Delta\Theta$ and of $\overline{\tau_0}$ are given in table 58 and in figure 24. This shows:

1. In regions deeper than $\tau_0 = 0{,}30$ the temperatures from model VII are very probably correct.
2. In higher region there is a small but clear indication that a negative temperature correc-

FIGURE 24

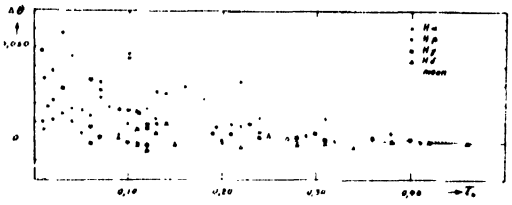

Tentative temperature correction in the highest layers of the solar atmosphere.

tion is necessary; this correction is slightly greater than the mean error, with which it has been determined.

At $\tau_0 = 0,20$ it is $\Delta(\omega) = + 0,008$: $\Delta T = - 40^0$
$\tau_0 = 0,10$ $\Delta(\omega) = + 0,014$: $\Delta T = - 70^0$
$\tau_0 = 0,01$ $\Delta(\omega) = + 0,026$: $\Delta T = - 90^0$

With the corrected model of the sun the limb temperature would be 4180^0.

Though it is tempting to apply this correction, we shall keep to model VII, since it will be shown in the following chapter that the limb observations of the *continuous radiation* suggest a positive temperature correction in the layers above $\tau_0 = 0,15$. As long as this discrepancy is not solved, model VII will be considered as a good intermediary between the models, valid for the description of the hydrogen lines and those which describe the continuous radiation.

§ 8. *The profiles of the high Balmer lines* H_{2-8} ... H_{2-12}.

The computed profiles are given in table 59. It is to be noted that these profiles have been calculated without correction for complete redistribution. This makes the cores of the lines *too bright*. (As compared with "absorption" the cores of the lines, computed with redistribution are darker in this case).

This is clearly visible in figure 25. There,

TABLE 59. Calculated residual intensities in the high Balmer lines H_{2-8}; H_{2-10}; H_{2-11} and H_{2-12}. All residual intensities are multiplied by a factor 1000.

$\Delta\lambda$ \ cos θ		1,000	0,755	0,484	0,142	1,000	0,755	0,484	0,142	
H_{2-8}	0,0	(0,401)	(0,418)	(0,447)	(0,587)	(0,551)	(0,581)	(0,635)	(0,780)	H_{2-10}
	0,2	(0,422)	(0,443)	(0,479)	(0,628)	(0,559)	(0,590)	(0,650)	(0,816)	
	0,4	0,502	0,539	0,601	0,704	0,589	0,626	0,694	0,871	
	0,6	0,560	0,604	0,676	0,759	0,626	0,666	0,740	0,919	
	1,0	0,631	0,675	0,747	0,827	0,674	0,714	0,788	0,958	
	2,0	0,776	0,814	0,877	0,984	0,795	0,828	0,885	0,985	
	4,0	0,895	0,918	0,952	0,996	0,903	0,925	0,957	0,996	
	10,0	0,980	0,986	0,993	1,000	0,987	0,992	0,997	1,000	
H_{2-11}	0,0	(0,618)	(0,646)	(0,704)	(0,835)	(0,683)	(0,705)	(0,756)	(0,887)	H_{2-12}
	0,2	(0,618)	(0,646)	(0,704)	(0,835)					
	0,4	0,641	0,673	0,741	0,914					
	0,6	0,663	0,696	0,764	0,924	0,712	0,738	0,796	0,958	
	1,0	0,704	0,737	0,802	0,962	0,750	0,779	0,840	0,976	
	2,0	0,797	0,826	0,880	0,986	0,822	0,846	0,893	0,986	
	4,0	0,891	0,912	0,945	0,966	0,902	0,920	0,951	0,998	
	10,0	0,961	0,970	0,984	1,000	0,961	0,970	0,984	1,000	

the computed profiles are given together with the observed ones, interpolated from tables 10 to 13 (chapter II).

The comparison of the observations with the calculations shows that the agreement is satisfactory in the central parts of the disc, if the great uncertainty of the observed profiles is taken into account. The line H_{2-10}, which is extremely difficult to observe in the solar spectrum, shows deviations.

The calculated cores of the lines are generally too bright, which may be caused by the neglect of the influence of redistribution. We may estimare the magnitude of this correction by comparing it with that for the line H_{2-8}. There the correction is for $\Delta\lambda = 0,0$:

at cos θ = 1,000 : 6,9%
0,755 : 8,3%
0,484 : 11,0%
0,142 : 22,9%

The fact that the ultra violet Balmer lines are

FIGURE 25

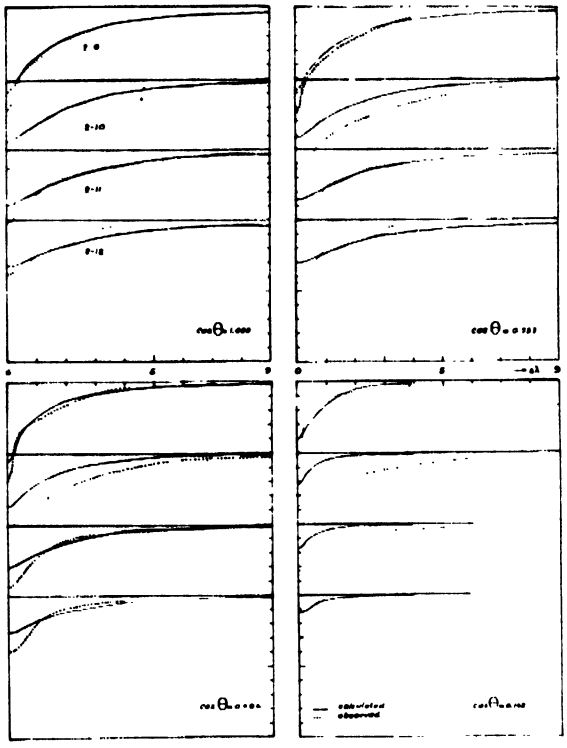

Comparison of the computed and the observed profiles of the Balmer lines H_{2-8}, H_{2-10}, H_{2-11} and H_{2-12}. The agreement is very good for H_{2-8} and is still fairly good for the other lines, excepting H_{2-10}, which line is, however, very strongly blended in the solar spectrum and thus is difficult to observe. Differences occur also near the sun's limb and in the cores of the lines. These latter may be due to the neglected influence of redistribution.

FIGURE 26

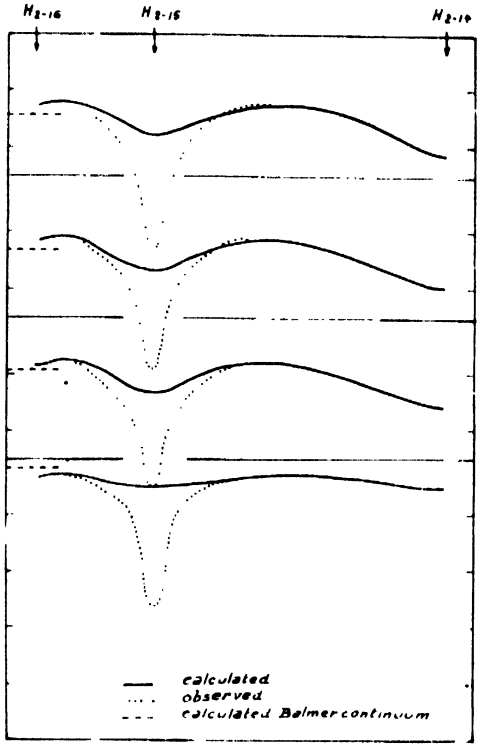

Observed and computed intensity profiles in the solar spectrum between H_{2-14} and H_{2-16}. The profiles are drawn with respect to a fictive continuous spectrum which would exist if the Balmer lines would not occur in the solar spectrum. One unit of the scale of ordinates is 0,1 times the intensity of this continuum. The four curves are valid for respectively cos θ = 1,00; 0,755; 0,484 and 0,142.

formed deeper in the atmosphere than H_{2-8} will probably make the corrections for these lines smaller than for H_{2-8}.

Hence, the application of this correction would indeed greatly reduce the remaining differences between observations and calculations. We did *not* calculate this correction, because the calculations are fairly complicated and because the observations are uncertain, especially in the cores of the lines.

§ 9. *The lines H_{2-14}, H_{2-15} and H_{2-16} and the Balmer discontinuity.*

Near the Balmer discontinuity the blending of the lines becomes important. This is already the case in the region of H_{2-15}. In order to study this effect in detail, we have calculated the profile of the whole region between the centres of H_{2-14} and H_{2-16}, taking into account the lines from H_{2-13} to H_{2-17}. The other Balmer lines have no influence on this region of the spectrum. The resulting profile is tabulated for four cos θ-values in table 60 and in figure 26. In these table and figure we have also given the value of the Balmer discontinuity, calculated as the ratio between the continuous spectra at 3647^+ and 3647^- A, neglecting the influence of the Balmer lines.

The comparison of the observations with the calculations shows that the differences are great. It is certain, that they cannot be reduced materially by the addition of the influence of redistribution, because these lines are formed too deep in the solar atmosphere. The core of H_{2-15} is formed at optical depths, ranging between $\tau_0 = 2,7$ (centre of disc) and 0,9 (cos θ = 0,14); at these depths the influence of redistribution is negligible.

It is more probable that a great part of the differences may be explained as observational errors, since this part of the spectrum can only be observed with great uncertainty. The influence of the crowded Fraunhofer lines on these broad, shallow lines is certainly very

TABLE 60. Calculated profile of the spectrum between the wavelengths 3721,94 A (centre of H_{2-14}) and 3703,86 A (centre of H_{2-16}). All values are expressed in the intensity of the continuous spectrum which would be observed if the Balmer lines did not exist. The $\Delta\lambda$-values are chosen with respect to the centre of H_{2-15}.

$\Delta\lambda$		cos θ =	1,000	0,755	0,484	0,142
- 4,0	centre of H_{2-16}		871	888	920	969
- 1,0			833	846	880	956
0,0	centre of H_{2-15}		818	831	863	950
+ 1,0			835	850	882	956
+ 4,0			871	888	920	969
+10,0	centre of H_{2-14}		784	800	840	946
	Balmer Jump		855	870	904	983

important but it is difficult to estimate its magnitude.

We finally turn to the discussion of the Balmer discontinuity (table 61). It gives (*a*) the Balmer jump for different values of cosθ, as derived from the observations of CHALONGE *et al.*[21,20]; (*b*) the computed values of the Balmer jump and finally (*c*) the mean optical depths τ_0. There seems to be agreement near the sun's limb but in the centre of the disc the differences amount to a factor 2 (figure 27).
In order to solve this discrepancy we want to investigate in how far it may be attributed to errors in the adopted electron pressures. The influence of the electron pressure on the continuous Balmer absorption is not negligible; we may use the following approximate formula:

$$\Delta D = -13,56\,\Delta\omega - \Delta \log P_e$$

(This formula represents the influence of variations of temperature and electron pressure on the continuous Balmer absorption coefficient κ_λ we assume that it applies also to ΔD).
Since we may assume that the temperature distribution in the solar atmosphere is well known,

FIGURE 27

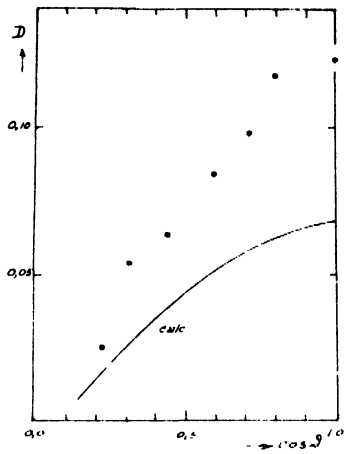

A comparison of the observed and the computed values of the Balmer jump in the solar spectrum. The differences between both in the central part of the disc might be explained by other values of the electron pressure in the deep layers.

we have not to consider a temperature correction; thus:

$$\Delta D = -\Delta \log P_e$$

TABLE 61. Observed and calculated values of the Balmer jump; $D = \log I_{3647^+} - \log I_{3647^-}$
The "computed" values are derived by interpolation.
Corrections to be applied to the electron pressures of model VII.

cos θ	1,00	0,80	0,71	0,60	0,44	0,31	0,22
D_{obs}	0,123	0,118	0,098	0,084	0,064	0,054	0,025
D_{calc}	0,068	0,063	0,059	0,052	0,040	0,028	0,018
τ_0	2,80	2,40	2,20	1,98	1,58	1,24	1,03
$\Delta \log P_e$	-0,055	-0,055	-0,039	-0,032	-0,024	-0,026	-0,007
$\log P_e$ "obs"	2,50	2,42	2,38	2,33	2,14	1,95	1,85

This yields the corrections to log P_e, listed in the fifth row of table 61; the corrected values of log P_e are given in the last row (corresponding to the τ_0-values given in the fourth row). We note, that these corrections are fairly small and have no sensible influence on the calculated line profiles.

In this way it is possible to derive observationally the values of the electron pressure in the solar atmosphere from the observatuons. In the following chapter (IX) log P_e will be computed theoretically; the result will be compared with the data found here.

CHAPTER IX

VERIFICATION OF MODEL VII BASED ON THE CONTINUOUS RADIATION OF THE SUN. THE OBSERVATIONAL DATA ON THE CONTINUOUS ABSORPTION COEFFICIENT. COMPARISON WITH OTHER MODELS OF THE SOLAR ATMOSPHERE. THE RADIATIVE AND AERODYNAMIC PROPERTIES OF MODEL VII

§ 1. *Introduction.*
In this chapter the distribution of the continuous radiation over λ and cos θ will be computed with model VII. It will be shown that there is agreement in a great wavelength region; differences in the far infrared spectrum indicate that in that wavelength region CHANDRASEKHAR and BREEN's absorption coefficients are probably not correct.
The pressure and the electron pressure are calculated for different values of the helium abundance, but the comparison with the "observed" P_e values is not conclusive; hence UNSÖLD's abundance ($N_H/N_{He} = 5$) will be maintained.
A comparison with other atmospheric models is given.
Finally some of the radiative and aerodynamic properties of the sun are discussed.

§ 2. *The energy-wavelength curve for the centre of the disc.*
The $I(\lambda)$-curve was calculated by numerical integration for the wavelength region between 0,4μ and 2,3μ. In table 62 and in figure 28 the results are given and compared with the observed energy-wavelength curve of PEYTURAUX[131], who has shown that the earlier curve, derived by ABBOT[1,2] and corrected by MULDERS[118] is probably not completely correct. Cf. also NICOLET[122]. Figure 28 shows agreement; the differences are never greater than 3 to 5% between 0,4 and 2,2μ. These differences may be understood if we consider the relative difficulty of the establishment of a reliable observational $I(\lambda)$-curve. If we further mention the very great differences between the observations and the energy-wavelength curve calculated with previous models, we conclude, that the present results are satisfactory (cf. figure 12).

§ 3. *The centre-to-limb variations at 5000 A.*
We compute the limb darkening for the wavelength 0,5μ; this wavelength is supposed representative for the region between 0,4 and 0,6μ, in that sense that an agreement found between theory and observations for that wavelength makes agreement in the whole region probable.

TABLE 62. Computed energy-wavelength curve between 0,4 and 2,3μ.

λ(μ)	I (c.g.s. 10^{-14})
0,405	4,454
0,456	4,241
0,500	3,962
0,569	3,471
0,759	2,132
0,911	1,500
1,013	1,224
1,139	0,903
1,302	0,665
1,459⁻	0,479
1,459⁺	0,483
1,519	0,438
1,823	0,247
2,278	0,108

FIGURE 28

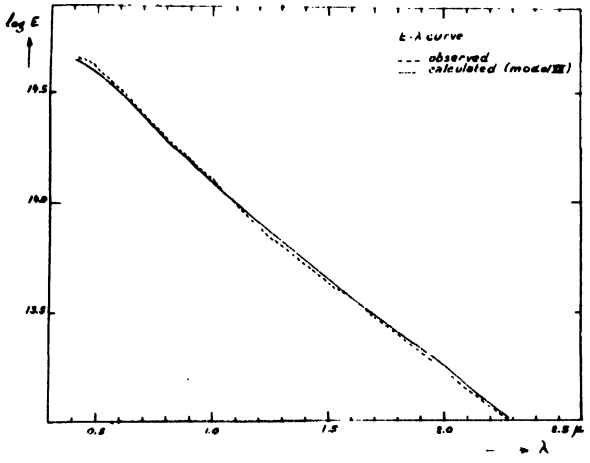

Energy-wavelength curve of the sun between 4000 and 23000 A, observed (Peyturaux) and computed (model VII).

In order to compare our results with the observational data, presented in figure 10 of chapter V, we compute $I(0,5\mu;\cos\theta)$ both for models III and VII. Then $\Delta I = I_{VIII} - I_{III}$ and $\Delta I/I_{III}$

is determined (See table 63). These data are plotted in figure 29, where the values of $\Delta I/I$ from figure 10 are also given.

TABLE 63. Computed limb darkening at 5000 A (model VII), compared with the limb darkening, according to model III. The comparison between model III and the *observed* values is given in figure 10.

sin θ	cos θ	I_{VII} (.10^{-14})	I_{III} (.10^{-14})	$\frac{\Delta I}{I_{III}}$ (%)
0,00	1,00	3,962	4,407	10,1
0,30	0,954	3,871	4,277	9,5
0,50	0,867	3,704	4,044	8,4
0,60	0,800	3,559	3,844	8,0
0,70	0,710	3,354	3,569	6,0
0,80	0,600	3,068	3,203	4,2
0,90	0,426	2,592	2,654	2,3
0,95	0,313	2,225	2,274	2,2
0,96	0,280	2,041	2,131	4,2
0,97	0,244	1,896	2,007	5,4
0,98	0,200	1,701	1,852	8,1
0,985	0,175	1,579	1,739	9,2
0,99	0,140	1,391	1,628	14,6
0,995	0,092	1,110	1,446	23,2

FIGURE 29

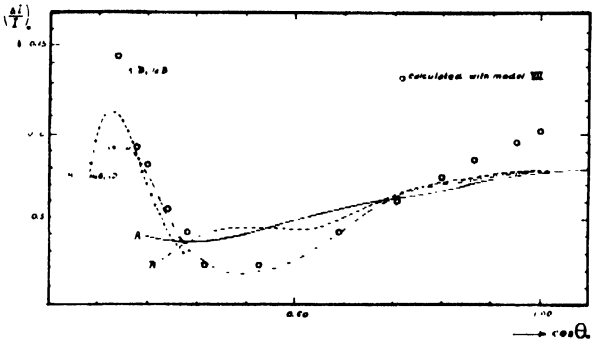

Comparison of the observed limb darkening of the sun with the limb darkening, computed from model VII (open circles); λ = 5000 A.
The "observed" curves are the same as those, given in figure 10.

Discussion. Agreement is found in the mean region of the curve, mainly for $0,15 < \cos\theta < 0,85$. In the central part of the disc a deviation of $\Delta I/I \approx 2\%$ is found; this is the difference between the observed and the computed energy-wavelength curves at 5000 A. (cf. figure 28).
A change in the temperature, which would make agreement at 5000 A, changes at the same time the energy-wavelength curve in the whole region, which certainly would increase the differences in the other part of the spectrum. Hence it seems better not to apply temperature corrections to the deep layers.

We secondly investigate the high regions of the atmosphere. Figure 29 shows, that the observations of the limb darkening of the continuous spectrum, made by MINNAERT, Van den HOVEN van GENDEREN and Van DIGGELEN[110] deviate from the computations at small values of $\cos\theta$; according to the extrapolated observations the limb temperature would be higher than the values derived from model VII. This fact disagrees with the results found in chapter VIII, section 7. The solution of this problem seems not yet clear.

§ 4. *The centre-to-limb variations between 0,7 and 10,2μ and the observational data on the continuous absorption coefficient.*

The data of this section are for a great part reproduced from the paper by NEVEN and De JAGER[12]. In that paper, the limb darkening of the sun was derived from model VII between the wavelengths 0,7μ and 10,2μ. Since it was found, that the calculated limb darkening agrees with the observed values between the limits of error, indicated by the scatter of the points (see figure 30), it has been concluded that model VII as well as the continuous absorption coefficients, computed by CHANDRASEKHAR and BREEN[25] are correct within the limits of error. In any case, the scatter of the points belonging to different sets of limb darkening observations (ABBOT[1,2], PEYTURAUX[132], PIERCE, McMATH, GOLDBERG and MOHLER[137]) is so great, that it is at present not yet possible to detect errors in the calculated values of the continuous absorption coefficient in the region between 0,7 and 2,2μ. Cf. figure 30. Deviations, occuring between the observed and the calculated limb darkening for $\lambda > 2,2$, may be interpreted as due to errors in the adopted continuous absorption coefficients. An unknown absorbing constituent seems to exist, the influence of which should be added to that of H^-.
The ratio between the "observed" and the theoretical absorption coefficients was roughly calculated to be: 1,2 at 3,5μ; 1,7 at 8,3μ and 1,6 at 10,2μ. (cf. figure 31).
PEYRURAUX has recently published a model giving for two wavelengths in the far infrared region (8,3 and 10,2μ) a better agreement between the computed and the observed limb darkening than is predicted by our model VII. This would reduce the factors given above (cf. [207]).
This agreement is obtained, however, by reducing the temperature gradient in the highest layers of the atmosphere; this yields a limb temperature of about 4500°. This temperature seems *too high*, however, to explain the central parts of the hydrogen lines and of the other Fraunhofer lines.
It seems preferable, to keep the low limb temperature of the sun and to accept provisionally

FIGURE 30

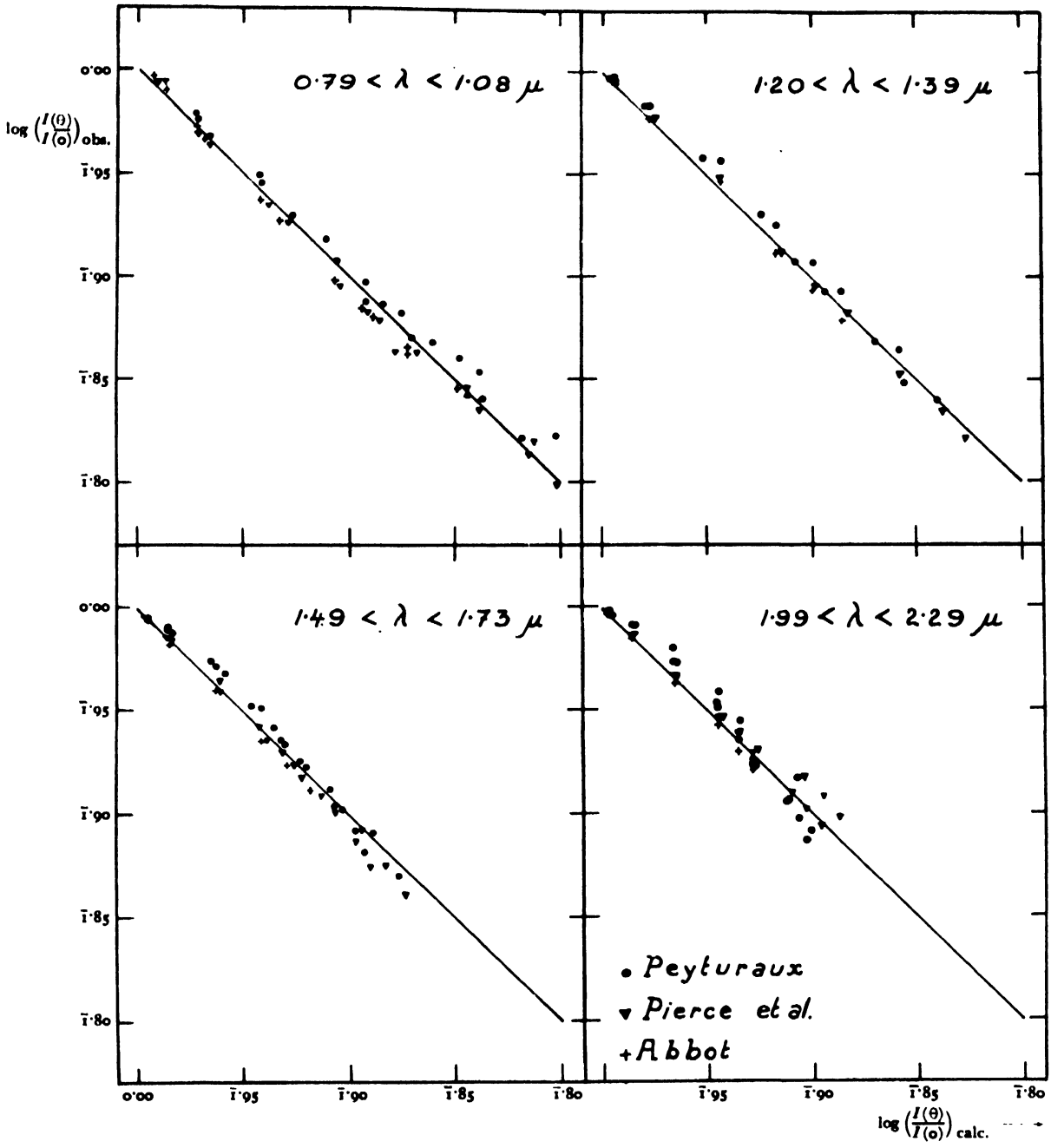

Comparison of the observed and the calculated values of the relative limb darkening in the near infrared region (logarithmic scales). Full-drawn is the 45° line.

FIGURE 31

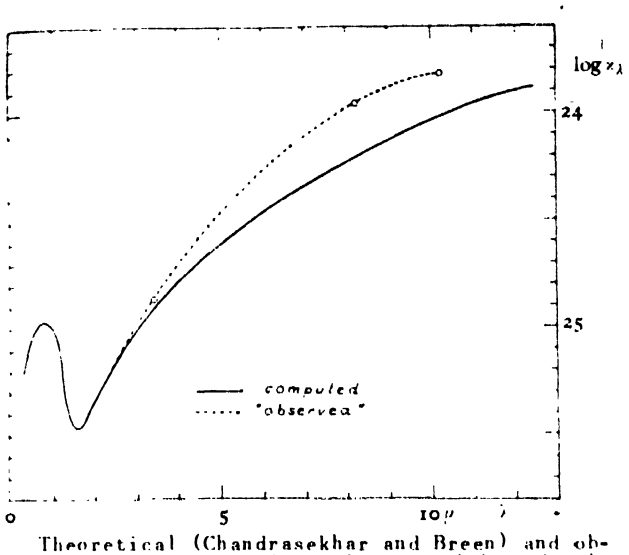

Theoretical (Chandrasekhar and Breen) and observed continuous absorption coefficient in the infrared; $\omega = 1,0$.

the difference in the far infrared, the more so, as PEYTURAUX himself did not succeed in making these differences completely disappear.

§ 5. *The distribution of pressure and electron pressure in the atmosphere and the abundance of helium.*

The electron pressure and the gas pressure, hitherto adopted for model VII had been derived by assuming an abundance of hydrogen to metals log A = 3,8. For the abundance ratio hydrogen: helium (B), log B = 0,7 has been adopted, following UNSÖLD[179], who found from the spectrum of an eruptive protuberance that log B = 0,7 ± 0,5. Although still poor, this is the first direct determination of the abundance of He in the solar atmosphere.

Recently, CLAAS[29] has published a new determination of the abundances in the solar atmosphere, giving log A = 3,95. Hence, the pressure and the electron pressure in the atmosphere have been computed once more, assuming

a) log A = 3,95

b) log B = 0,4; 0,7 and 1,0 respectively.

The different assumptions under b) have been made in order to investigate whether it is possible to determine the abundance of helium in the solar atmosphere with the aid of the "observed" electron pressures (table 61). The calculations have been made with BARBIER's method, in three approximations, using the values of table 53 as a first approximation. The results are given in table 64. Evidently the helium abundance has no great influence on the electron pressure and it is clear that it is not possible to decide between the three abundances on the basis of the data from table 61; hence we shall keep to log B = 0,7, which is UNSÖLD's value.

§ 6. *Comparison of model VII with other observational models of the solar atmosphere.*

In figure 32 the following models are compared: (*a*) BARBIER[8]; (*b*) De JAGER[68] (= model III); (*c*) VOIGT[184]; (*d*) Ten BRUGGENCATE, GOLLNOW and JÄGER[15]; (*e*) model V and (*f*) model VII.

Model (*a*) has been derived from the limb darkening of the continuous spectrum. Models (*b*), (*c*) and (*d*), derived in different ways are all corrections of BARBIER's original model and are hence, not independent. As, however, our model III is not wholly correct, since it fails to explain the energy-wavelength curve of the sun (cf. chapter V), the same applies probably to models (*a*), (*c*) and (*d*). It would be very interesting to compare e.g. VOIGT's result with another model, such as model VII or V.

Hence it seems, that there are at present no reliable observational models, to compare our models V and VII with (the model of PLASKETT[139, 140] developed from the limb darkening of the continuous radiation at 5500 A yields a temperature curve which is much too high to be correct).

Recently, PEYTURAUX[207] derived a new model of the solar atmosphere, using his limb darkening observations in the infrared part of the spectrum. Since he does not give a relation between I and τ, a comparison is difficult. The comparison will be performed in § 7.

From a discussion of the limb darkening and the energy-wavelength curve of the sun in the wavelength region between 0,5 and 2,2μ PIERCE and ALLER[138] determined the "limb temperature" of the sun. No temperature function is derived. It is not certain whether their limb temperature is correct: in discussions of this kind, the limb temperature is always rather uncertain, since its determination is always based entirely on an extrapolation of the limb darkening observations (see figure 1 of the quoted paper). The error, made in reductions of this kind is often underestimated. The limb temperature should be determined more directly: either by using the cores of strong Fraunhofer lines or by direct limb photometry during eclipses.

§ 7. *Comparison of model VII with theoretical models and with PEYTURAUX's model.*

A complete theoretical model should give the variation of temperature and pressure in the solar atmosphere, taking at the same time into account the existence of a zone in radiative equilibrium, the existence of a convection zone and the influence of the selective absorption

TABLE 64. Values of gas pressure and electron pressure in the solar atmosphere, computed with the temperature distribution of model VII with log A = 3,95, after CLAAS and with log B = 0,40; 0,70 and 1,00 respectively.
The results given here, are found after three approximations (method of BARBIER).

		log B = 0,4		log B = 0,7		log B = 1,0		
τ_0	Θ_{VII}	log P_e	log P	log P_e	log P	log P_e	log P	h (logB=0,7)
0,01	1,180	- 0,20	4.25	- 0,21	4,17	- 0,23	4,11	100 km
0,02	1,136	+ 0,06	4,40	+ 0,04	4,32	+ 0,03	4,27	131
0,03	1,098	0,20	4,49	0,19	4,41	0,17	4,36	150
0,04	1,075	0,29	4,56	0,28	4,48	0,26	4,42	165
0,06	1,043	0,43	4,65	0,41	4,57	0,40	4,52	185
0,08	1,020	0,52	4,72	0,51	4,64	0,49	4,58	201
0,10	1,003	0,59	4,77	0,58	4,69	0,56	4,64	213
0,15	0,972	0,72	4,87	0,71	4,79	0,69	4,73	237
0,20	0,941	0,83	4,94	0,82	4,86	0,80	4,80	254
0,30	0,883	1,06	5,03	1,05	4,95	1,03	4,90	277
0,40	0,843	1,30	5,09	1,28	5,01	1,27	4,96	293
0,50	0,829	1,42	5,13	1,41	5,05	1,39	5,00	304
0,60	0,819	1,50	5,16	1,48	5,07	1,47	5,03	310
0,80	0,803	1,62	5,21	1,61	5,12	1,59	5,07	327
1,00	0,785	1,78	5,24	1,76	5,16	1,75	5,11	336
1,20	0,769	1,90	5,27	1,89	5,19	1,87	5,13	345
1,40	0,754	2,01	5,29	2,00	5,21	1,98	5,15	351
1,60	0,739	2,13	5,30	2,11	5,22	2,10	5,17	254
1,80	0,728	2,20	5,32	2,19	5,24	2,18	5,18	360
2,00	0,718	2,28	5,33	2,27	5,25	2,25	5,19	363
2,50	0,700	2,42	5,35	2,41	5,27	2,39	5,21	370
3,00	0,690	2,49	5,37	2,48	5,29	2,46	5,23	377
4,00	0,670	2,69	5,39	2,68	5,31	2,65	5,26	387
5,00	0,658	2,80	5,41	2,79	5,33	2,77	5,28	396
7,00	0,644	2,95	5,44	2,94	5,36	2,92	5,31	407
9,00	0,637	3,02	5,47	3,00	5,39	2,99	5,33	418

in the Fraunhofer lines on the model. No existing model fulfils all demands. The best models, at present available, are probably those of MICHARD[102] and LABS[86] (zero order approximation). A correction for the influence of the selective absorption by the Fraunhofer lines has been applied to MICHARD's model by PECKER[130]. His treatment has, however, been criticized by LABS[86] and MINNAERT[111]: PECKER's neglect of the resonnance lines and of the variation of collisional widening with depth seems not justified.

LABS has given a further approximation to his model for the influence of Fraunhofer lines; but though his limb temperature seems correct, his modified temperature in the deeper layers seems not sufficiently well established because his iteration converges too slowly.

Moreover, these models have been calculated without taking into account the existence of a convection zone. Hence, it is expected that deviations between the theoretical models and the observational one will in the first place occur in the deepest layers (granulation zone) and in the highest layers (region of the blanketing effect).

As the theoretical models are given in the form of a $T(P)$ relation and not of a relation between T and τ_λ, we compare in figure 33 the $T(P)$ relations for the theoretical models and for our model. Besides, PEYTURAUX's observational model, which is only given in the form of a relation between T and P is also inserted in the figure.

FIGURE 32

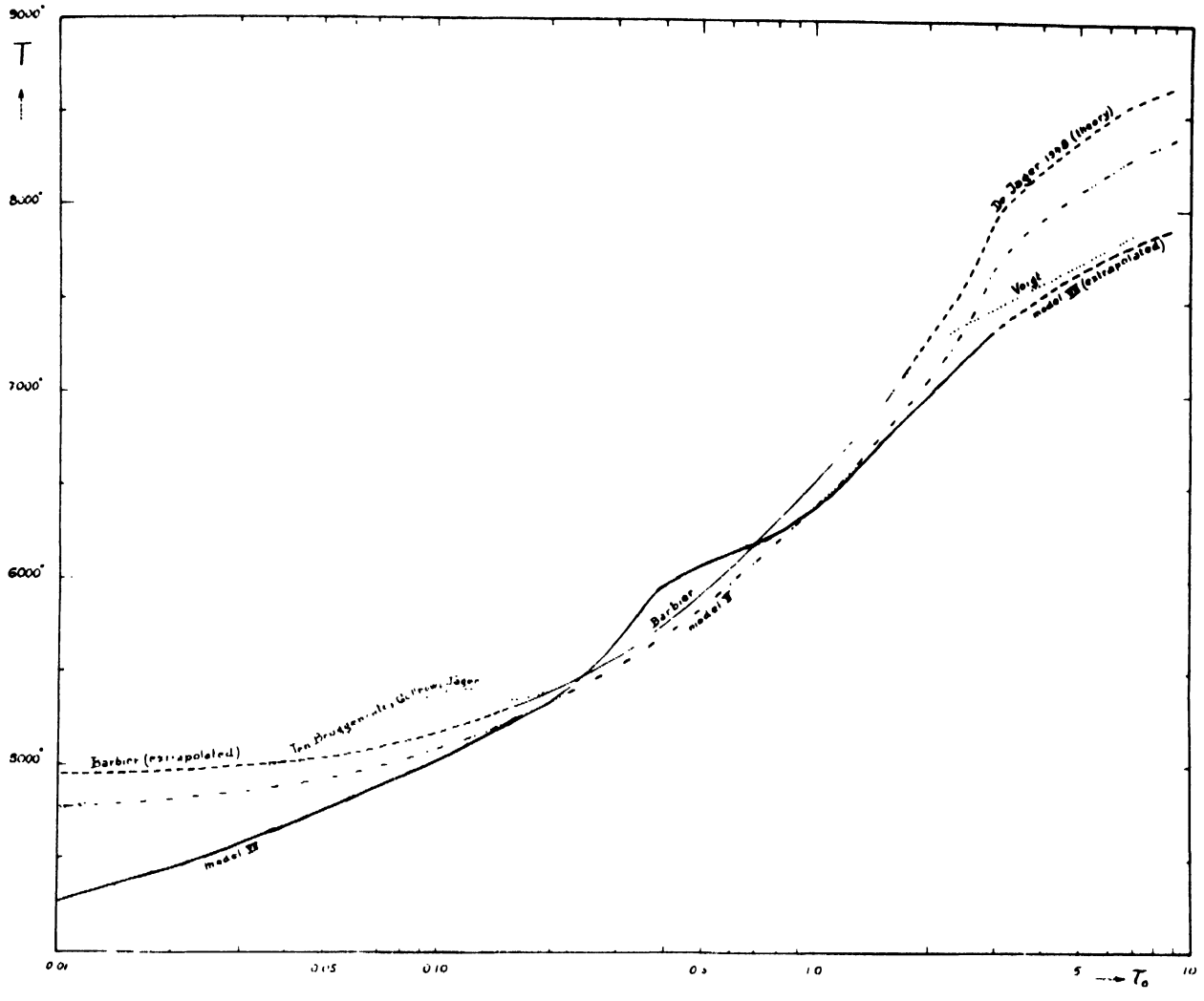

Comparison of observational models of the solar atmosphere.

The original relation, given by MICHARD has been calculated for a solar atmosphere without helium (R = 0). To make all curves comparable, MICHARD's relation has to be changed. The influence of an addition of He is to increase the pressure, corresponding with a certain T-value in the ratio 1,46. This may be shown as follows. In an atmosphere without helium (cf. BARBIER[8]):

$$p^2 = \frac{2gm_H}{\kappa_0} \int_0^{\tau_0} \frac{d\tau_0}{\varphi(T)P_e/P}$$

If helium is added, with R = 5, then the constant before the integral sign changes into

$$1{,}8\ \frac{2gm_H}{\kappa_0}$$

Moreover, the values of P_e/P all decrease in the ratio

$$\frac{N_H + N_e}{N_H + N_{He} + N_e} \approx \frac{N_H}{N_H + N_{He}} = 0{,}83.$$

Hence, P^2 increases by a factor $\frac{1{,}8}{0{,}83} = 2{,}16$ and P by a factor 1,46.

The best agreement between the theoretical models and our model occurs in the main part of

FIGURE 33

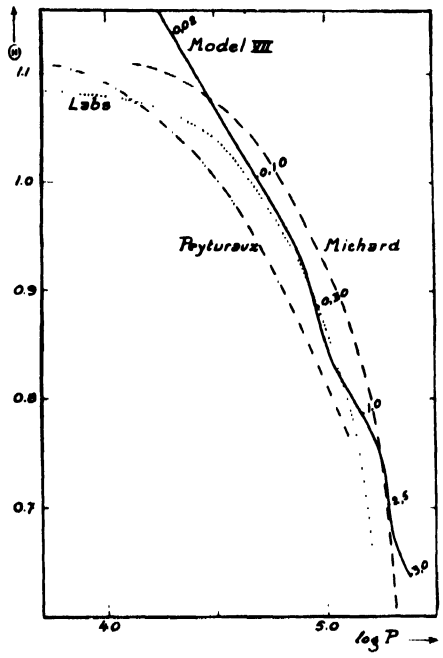

Comparison of the $(\omega; \log P)$ relations for the *theoretical* models of Michard and Labs and the *observational* models of Peyturaux and De Jager. The numbers denote τ_0-values.

the atmosphere; in the high and the deep layers our "observed" temperatures are lower than the computed ones; this agrees with our predictions: it is the granulation zone and the blanketing zone, which manifest themselves.
We now turn to PEYTURAUX's model[207]: there the temperatures are higher than for the other three models; this disagreement is not easy to understand since it should predict too high a value for the energy-wavelength curve. His agreement with the theoretical curves near the sun's surface means in fact that the surface temperature of his model is about 4500°, which seems to be too high.

§ 8. *The convection region in the solar atmosphere.*
If the temperature and the pressure in the atmosphere are known, it is possible to find the boundaries of the convection zone if existing. Practically always, K. SCHWARZSCHILD's relation

$$\left(\frac{d \log T}{d \log P}\right)_{adiab} = \left(\frac{d \log T}{d \log P}\right)_{rad} \qquad (IX,1)$$

is used; the boundary of the convection zone is at the level where the relation (IX,1) is fulfilled. However, SCHWARZSCHILD's relation is not entirely correct, since it is only valid in an atmosphere *without* radiation. In the course of an investigation on the solar granulation zone, WOOLLEY has developed another relation, which hitherto has practically been neglected. Cf.[194,68]. He showed that for a mixture of gas and radiation, formula (IX,1) should be replaced by

$$\left|\frac{dT}{d\tau}\right|_{rad} = \left|\frac{dT}{d\tau}\right|_{adiab} \qquad (IX,2)$$

This relation reduces to SCHWARZSCHILD's in the absence of radiation. In other cases it diverges from (IX,1).

The boundary of the convection zone has been determined for model VII, using WOOLLEY's condition (IX,2); the upper boundary is found to be at about $\tau_0 = 2,4$. In the higher regions no convection seems to occur.
This limit of the granulation zone lies rather deeper than WALDMEIER's observational limit of $\tau_0 = 1,6$[185]. However, this latter quantity has been obtained by visual observations and is not very exact. Moreover, if the upper limit of the convection zone lies at $\tau_0 = 2,4$, then the higher layers are still not uniformly heated by the lower lying levels. *Convection* may end at 2,4 but the temperature differences due to unequal heating must be detectable even in the highest layers.
The problem of the influence of the convection zone on the higher layers has in a general way been treated by RUDKJÖBING[152], but it has never been discussed in detail in the way, indicated above (See also work of Mrs PECKER[208] and of CAYREL[209]).

§ 9. *Aerodynamics of the high atmosphere.*
In this section we discuss in a preliminary way some provisional results of our spectroheliographic observations at Meudon. The detailed results and a more thorough investigation will be postponed to a later date.

Flocculi manifect themselves as big irregular structures with a mean linear dimension of the order of 20 000 - 50 000 km. Their general character is the same in H_α, H_β, H_γ and H_δ; but in the core of H_α the character changes and a transition from the big structure to a smaller, more granular structure is obvious. In the following we distinguish between the flocculi and the "granular" flocculi. The dimensions of the first are about 30 000 km to 70 000 km; the latter range between 5000 and 10 000 km.
In table 65 the mean intensity variations between dark and bright patches is given. It is possible to use these data to determine the mean depths of that part of the atmosphere, where the flocculi occur. In principle, if on

TABLE 65. Preliminary values of the mean intensity differences between dark and light patches in the hydrogen flocculi. The exposures show hardly any centre-to-limb variations in the relative intensities except for H_γ ($\Delta\lambda$ = 0,4 and 0,6 A) and $H\delta$ ($\Delta\lambda$ = 0,4 and 0,6 A), where no flocculi seem to be visible near the limb of the sun.

$\Delta\lambda$	0,0	0,2	0,4	0,6	0,8	1,0
$H\alpha$	0,04*	0,02*	0,06	0,05		0,02
$H\beta$	0,03	0,03	0,025	0,02	0,02	
$H\gamma$	0,02	0,04	(0,01)	(0,01)		
$H\delta$	0,025	0,02	(0,01)	(0,01)		

*) Small (granular) flocculi.

a spectroheliogram a dark patch is observed, it may have been caused by an abnormally cold region at any possible depth in the atmosphere. But as the study of the spectroheliograms shows that in proceeding from the cores to the far wings of a line, a certain flocculus appears and disappears at well defined wavelengths, the flocculi must exist between certain rather sharply defined limits of depth in the atmosphere. These depths may be found, the mean optical depth being known from where the light, emitted at certain wavelengths originates. Cf. table 66.

TABLE 66. Computed mean optical and geometrical depths for various wavelengths distances in the cores of the Balmer lines, see also table 65.

$\Delta\lambda$(A)	0,0	0,2	0,4	0,6	0,8	1,0
$H\alpha$	0,009	0,012	0,021	0,06	0,17	0,20
$H\beta$	0,016	0,025	0,064	0,20	0,25	
$H\gamma$	0,043	0,07	0,20	0,25		
$H\delta$	0,07	0,18	0,23			
$H\alpha$	-200 *	+ 110	135	193	250	261
$H\beta$	+115	145	198	261	275	
$H\gamma$	176	200	261	275		
$H\delta$	200	255	266			

*) Upper limit of depth.

This table shows the important result that the big flocculi only exist between τ_0 = 0,01 and 0,25 or 0,30, corresponding with depths of 100 and 275 km below the surface of the sun, much deeper than has generally been assumed. It is satisfactory to note that the lower limit is nearly identical for all hydrogen lines.

It is difficult to say whether the flocculi have something to do with the convection zone, which possibly may occur – according to UNSÖLD[181] – above τ = 0,3. This question is strongly connected to the whole problem of the origin of the flocculi; a critical theoretical discussion seems necessary to establish such a connection, if existing. However, it is remarkable that the "hump", observed by us in the temperature distribution, occurs nearly exactly at the same height as the lowest limit of the region of the flocculi.

The granular flocculi occur at greater heights; probably from τ_0 = 0,01, a hundred km under the surface of the sun, up to higher levels. Since nothing is visible of the big flocculi if photographed with the most central part of H_α, one should conclude that the big flocculi are flat structures with a linear horizontal dimension of about 40 000 km and a thickness, not greater than 300 km. Such a structure might seem unreasonable *a priori* but analogous structures are known; an altostratus, covering a great part of Holland would have the same relative dimensions.

New and interesting view-points manifest themselves if the *life time* of the flocculi is considered. A rough determination shows that the life time of the big flocculi is of the order of some 12 to 24 hours. The hypothesis, that these structures have something to do with the dissipation of energy of the noise waves, considered by BIERMANN and SCHATZMAN, must therefore be rejected, as the velocity of sound in these layers is so great that the flocculi would then have a life time of ten to twenty minutes only *).

We are inclined to consider them as the basic structures of very small filaments (following UNSÖLD).
The life time of the granular flocculi has been found to be fairly small – it is of the order of some fifteen minutes. It may be possible that these are related both to the dissipation of the noise waves in the high chromosphere and to the base of the chromospheric spicules. It would be highly interesting to study the observed differences in intensity in the spicules and in the granular flocculi with regard to the temperature and the aerodynamics of the chromosphere.

*) Personal communication by Dr Schatzman.

CHAPTER X

ESSAY ON AN INDUCTIVE DETERMINATION OF THE WIDENING FUNCTIONS FOR THE LINES $H_\alpha \ldots H_\gamma$

§ 1. *Introduction.*
In principle it is possible to find the excitation coefficients in the lines, since the variation of the ergiebigkeit with depth is known (cf. chapter VII). For a certain geometrical depth, the relation holds:

$$\frac{(dS/d\tau)_{\lambda=\lambda_1}}{(dS/d\tau)_{\lambda=\lambda_2}} = \frac{(\sigma_\nu+\kappa_\nu+\kappa_\lambda)_{\lambda_2}}{(\sigma_\nu+\kappa_\nu+\kappa_\lambda)_{\lambda_1}} \qquad (X,1)$$

If we suppose that $S = B$, the first part of (X,1) is known and hence the second part also. It has already been illustrated in chapter VIII that this assumption is valid for the greatest part of the atmosphere. The application of (X,1) will enable us to find the excitation coefficients in the strong hydrogen lines inductively; the results will be compared with theoretical values.

§ 2. *Relative values of the excitation coefficients in the Balmer lines.*
Since $B(\tau) = a - be^{-c\tau}$
as was supposed in the equation (VII,2),

$$\frac{dB}{d\tau} = c(a - B(\tau)) \qquad (X,2)$$

Substitution of a value B_1 for B in (X,2) gives the values of $dB_1/d\tau$ as a function of $\Delta\lambda$, since a and c are known. (The method cannot be applied if the assumed value $B_1 > a$; that is to say, if we want to examine a region of the atmosphere, too deep for investigation with radiation of this wavelength).
The inverse, $(d\tau/dB)$, is proportional to the excitation coefficient; it can be expressed in the continuous absorption coefficient for that depth, κ_λ, by forming

$$\frac{(d\tau/dB)_{\Delta\lambda}}{(d\tau/dB)_{\lambda_{cont.}}}$$

Now, in plotting the values of $(d\tau/dB)$ against $\Delta\lambda$ it is observed that they tend for great values of $\Delta\lambda$ to a constant value. We will assume that this constant value is proportional to the continuous absorption coefficient for that depth. For the deep layers the continuous absorption coefficient could not always be determined in this way (e.g. for $\mu = 0{,}716$); here the value of $d\tau/dB$, derived from model V was used to find the data, given in the table. Sometimes, especially for the deep layers, no values of $(dB/d\tau)$ are found for the small wavelength distances: this occurs when the particular value for $B(\tau)$ chosen in (X,2) is greater than a; then no solution is possible.

§ 3. *Absolute values of the excitation coefficients in the Balmer lines.*
We next want to express the excitation coefficients in absolute units, and to find the excitation coefficient *per neutral hydrogen atom.*
Now

$$\left(\frac{d\tau}{dB}\right)_{\Delta\lambda} : \left(\frac{d\tau}{dB}\right)_{cont.} = \frac{\alpha_H N_H + \alpha_{H^-} N_{H^-}}{\alpha_{H^-} N_{H^-}}$$

with
α_H = selective excitation coefficient per neutral hydrogen atom;
N_H = number of neutral hydrogen atoms per unit of volume;
α_{H^-} = continuous absorption coefficient per neutral hydrogen atom;
N_{H^-} = number of H^- ions per unit volume.
From this we derive

$$\frac{\alpha_H . N_H}{\alpha_{H^-} N_{H^-}} \qquad (X,3)$$

In CHANDRASEKHAR and BREEN's tables [25] the quantity

$$\frac{\alpha_{H^-} N_{H^-}}{N_H P_e}$$

is given. Multiplying this by the electron pressure P_e for the depth i.q., we find

$$\frac{\alpha_{H^-} N_{H^-}}{N_H} \qquad (X,4)$$

and a comparison of (X,3) and (X,4) gives the desired quantity α_H; this is the selective excitation coefficient per neutral hydrogen atom *).
(See table 67, where an example of the calculations is given).

*) This procedure is permitted since the influence of the continuous neutral hydrogen absorption is negligible. This is indeed so in the fairly high parts of the atmosphere, discussed here.

TABLE 67. Example of the calculation of the "observed" values of the excitation coefficients. In this example calculations are given for Hα; $\Theta = 0{,}993$. At that depth $\kappa_\lambda . P_e = 42{,}3 . 10^{-26}$.

$\Delta\lambda$	0,6	0,8	1,0	1,25	1,5	2,0	3,0	4,0
$dB/d\tau . 10^{-14}$	1,06	2,34	3,05	3,41	3,59	3,80	3,80	3,71
$\left(\frac{d\tau}{dB}\right)_{\Delta\lambda} : \left(\frac{d\tau}{dB}\right)_{cont.}$	3,56	1,62	1,24	1,11	1,06	1,00	1,00	1,02
$\left[\frac{\left(\frac{d\tau}{dB}\right)_{\Delta\lambda}}{\left(\frac{d\tau}{dB}\right)_{cont.}}\right] - 1 \quad . \kappa_\lambda P_e . 10^{26}$	108	26	10	4,6	2,5	0	0	0,8
theoretical values (widening by ions and electrons)	80	26	14	8	5	2,5	1,0	0,5

A weak link in this method is the introduction of the electron pressure; this value must be derived from a model of the atmosphere. We have taken the values from model V; for the main part of the atmosphere they are not very different from those of model VII. The uncertainty in the communicated values is estimated to be about ± 0,20 (on a logarithmic scale), as a consequence of the uncertainty in the reduction.

§ 4. *Comparison with the theoretical values.*
The data obtained in the preceding section will be compared with the theoretical values, which have been calculated for model VII. It was assumed that the profile of the excitation coefficient is widened by the Statistical Stark effect of *ions and electrons*, since the discussion in chapter VI (see figure 18) showed that for the lines Hα to Hδ widening by ions and electrons explains the observations better than widening by ions alone.
These values are computed for the same depths as those of the preceding section. Figure 34 gives the mutual comparison.
The comparison of the "observed" values with the theoretical ones shows that deviations as great as a factor 10 sometimes occur; it is difficult to find a regularity in them.

These results are compared with those of figure 18 and it is satisfactory to note that the earlier results, though derived in an entirely different way, are qualitatively in agreement with the new determinations.
Let us, for instance, examine H_{2-3}. In chapter VI and figure 18 it was shown that the excitation coefficient for H_{2-3} is about a factor 9 greater than the theoretical value, calculated for statistical widening for ions alone (see table 45). Figure 34 *seems* to indicate a contradictory value; but this is not so in fact, for two reasons:

a) our latter theoretical values are valid for widening by ions and electrons; this causes an increase in the excitation coefficients with respect to those computed for widening by ions alone by a factor $5/2 . (2)^{2/3} \approx 4$.
b) Let us consider the results of table 43; the figures in it refer to the wavelength distances $\Delta\lambda = 2$ to 4 A. These distances correspond to layers with temperatures between $\Theta = 0{,}83$ to 0,77, agreeing with the curve in figure 34 for the temperature $\Theta = 0{,}798$. The figure clearly shows that in the wavelength region between 2 and 4 A figure 34 is indeed in harmony with the earlier results found in chaper VI.
In the same way it can be shown for the other hydrogen lines that our new results agree qualitatively with the old ones. But the new values are more detailed and probably better.

§ 5. *Verification of the new excitation coefficients by numerical integration over the solar atmosphere.*
The only direct way to examine whether the new values are reliable is the calculation of the emergent radiation for different lines and wavelength distances with the aid of numerical integration. This will be done in this section. Two difficulties occur.
a) The excitation coefficients have been found from the *observed* intensities in the lines. If next the line intensities would be calculated by following exactly the same procedure but in the inverse direction, we would practically find again our initial data – the observed intensities. The new, calculated intensities, as compared with the observed values, would only be smoother owing to the way of reduction, but this result would not be very interesting. We therefore propose to calculate the line profiles, using model VII of the solar atmosphere. In this model the $B(\tau)$-relation is far more complicated than the relations

FIGURE 34

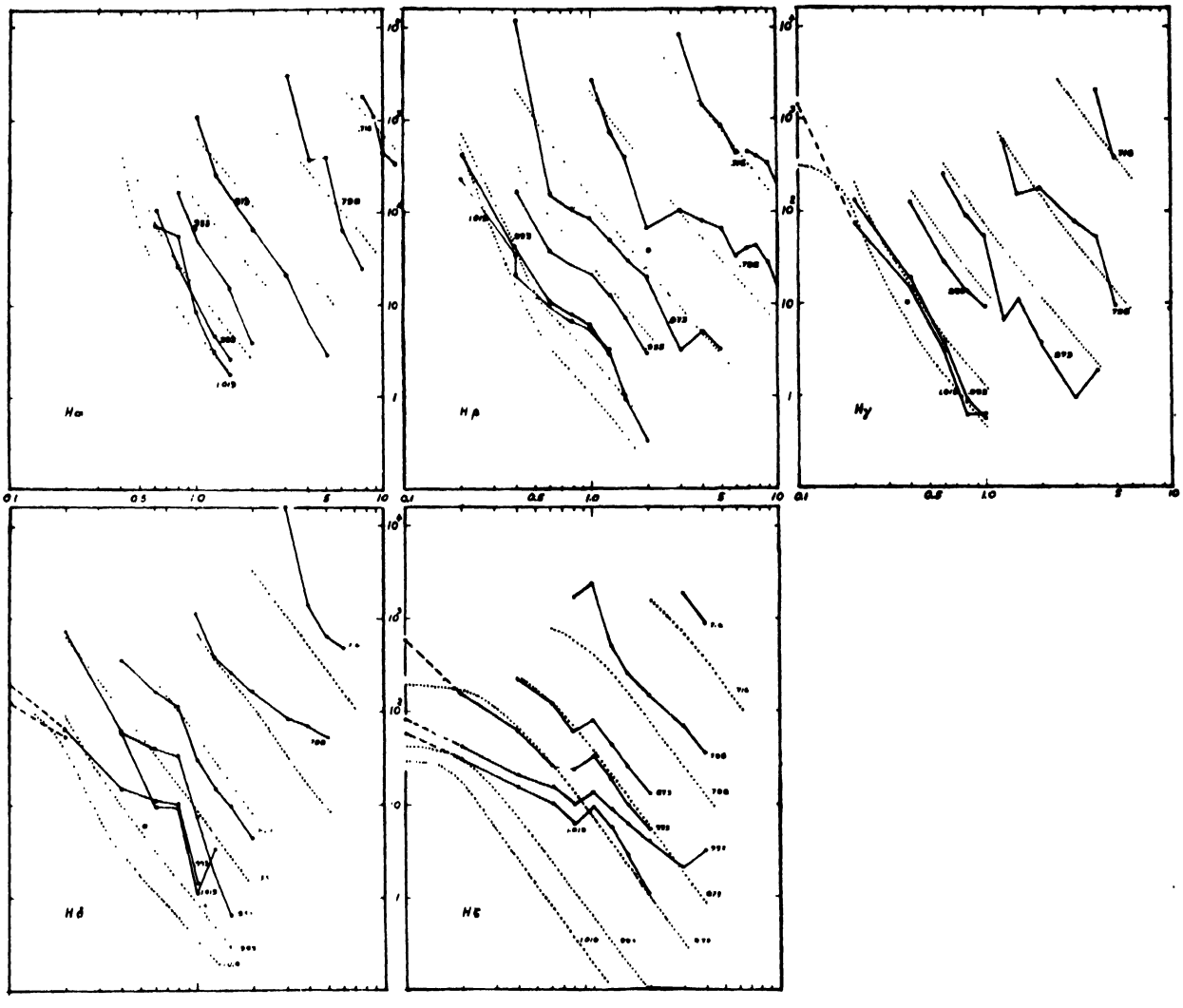

Observed and computed excitation coefficients in the lines H_α ... H_ζ. The computed coefficients have been derived on the basis of statistical widening by ions and electrons.
Abscissa: wavelength distances to the centre of the line (Angstrom units).
Ordinate: line excitation coefficients per hydrogen atom and per unit of electron pressure. The curves in the figure are given as functions of the parameter Θ (= 5040/T). One unit is 10^{-26} c.g.s.

$$B(\tau) = a - be^{-c\tau}$$

which were used in the derivation of the "observed" excitation coefficients. Hence the calculations will serve as a check whether the excitation coefficients are reliable.

b) The excitation coefficients of figure 34 are only known in a restricted region of $\Delta\lambda$ and Θ. Outside these regions the values were found not to be reliable, their contribution to the line formation being too small. As, for this reason, their influence on the profiles is not important either, adopting a somewhat erroneous value for the unknown part of the functions is not objectionable. We assume that the excitation coefficient curves are prolongated according to the law

$$\kappa \sim \Delta\lambda^{-5/2}$$

and a curve of this form is connected to the end points of the curves in figure 34.

The *calculations* have been made for the lines H_{2-3} ($\Delta\lambda$ = 0,8; 1,5 and 5,0 A), for H_{2-4} ($\Delta\lambda$ = 0,8; 1,5 and 5,0 A) and for H_{2-5} ($\Delta\lambda$ = 1,0 and 2,0 A).

In these calculations the optical depths in the region of the lines are expressed in the optical depths τ_λ with the formula

$$\frac{d\tau_\nu}{d\tau_\lambda} = \frac{\alpha_H}{\alpha_H - P_c}$$

The results and their comparison with the observations are given in table 68A. Obviously there is a general agreement, but this is perfect for none of the three lines; in one case the difference between observations and calculations amounts to nearly 20%; generally it is much smaller. The mean value of the difference is 2% for H_{2-3}; it is 9% for H_{2-4} and 4% for H_{2-5}. But two things must be taken into account:

a. The error is small for great wavelength distances, evidently because of the fact that for great wavelength distances the value of the excitation coefficient is small, so that its influence on the line intensities is also small. For great wavelength distances the emitted radiation approaches the value for the continuous radiation; which is evident since model VII explains the *continuous radiation* correctly.

b. Further the calculated values are always greater than the observed ones. This means that the excitation coefficients used by us are still *too small* and have to be increased to reach agreement.

TABLE 68. Comparison of the observed line intensities and the intensities, computed with the excitation coefficients of figure 34.

A	cos θ \ Δλ	H_α			H_β			H_γ		cos θ \ Δλ	1,0	1,25	2,0	B
		0,8	1,5	5,0	0,8	1,5	5,0	1,0	2,0					
computed:	1,000	1,780	2,243	2,573	2,691	3,238	3,692	2,960	3,502	1,000	1,84	2,03	2,07	
	0,755	1,670	2,115	2,390	2,495	2,944	3,292	2,731	3,160	0,800	1,77	1,94	1,98	model V
	0,484	1,499	1,893	2,094	2,160	2,508	2,710	2,352	2,638	0,436	1,60	1,73	1,76	
	0,124	1,130	1,304	1,339	1,276	1,444	1,464	1,323	1,358	0,176	1,35	1,41	1,43	
observed:	1,000	1,68	2,14	2,60	2,34	2,99	3,65	2,70	3,40	1,000	2,04	2,30	2,41	
	0,755	1,57	2,11	2,38	2,15	2,67	3,27	2,62	3,16	0,800	1,92	2,17	2,28	model VII
	0,484	1,47	1,82	2,07	1,78	2,18	2,53	2,19	2,63	0,436	1,69	1,85	1,95	
	0,124	0,97	1,26	1,33	1,12	1,31	1,46	1,20	1,30	0,176	1,30	1,42	1,45	
										1,000	1,91	2,05	2,22	
										0,800	1,77	1,90	2,08	observed
										0,436	1,58	1,67	1,67	
										0,176	1,30	1,36	1,40	

It is possible to show, that these systematic differences are due to the model which has been used for computing the absolute values of the excitation coefficients. Model VII is not a smooth model like the models which have been derived from the continuous radiation of the sun, but it presents some irregularities.

On the other hand, the excitation coefficients have been found, assuming a smooth ($B;\tau$) relation – formula (X,2). It seems probable that a smooth model of the atmosphere would give better results.

Hence, computations, analogous to the former ones have been made for H_α, $\Delta\lambda$ = 1,0; 1,25 and 2,0, and for model VII and model V. Table 66B, where the results have been listed, shows that the agreement is better for model V. This result does nog signify that model V explains the Balmer line profiles better than model VII, since the reverse is the case, but it means that the method of deriving the values for the line excitation coefficients inductively has certainly its limits. Although in principle it is attractive to calculate the observational values of the excitation coefficients, the method works only well in the case of very exact measurements.

The cause of these uncertainties is the fact that in this reduction twice a process of differentiation has been applied to *the same observational results*: the first time, when solving the integral equation (X,2), which led to the observational B-values and the second time, when deriving from these B-values the excitation coefficients. This makes the result extremely uncertain.

This same problem has already been encountered in deriving a model of the atmosphere from the limb darkening of the continuous spectrum. There already, it has been shown that even very exact

observations admit several solutions, owing to the fact that the observational data are only known in a limited range of ϑ and owing to the scatter of the observations. Since in our case of the hydrogen lines the quality of the observations is less accurate than the quality of the very exact observations of the limb darkening of the continuous spectrum, the uncertainty in the results is greater. The uncertainty in a *deduced* quantity, such as the optical depth $\tau_{\lambda+\nu}$ or the line excitation coefficient, which is great already when using the limb darkening of the continuous spectrum (see e.g. [23]) is still greater for the Fraunhofer lines.

For the time being the following conclusion may perhaps be drawn:

If we take into account the great scatter of the points, then the "observed" excitation coefficients, given in figure 34, may probably be considered to be in most cases roughly in agreement with the excitation coefficients calculated with the aid of statistical Stark widening by ions and electrons. The scatter of the points is very great, however; this great uncertainty shows that it is not sufficient to compute the excitation coefficients inductively but that these must always be controled by a deductive calculation.

CHAPTER XI

INDUCTIVE DETERMINATION OF THE WIDENING FUNCTIONS FOR THE PASCHEN AND BRACKETT LINES

§ 1. *Introduction.*
This subject was already discussed earlier and the results of it were published elsewhere [72]. In this chapter a very short review is given. No details of the calculations are included.

§ 2. *The method.*
This is fairly simple. Firstly the line profiles are calculated by assuming statistical widening by ions alone making use of model VII. It is found that the observed profiles are much wider and shallower than the calculated ones. Then the following assumption was introduced: let us assume that the excitation coefficients are indeed statistically widened but that the *form* of the widening function is another than is generally assumed. (The normal form of this function is given in figure 14). We next want to find this new function for each line independently. This is determined in several steps.
Firstly it is assumed that the deviations between the observed and the calculated line profiles can be explained by the assumption that the true excitation coefficient at a certain wavelength $\Delta\lambda$ in the line is equal to the excitation coefficient adopted in the calculations for the wavelength $\Delta\lambda'$ for which $r_{calc.}(\Delta\lambda') = r_{obs}(\Delta\lambda)$; r is the depression in the line profile. This is more or less the same procedure which has been applied to the Balmer line wings in chapter VI. In principle this means that the whole variation of the excitation coefficient with depth at the wavelength $\Delta\lambda$ should be put equal to the function adopted for the wavelength $\Delta\lambda'$; but in practice this equality was adopted only for one depth: the mean optical depth where the dip of the line profile is formed.

This procedure enables us to find a new widening function; this function is used for the calculation of a new profile, by which a further correction is determined. This was continued till the deviations between the observed profiles and the calculated ones are of the order of 1%. The "observed" widening functions, thus determined are given in figure 35. The probable errors of these data are fairly great; they are estimated at about ± 20%.

§ 3. *Discussion.*
The "observed" widening functions are clearly wider than the theoretical function, derived on the basis of the classical theories. The discrepancy is greater for the Brackett lines than for the Paschen lines.
Because of the great scatter of the points, it is difficult to find whether really a mean curve may be drawn through the dots; the dotted curves, drawn in figure 35 are therefore very uncertain. They are obtained from the theoretical curves by a widening of the wings and a corresponding lowering of the central intensity, $\int \kappa_\nu d\nu$ remaining constant. The widening factors are:

for the Paschen lines	2,3
for the Brackett lines	3,1

Moreover, in the preceding chapter it has been found

for the Balmer lines	1,3

From the preceding discussion it is clear that this widening is much too great for the assumption to explain the widening by ions *and* electrons. – Our calculations have been made for widening by ions alone, but the introduction of electrons causes only a widening by a factor 1,34, which is insufficient.

Let us, finally, examine, whether the scatter of the points around the dotted mean widening curve is physically real or whether it is only a consequence of the normal errors in the measurements. For this purpose it is necessary to investigate the influence of a change in the adopted $s_n S(\beta)$ value on the resulting line depression. This influence can be calculated immediately with the aid of the several approximations, already used for finding the ultimate widening functions.
For H_{4-7} at $\beta = 5,5$, where this line shows the greatest deviations from the mean curve, the individual "observed" $s_n S(\beta)$ value and the "mean" value from the dotted curve amount to 0,10 and 0,036. By interpolation (see [72], table 3) we find that these figures correspond to line intensities of 0,828 and 0,88. These numbers differ by 5%, which seems to exceed the possible systematic error in the observations.

FIGURE 35

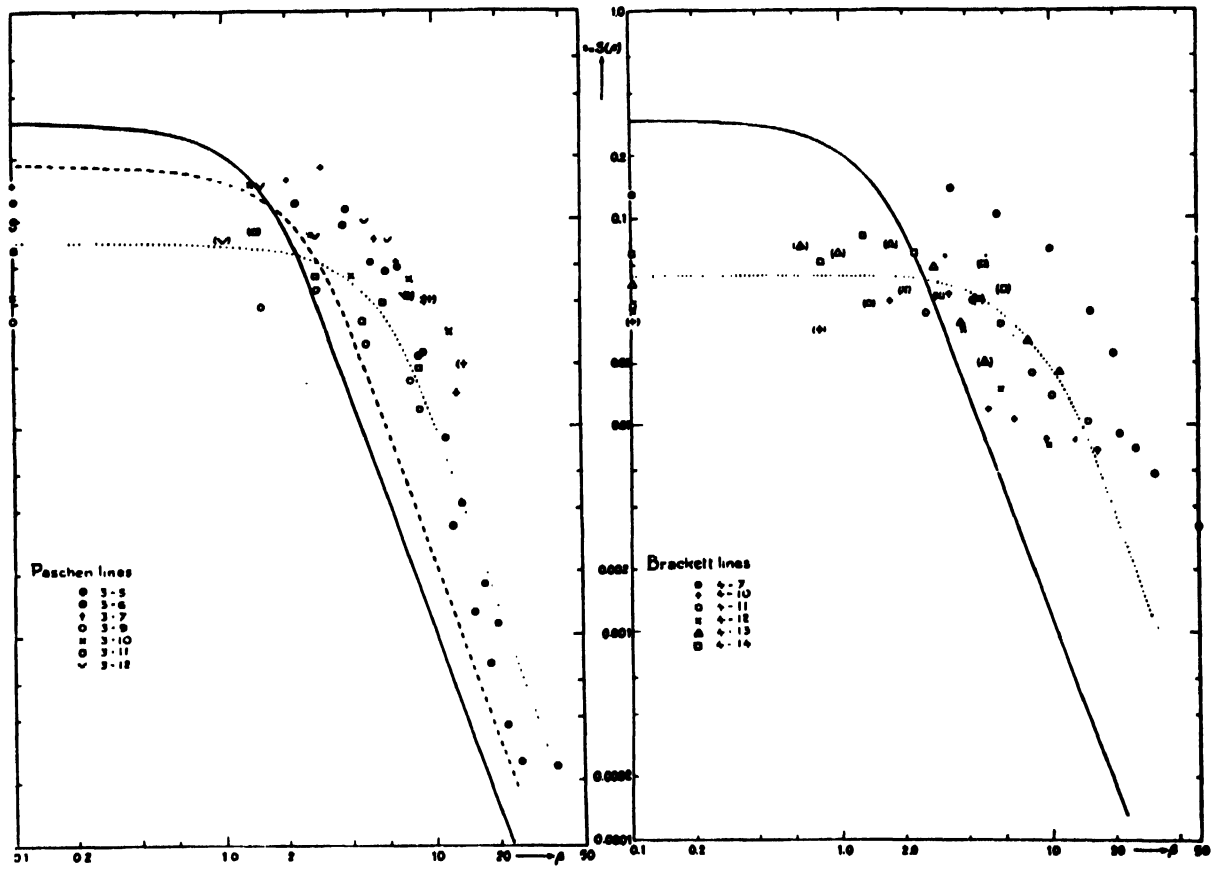

"Observed" excitation coefficients in the Paschen and Brackett lines. Full-drawn is the line computed for statistical Stark widening by ions only. The "observed" values may be represented by the dotted curve, which seems to be the best mean curve. This curve is widened with report to the full drawn one; the widening factors are 2,3 for the Paschen lines and 3,1 for the Brackett lines. The dashed curve is computed for statistical widening by ions and electrons.

Conclusion: This discussion shows that the widening factors, presented above must be considered as a rough approximation of the true situation. It is well possible that the true law of line widening is a complicated function of the atomic transition considered and of the depth in the solar atmosphere. In order to find these function with a greater precision than the functions, found here, it seems that centre-to-limb observations of the Paschen and Brackett lines are necessary.

CHAPTER XII

SOME CASES OF BLENDING (H_ε AND D_α AND THE ABUNDANCE OF DEUTERIUM)

§ 1. *Introduction.*

The blending of "normal" solar lines and hydrogen lines presents an interesting problem: the cores of strong hydrogen lines originate in a superficial layer of the suns atmosphere; and as the line absorption increases strongly with depth, the region of line formation is relatively thin in the atmosphere. This causes that a metal line, which may be formed at a greater optical depth than the core of the hydrogen line may be practically invisible if it is blended with the central part of a strong hydrogen line.

But the *wings* of the Balmer lines and the cores of the high series members and of most of the Paschen and Brackett lines are formed in *deep* layers of the atmosphere and the contribution of the *higher* layers to the line profile is negligible. Hence, a high series member, which is blended with a broad metal line will hardly be visible in the solar spectrum.

An example of this second case is the line H_ε which is blended with the Ca^+ line at 3968,5 A, the distance between the line centres being 1,6 A. Since the Ca^+ line is formed in superficial layers, nothing can be detected of the wings of H_ε and only a trace is visible of its core.

The most interesting example of hydrogen blending is, however, the case in which a *faint* hydrogen line (formed in deep layers) is blended with a strong hydrogen line (formed in high layers). In that case the faint line will hardly be visible. Such a case exist in the sun since all lines of the deuterium spectrum are blended with the corresponding hydrogen lines. In this chapter a quantitative discussion is given of the two cases described above.

§ 2. *The blending of H_ε by Ca^+ 3968,5 A; the optical depths.*

The optical depths in the *hydrogen line* H_ε have been computed in the same way as those for the other Balmer lines, using model VII of the atmosphere and assuming statistical widening by ions and electrons; the method has already been described in full in chapter VIII; no further details will be given here.

In the *Ca^+ line* the line excitation coefficients have been calculated in a more or less approximate way. We assume:

a. a Milne-Eddington model of the atmosphere;
b. $\kappa_\nu = 0$; only scattering is dealt with;
c. σ_ν/κ_ν is constant as a function of depth;
d. in the continuous spectrum: $B = 1 + \beta\tau_\lambda$, with $\beta = 4,5$ (Cf. HOUTGAST[62]).

With this model the line depression was computed for the combinations of the following values of $\cos\theta$ and $\sigma_\nu/\kappa_\lambda$:

$\cos\theta$ = 0,1; 0,33; 0,67; 1,00.

$\sigma_\nu/\kappa_\lambda$ = 1; 3; 10; 30; 100; 300; 1000.

The results are given in table 69. With the aid of HOUTGAST's observations of the centre-to-limb variations of the Ca^+ lines the ratio between σ_ν and κ_λ could be determined by interpolation from table 69 for each of the wavelengths for which observations are communicated by HOUTGAST and for the four values of $\cos\theta$, given in the table.

It was found, that the values of $\sigma_\nu/\kappa_\lambda$ thus derived, were only functions of $\Delta\lambda$ and not of $\cos\theta$. The resulting mean values are given in table 70.

With these values the optical depths in the lines have been computed at the same wavelengths for which they had already been derived for the hydrogen line H_ε.

TABLE 69. Residual intensities, calculated for the Milne-Eddingston model at 4000 A. $\kappa_\nu = 0$; $B = 1 + 4,5\,\tau_\lambda$.

$\frac{\sigma_\nu}{\kappa_\lambda}$	1	3	10	30	100	300	1000
$\cos\theta$ = 0,10	0,904	0,645	0,390	0,213	0,110	0,103	0,011
0,33	0,745	0,522	0,300	0,209	0,087	0,072	0,014
0,67	0,652	0,433	0,243	0,126	0,073	0,059	0,012
1,00	0,610	0,390	0,212	0,122	0,067	0,035	0,013

TABLE 70. Observational values of $\frac{\sigma_\nu}{\kappa_\lambda}$ for the line Ca^+ 3968,5 A.

$\Delta\lambda$(A)	0,0	0,63	1,26	1,86	2,78	4,13	6,85	8,9	15,7
cos θ = 1,00	60	28	18	13	8	5	1,5	-	-
0,67	80	30	16	13	8	5	1,6	-	-
0,33	55	30	16	12	8	5	2	1,3	-
0,10	30	24	26	16	7	5	2	-	-
mean value	56	28	19	14	8	5	1,8	(1,0) (extrapolated)	(0,15)

§ 3. *H_ε; the results.*
Next, two profiles of the Ca^+ line have been calculated: one without the extra hydrogen line absorption and another with the addition of the hydrogen line (See table 71). The calculations have been made numerically, with model VII. For the Ca^+ line the *constant* ratio between σ_ν and κ_λ has been used, while for the hydrogen line the variation of the line excitation coefficient with depth has been taken into account in the way, already described earlier.
According to this table the profile of H_ε should be detectable chiefly near its core although a very small influence should be visible even to a distance of 10 A from the line centre. It seems, however, practically impossible to measure this latter depression in this broad Ca^+ line, which is much disturbed by other lines.
Indeed, at the wavelength of the centre of H_ε a small depression in the profile of the Ca^+ line can be detected in the Utrecht Atlas of the Solar Spectrum, which depression amounts to about 2,5%. This is smaller than the predicted value, this being 4,3% (see table 71). This difference may, however, easily be explained by

TABLE 71. Computed residual intensities in the region of the line H_ε, blended by Ca^+ 3958,5. The residual intensities r are multiplied by 1000.

$\Delta\lambda(H_\varepsilon)$	$\Delta\lambda(Ca^+)$	profile of	cos θ = 1,00		cos θ = 0,755		cos θ = 0,484		cos θ = 0,142		observed (ATLAS) cos θ = 1,00	
			r	Λ	r	Λ	r	Δ	r	Λ	r	Λ
- 1,0	+ 0,6	Ca^+	167	0	165	0	170	0	232	0	080	0
		H_ε + Ca^+	167		165		170		232		080	
0,0	+ 1,6	Ca^+	241	43	231	39	223	25	258	06	200	26
		H_ε + Ca^+	192		192		198		252		174	
+ 1,0	+ 2,6	Ca^+	354	14	346	09	340	04	428	0	295	04
		H_ε + Ca^+	340		337		336		428		291	
+ 10,0	+ 11,6	Ca^+	898	10	899	07	913	04	976	0	-	
		H_ε + Ca^+	888		892		909		976			

the approximative way in which the optical depths in Ca^+ 3986,5 were derived. Table 71 shows that the residual intensities of the Ca^+ line, computed by us, are greater than the observed values. This might mean that our excitation coefficients in the Ca^+ line, which had been derived from the observations, have nevertheless been chosen too small. An increase in the excitation coefficients would at the same time reduce the depression at the centre of the hydrogen line.
We conclude that it seems that *the blending of H_ε by the Ca^+ line at 3968,5 A may be explained quantitatively.*

§ 4. *The abundance of deuterium in the solar atmosphere.*
In his thesis, CLAAS[29] tried to find an upper limit for the abundance of deuterium by the consideration that the D_α line cannot be seen in the Atlas. Supposing that the equivalent width of this line is smaller than 2 mA, a

maximum abundance of deuterium could be found with the method of the weighting functions.
His upper limit, 4.10^{-9} is surprisingly low, since the terrestrial abundance of deuterium is about 2.10^{-4} (see e.g.[48]), a factor 5.10^{4} greater than CLAAS' upper limit.
It will be shown in this section that the blending of the deuterium line by H_α makes the deuterium profile almost completely invisible, thus explaining a part of this great factor.

The profile of the line H_α has been computed for two cases: with the deuterium line and without. Besides, the profile of the deuterium line without the hydrogen line has been calculated. The abundance 2.10^{-4} was tentatively adopted.
Since the method of calculation is known we give the results of the calculations without further details in table 72. We notice that a small depression, of about 2%, should be visible

TABLE 72. Calculated residual intensities of D_α.
All residual intensities r are multiplied by 1000.

$\Delta\lambda_{D\alpha}$	$\Delta\lambda_{H\alpha}$	profile of	cos θ = 1,00		cos θ = 0,755		cos θ = 0,484		cos θ = 0,142		observed (ATLAS) cos θ = 1,00	
			r	Δ	r	Δ	r	Δ	r	Δ	r	Δ
0	-1,8	H_α	797	23	829	21	872	17	968	10	812	06
		$H_\alpha + D_\alpha$	776		806		855		958		806	
-0,2	-2,0	H_α	826	07	857	05	898	03	976	0	830	09
		$H_\alpha + D_\alpha$	819		852		895		976		821	

Undisturbed profile of D_α:

Δλ =	0,0	0,2	0,4	0,6
r × 1000	877	893	961	986

at the core of the deuterium line; at $\Delta\lambda_{D\alpha} = -0,2$ A we predict a depression of 0,7%.
Turning to the Atlas, we do not agree with CLAAS that no trace of deuterium can be detected, as at $\Delta\lambda_{D\alpha}=0,0$ we are inclined to place the undisturbed continuum of H_α at a height of 0,812 and the disturbed profile at 0,806, thus giving a depression of 0,6%. This is a factor 3,5 smaller than the tentatively predicted value but the observation is uncertain: a small blending line at 6561,2 A makes the "deuterium" profile unreliable and it is possible that the true deuterium depression is of the order of 1%.
At $\Delta\lambda_{D\alpha} = -0,2$ A, where the profile of H_α is less disturbed, we observe a depression of 0,9%, the undisturbed continuum being placed at 0,830 and the line profile at 0,821. This value is of the same order of magnitude as the predicted value (0,7%).
We conclude that it is not impossible that deuterium is present in the solar atmosphere and that its abundance is of the same order of magnitude as the terrestrial abundance. The most probable value seems to be 1.10^{-4}.

Finally we notice how great the blending influence of H_α is. The unblended deuterium line should be a fairly strong line with a central dip of 12,3%; a half width of 0,67 A and an equivalent width of 92 mA. The blended profile, on the other hand, should have a central dip of 2,3% and an equivalent width of only 7 mA, a 13 times smaller than the unblended equivalent width. Hence, the influence of the blending explains a factor 13.
It is still necessary to explain why CLAAS found for the unblended line an equivalent width of 2 mA with an abundance of 4.10^{-9}, while we found an equivalent width of 92 mA with an abundance of 2.10^{-4}. This difference is due to the fact that CLAAS used for his calculations the method of the weighthing functions, which is not permitted for the hydrogen lines: the deuterium lines cannot be considered as faint lines but they are caused by a strong absorption in the deep layers. In the high layers practically no selective absorption occurs.

CHAPTER XIII

A WORKING MODEL OF THE CHROMOSPHERE AND CORONA

§ 1. *Introduction; program of this chapter.*
To understand the intensity distribution in H_α, observed in the chromosphere, a model of the chromosphere is necessary. Since there might also be a small chromospheric contribution to the central intensities of some Fraunhofer lines, observed in the normal solar spectrum, knowledge of the structure of the low chromosphere is of great importance. A model of the chromosphere will be derived in this chapter. As our knowledge of the outer layers of the sun is extremely poor, the model will be very uncertain.
Our *program* is first to derive from the available data on the temperatures in the chromosphere and corona a mean temperature curve. It is necessary to look for possible differences between the kinetic and the excitation temperatures; furthermore, values which are derived from Doppler widths of emission lines must be treated with caution, since they might be influenced by self-absorption (causing too flat a profile and hence too great a value for the kinetic temperature) and by turbulent motions.
We will also survey the determinations of the electron density. Then both - temperatures and densities - will be compared with the radio measurements of the quiet sun. This will give, finally our working model.
It must be remarked, that nearly all temperatures, communicated up to now, have been derived, neglecting the influence of the summation over the higher layers in the line of sight. This influence can only be taken into account, if a "working model" of the chromosphere is already known; this correction to the communicated values would necessarily be the first step after this investigation.

§ 2. *A review of temperature determinations in the chromosphere and corona.*
In this section we only discuss the temperatures determined by *optical* methods. In tables 73, 74 and 75, the kinetic temperature for electrons, the kinetic temperature for atoms and the excitation and ionisation temperatures are listed as they have been found by different authors. The same data are plotted in figures 36[a] and 36[b] (the excitation and ionisation temperatures are not represented graphically).
A discussion of these data is not given, though it is clear, that not all have the same value; some data are fairly exact, while others have only the value of an approximation.

A few authors have published profiles of emission lines in the chromosphere and in the corona. If the chemical element, emitting such a line is known, the profile may be used for deriving the Maxwellian velocity of the atoms. In this way the results of MENZEL[99] and KEENAN[76] are interpreted. The same has been done with the measurements of GROTRIAN[55,56] and LYOT[94,95] using EDLEN's identifications[43]. Finally, the Doppler velocity of the hydrogen atoms in the high chromosphere can be determined with the

TABLE 73. Kinetic temperatures for electrons in the chromosphere and corona.

h (km)	T or T	derived from	ref.
400	4 000°	Balmer continuum	33
400	10 000°	(the same observations)	79
670	5 240°	Balmer continuum	26; 196
1700	4 010°	Balmer continuum	
1300	< 30 000°	Balmer continuum	200
2000	2 000°	Balmer decrement	174
700000	1050 000°	Ne in corona	67
1400000	850 000°		
700000	1400 000°		4
2000000			

TABLE 74. Kinetic temperatures for atoms in the chromosphere and corona.

A. From WILDT's density gradients [196].

$\mu = 0,5$ in the high chromosphere ($h > 3000$ km);
$\mu = 1,5$ in the low chromosphere.

h (km)	T	element
800- 1500	13 300°	Sc II
1000- 1500	11 300°	Ti II
500--1200	11 800°	V II
500- 1000	10 330°	Cr I
800- 1500	15 300°	Mn II
500- 1200	13 300°	Fe I
500- 1200	11 800°	Fe II
500- 1000	11 800°	Ni I
500--1200	11 800°	Y II
500- 1200	11 800°	Zr II
500- 1200	17 800°	Ca I
1500- 4500	33 000°	Sc II
2000- 6000	33 000°	Ti II
2000- 6000	14 400°	Mg I
10000-14000	18 200°	Ca II
1000- 6000	10 300°	Sr II
500-12000	66 000°	He I

B. From Doppler profiles of emission lines.

h (km)	T	element	ref.
1 500	35 000°	H	145
18 000-38 000	2 500 000°	Fe	
56 000	3 370 000°	Fe	187
80 000	5 130 000°	Fe	
120 000	6 550 000°	Fe	

TABLE 75. Excitation and ionisation temperatures.

h (km)	T	ref.	derived from
700	5 000	11	relative intentisies of H and Ca^+
500	4 500	99	relative intensities of ionised and neutral lines
"corona"	630 000	186	degree of ionisation in corona
"corona"	600 000	204	intensity differences between Fe X and Fe XIV

TABLE 76. Kinetic temperatures derived from the Doppler widths of profiles, observed by Menzel, Keenan, De Jager, Grotrian and Lyot.

h (km)	T (°)	element	ref.
600	14 800		
1 030	16 400		
1 675	17 900	Fe	99
2 320	21 500		
1 200	10 000	H	76
3 500	50 000		
5 000	47 000	H	table 18
6 000	52 000		
21 000	2 300 000		94; 95
24 000	2 500 000	Fe	55; 56

author's chromospheric profiles of H_α, communicated in chapter III. These data are summarized in table 76 and included in figure 36[a].
Reviewing all determinations it is satisfactory to observe that they can be considered to form more or less *one homogeneous set;* through the observed points it is indeed possible to draw a mean curve, dotted in figure 36; the curve is drawn somewhat below the mean of the points in order to correct tentatively for the influence of the higher temperature layers in the line of sight.
It is not yet possible to make a distinction between the different kinds of temperatures which were considered separately, since nearly all temperatures which are communicated are *kinetic* temperatures. It would be of great importance if exact excitation temperatures could be determined in the high chromosphere (above 3000 km).

§ 3. *Review of electron density determinations in the chromosphere.*
Very little is known of the electron densities in the chromosphere. We shall review the available data, starting at the base and finishing with the corona.
a. Limb of the sun. At an optical depth $\tau_{5000} = 0,01$, a hundred km below the limb of the sun, where $\Theta = 1,180$, the value of $\log P_e = -0,21$ (model VII). From this follows:

$$\log N_e = 12,02.$$

b. Low chromosphere. For the 500 km level (corresponding with the low flash) MITCHELL[113]

FIGURE 36

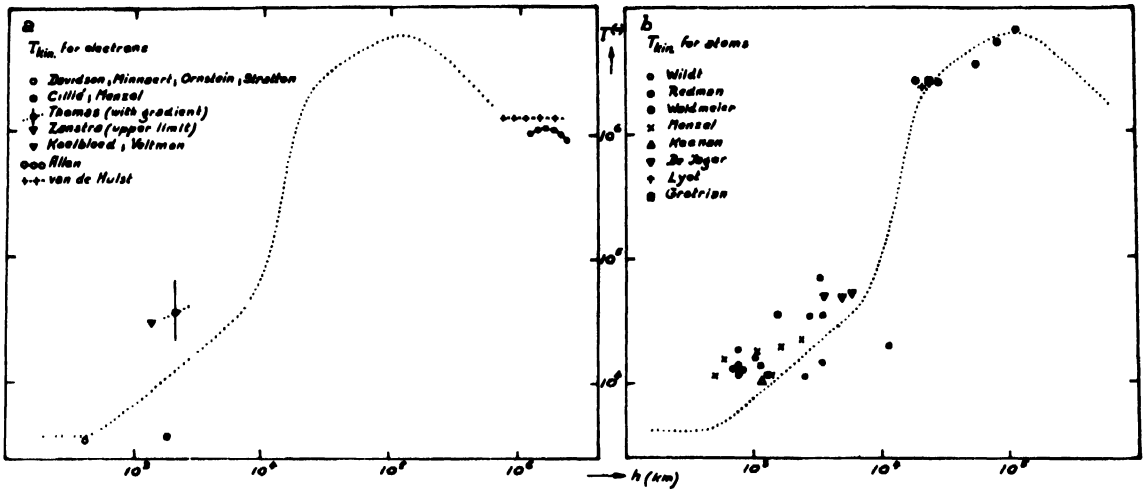

Kinetic temperatures for atoms and electrons in the solar chromosphere and corona. The dotted line is the "mean" curve, tentatively corrected for the influence of the higher layers in the line of sight.

notes that the first line which merges into the continuum of the Balmer and the Paschen series corresponds respectively with $n = 38$ and $n = 41$. These values may change from one eclipse to the other but must nevertheless be considered as reliable mean values.

Since the total half width of these lines depends both on the Stark effect and the Doppler effect, which are a.o. functions of T and P_e, these observations may be used to derive the electron density at the 500 km level. (The temperature is assumed to be known – figure 36).

The total half width of a profile, widened by Doppler and Stark effect, is known (chapter VIII). Table 77 gives the values of the total half width $2\,\Delta'\lambda_{SD}/s_n F_0$ as a function of the Doppler width $\Delta'\lambda_D/s_n F_0$. *Here*

$s_n = 2{,}56.10^{-3}.n^4(n^2-m^2)^{-2}(n(n-1)+2)$;

m is the lowest level, involved in the transition;

$F_0 = 46{,}8\ (P_e/T)^{2/3}$;

$\Delta'\lambda_D = 2{,}54.10^{-5}\ \omega^{-1/2}$, this is the half Doppler half-width.

We asaume now, that

$$\lambda_{n+1} - \lambda_{n-1} = 4\ \Delta'\lambda_{SD}$$

If further it is taken into account, that the s_n values for the Balmer and Paschen lines are to be multiplied by the correction factors 1,3 and 2,3 respectively (cf. chapters X and XI), we find with the adopted temperature of 4700° at 500 km:
from the Balmer lines: $\log P_e = \overline{2},83$ and $\log N_e = 10{,}99$;
from the Paschen lines: $\log P_e = \overline{1},22$ and $\log N_e = 11{,}40$.

There is some difference between the two values, but this cannot be ascribed to the influence of the apparatus widening, as in that case the P_e value derived from the Balmer lines oughts to be greater than the value for the Paschen lines.

Henceforth we shall adopt the mean value

$$\log N_e = 11{,}20 \text{ at } 500 \text{ km.}$$

c. Chromosphere between 1500 and 3000 km. In this region no determinations of the electron density are available, but WILDT[196] has given its *gradient* from a comparison between the gradients of Fe and Fe^+; it is found to be

$$d \log P_e / dh = -\ 0{,}20.10^{-8}\ \text{cm}^{-1} \qquad \text{(XIII,1)}$$

Since in this region $d \log T / dh = +\ 0{,}17.10^{-8}$ cm^{-1}, (§ 2) we find

$$d \log N_e / dh = -\ 0{,}37.10^{-8}\ \text{cm}^{-1}$$

d. High chromosphere and corona. The electron density in this region has been determined, assuming that the observed intensity of light in the corona is due to the scattering of sunlight by free electrons. We shall use Van de HULST's data; a mean value between the equatorial and polar electron densities is assumed.

All data from this section are combined in figure 37b and a curve, connecting them, is drawn (the dashed curve in the figure). The uncertainty of this curve is great, however!

FIGURE 37

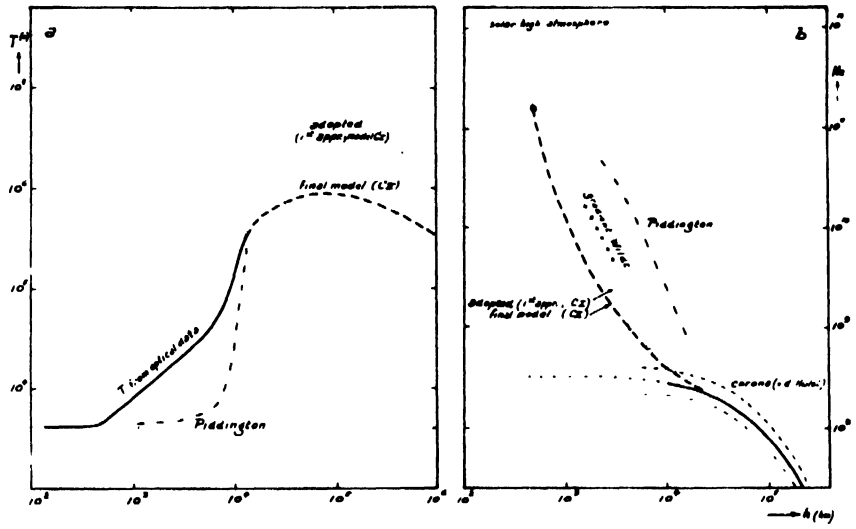

Distribution of temperature and electron density in the chromosphere and corona.

§ 4. *Discussion of some radio models of the chromosphere and corona.*

The extremely interesting intensity distribution in the solar radiospectrum shows that the apparent temperature rises from some thousands of degrees up to some millions of degrees, according to the wavelength considered (table 78).

TABLE 77. The total half-width $2\Delta'\lambda_{SD}$ of a line, widened by the Stark effect and the Doppler effect. The table gives the values of $2\Delta'\lambda_{SD}/s\eta F_0$ as a function of $\Delta\lambda_D/s\eta F_0$.

$\frac{\Delta\lambda_D}{s\eta F_0}$	$\frac{2\,\Delta'\lambda_{SD}}{s\eta F_0}$
0	2,92
0,3	2,94
0,5	3,06
0,7	3,18
1,0	3,58
2,0	5,04
3,0	6,75
5,0	8,90
7,0	11,3
10	15,2
20	29,6
30	44,4
40	59,2

TABLE 78. Apparent temperature deduced from the measurements of the radio-radiation of the quiet sun.

λ(cm)	$T_a.10^{-3}$	ref.	λ(cm)	$T_a.10^{-3}$	ref.
0,85	6,74	57; 58	55	240	88
1,25	2,00	159	60	240	164
1,25	10,5	39	62,5	590	142
1,25	10,0	133	150	1 200	32
3,15	12,0	120	150	1 000	90
3,18	22	154	150	700	127
3,18	19,3	112	150	1 000	127
3,28	18,0	159	150	600	205
10,0	18,0	159	172	650	153
10,0	25,0	32	187	1 800	142
10,0	54	134	187	900	12; 13
10,7	56	31	245	2 000	96
25	150	32	375	1 300	153
25	200	90; 135	670	2 000	96
50	500	32			
50	500	90			

Many astrophysicists used these data for the derivation of a model of the chromosphere and of the corona. Most of these models are too much simplified: the corona as well as the chromosphere have been assumed to be isothermal, a discontinuity occuring at a height of about 10000 km.

It is, in fact, curious that the generally adopted standpoint seems to be, that it is not possible to give a consistent description of the temperature in the chromosphere; more is supposed to be known about the electron density as a function of the height. This is e.g. HAGEN's[57,58] standpoint, who adopts the validity of formula (XIII, 1) in the *whole region* between about 400 and 15000 km, which is obviously not justified. PIDDINGTON's[136] model, derived in nearly the same way, is also unreliable, because he made a computing error[78] and practically neglected the optical measurements. It can be shown, that the intensity of the emitted radiation, calculated with his model, deviates strongly from the observed values. As PIDDINGTON's model will nevertheless sometimes be used in the following for comparison, we give in figure 37a his temperature curve next to our "optical" curve and in figure 37b his N_e curve together with the most probable N_e curve as derived by us. It will be clear that the differences are considerable.

§ 5. *Intensity of the radio radiation of the new model.*

The mean temperature curve from § 2 and figure 37a and the tentative electron density curve from § 3 and figure 37b define a new model of the chromosphere and corona, which will henceforth be called *model CI*. An independent test for this model will be the calculation of the emission in the region of the radio wavelengths. This calculation has been performed by numerical integration for nine values of r/R. In these calculations the absorption coefficient was found by KRAMERS' formula, used in MARTYN's[97] form:

$$\kappa = \zeta\, Ne^2/f^2\, Te^{3/2} \quad [\mathrm{cm}^{-1}]$$

$f = c/\lambda$

The value of ζ is, after PIDDINGTON[136]:

for λ = 1 3 10 30 100 300 1000 cm

ζ = 0,06; 0,07; 0,08; 0,09; 0,11; 0,13; 0,15

Some of these data are found after a slight extrapolation of PIDDINGTON's results.

Since in the region of the radio wavelengths PLANCK's law reduces to that of RAYLEIGH-JEANS, the black body radiation at a certain temperature is proportional to T. Hence the *brightness temperature* T_b at a certain point is found as

$$T_b = \int_0^\infty T(\tau_\lambda)\; e^{-\tau_\lambda}\, d\tau_\lambda$$

Finally, the *apparent temperature* T_a is

$$T_a = 2 \int_0^\infty \rho\, T(\rho)\, d\rho; \quad (\rho = r/R)$$

The results of the integrations are given in figure 38a (dashed curve). When they are compared with the observed values, given in table 78 and in figure 38a (dots and full-drawn curve) it is obvious that the agreement is satisfactory for $\lambda < 100$ cm; the temperature, adopted in the corona seems to be too high.

In this figure we have also given for comparison the apparent temperatures computed with PIDDINGTON's model; this calculation was less exact than the preceding one but must nevertheless be considered as reliable; the probable error in the computed points is about ± 0,05 (logarithmic scale). It is clear that this model is not in agreement with the observations and since there is a great resemblance between this model and that of HAGEN[57,58], it is assumed that our criticism must also apply to the latter model.

§ 6. *The corrected model of the chromosphere and corona.*

In § 5 we have derived from a provisional model called CI (*a*) the apparent temperature T_a as a function of the wavelength and (*b*) the variation of the brightness temperature T_b with r/R for several wavelengths. We shall now modify this model in order to correct the remaining discrepancies. This will lead to a new model; it will be based for the chromosphere on the *temperature curve* from figure 36, leaving aside as an unknown, the electron densities; in the corona we use the *electron densities* after Van de HULST as a basis, leaving open the possibility to change the temperature curve.

ad a. The corrections $\Delta \log N_e$ (in the chromosphere and $\Delta \log T$ (in the corona) are found with the aid of some trial integrations over some (9) models with different N_e and T curves. From these results we were able to investigate the influence of a variation of T or N_e on the apparent temperature, and, this being known, to determine the corrections to the model with the aid of these empirical differential formulae. The details of the calculations will not be given.

ad b. It is more difficult and less reliable to use the observed centre-to-limb variation, both because of the fact that these observations are less precise than these concerning the intensity of the integrated light, and because of the more complicated relation between ΔT o. ΔN_e and the emitted radiation. We have only determined corrections for the optically *thin* parts of the corona, where the influence of temperature variations will approximatingly increase or decrease the optical thickness of the layer, according to

$$\frac{\Delta\tau_\lambda}{\tau_\lambda} = -\frac{3}{2}\frac{\Delta T}{T}$$

FIGURE 38

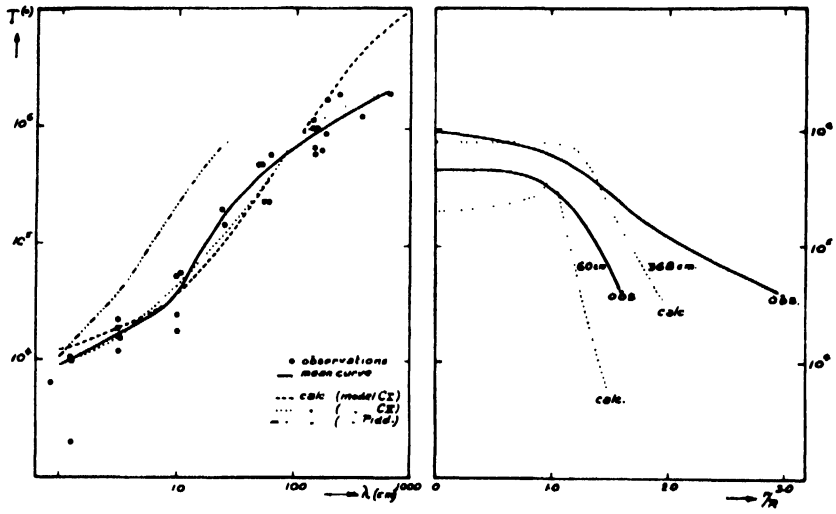

(left) The apparent temperature T_B of the sun in the region of the radiospectrum.
(right) The radial distribution of the brightness temperature T_b for 60 and 368 cm; calculated and observed values.

(This formula is justified is the layer considered is thin, both optically and geometrically. This is more or less the case at great diatances to the sun's limb).
In this way corrections have been found and a new model was determined by taking mean values between the results of *a* and *b*.
Second step: New calculations have been set up for this new model, in the same way as has been done with model CI. This yields the final model CII, which is given in table 79. The intensity distribution, computed with this model, is given in table 80. The apparent temperature for model CII is also given in figure 38a; the agreement between the observations and the calculations is now perfect in the whole spectral region.

§ 7. *Comparison with centre-to-limb variations at 60 and 368 cm.*

The weak point in our model is shown, when the calculated centre to limb variation is compared with radio-interferometric observations of the intensity distribution over the disc[164,96]. Although we have tried in the preceding section to find a model for which the agreement with the radio observations is as good as possible, the remaining differences are striking (cf. figure 38b). The agreement for 368 cm may be considered as tolerable, if we consider that the observations at great distances to the sun, say $r/R > 2$ are not reliable – the corrections for the influence of the apparatus function are very great in that region. The differences are

TABLE 79. The working model of the chromosphere and corona. (model CII).

h ($.10^{-11}$)	T ($.10^{-6}$)	N_e ($.10^{-9}$)
0,000 6	0,005 3	42,6
0,001 0	0,008 3	11,8
0,0015	0,012 0	4,68
0,0025	0,018 0	1,95
0,0040	0,027	1,04
0,0060	0,040	0,616
0,008	0,063	0,457
0,010	0,118	0,375
0,0125	0,309	0,330
0,015	0,427	0,289
0,025	0,632	0,229
0,040	0,776	0,184
0,060	0,86	0,132
0,100	0,86	0,080
0,150	0,800	0,045 7
0,250	0,683	0,020 9
0,400	0,562	0,007 9
0,600	0,446	0,003 6
1,00	0,340	0,00069
1,50	0,320	0,00014
2,5	0,32	0,000039
4,0	0,32	0,000016
6,0	0,32	0,000009

greater for 60 cm; it is remarkable there, that the limb brightening, so obvious in the predicted curve is absent in the observations. It is possible that the chromospheric bright ring has

TABLE 80. Centre-to-limb variation of the brightness temperature. The apparent temperature and the percentage of radiation outside the solar disc. All values have been computed with model CII. All T values are multiplied by 1000.

r/R	0,0	0,5	0,9	0,99	1,01	1,2	1,5	2,0	3,0	T_a	% int. outside disc
λ = 1	7,9	7,9	9,0	10,9	0,97					8,75	--
3	12,8	13,0	15,3	19,3	10,9					14,7	4%
10	25,9	29,7	36,8	51,7	102					43,5	15%
30	81,3	89,8	116	180	243	15,8				142	28%
100	359	436	516	641	688	192	19,9			743	37%
300	781	782	784	816	786	689	180	17,6		1570	50%
1000	580	574	636	553	563	552	525	192	1,8	2164	72%

been entirely smoothed out by the apparatus. The way, in which the observations are generally published is not right: it would be better to give the *uncorrected* functions *together* with the apparatus profile. For a comparison of the observations with the theoretical results, the latter could then be smoothed out by the apparatus profile and then the agreement between *this* result and the observations could be checked.

It is interesting to notice in this respect that REULE[206], after an investigation of a great number of possible models of the corona, concluded that it is *impossible* to explain the observations of STANIER[164] on the basis of the generally adopted density distribution in the corona.

Hence, we are inclined to believe that the best way to compare at present theory with observations is to make use of *eclipse observations*. These are free from the ambiguity of interference observations.

§ 8. *The intensity of radio-radiation outside the disc.*

Observations, made during partial eclipses are of less value: hence we restrict ourselves to the observations made during annular and total eclipses[36,37,89,210,211].

We summarize the observed ratios between the radiation at minimum of the eclipse and the total radiation observed before or after the eclipse. These are compared with the calculated ratios, according to table 80 but corrected for the influence of the differences between the radii of the sun and the moon:

			obs:	calc:
Hagen *et al*,	3 cm;	12-9-'50;	5,6%;	2%;
Hagen *et al*,	10 cm;	12-9-'50;	16 %;	13%;
Hagen *et al*,,	65 cm;	12-9-'50;	27 %;	29%;
Denisse *et al*,	3 cm;	1-9-'51;	16 %;	12%;
Denisse *et al*,	178 cm;	1-9-'51;	48 %;	43%;
Laffineur *et al*,	55 cm;	25-2-'52;	19,5%;	24%;
Laffineur *et al*,	117 cm;	25-2-'52;	30,5%;	31%;

FIGURE 39

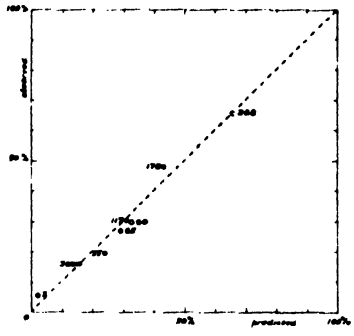

Comparison of the observed and computed ratios between the radio-intensity outside the solar disc and the total radiation. Filled circles denote eclips observations; open circles represent results, derived from interferometric observations. The numbers are wavelength in cm.

The agreement between the observed and the computed values may be called satisfactory. This may be considered as a support to our view, stated above, that the interferometric observations are probably not wholly trustworthy and smooth out the bright ring.

To test his hypothesis further, we compute the percentage of radiation outside the solar disc, as it has been observed interferometrically by STANIER[164] and MACHIN[96]. This quantity should be less affected by the uncertainty due to the apparatus function than would be the case for the exact *form* of the brightness distribution.

We find at 60 cm:	observed ratio	30%
	predicted	33,5%
at 368 cm:	observed ratio	66%
	predicted	66%

These results, which are given in figure 39, together with tne eclipse results, show that our model seems to be well in agreement with these observations; but more observations are certainly necessary.

CHAPTER XIV

H_α IN THE CHROMOSPHERE

§ 1. *Introduction.*
One of the most serious problems related to the hydrogen spectrum of the sun is the explanation of the hydrogen lines in the chromosphere. At present two difficulties seem to prevent the understanding of this spectrum: the population of the atomic levels deviates from that, predicted from BOLTZMANN's and SAHA's laws; and the dynamic character of the chromosphere makes a quantitative discussion very difficult.
These are the reasons that it is not possible for the moment to study the hydrogen spectrum of the chromosphere inductively: the uncertainty is too great. Moreover, we still lack sufficiently accurate observations of the line profiles and their absolute values (our observations, given in chapter III seem to be the only available at present). The aim of this chapter is more modest: we want to calculate the variation of the intensity in the centre of H_α as a function of the distance to the limb of the sun. The result of these calculations will be compared with our observations (table 18; chapter III); agreement will be found in the low chromosphere, while in the high part of the chromosphere great differences occur. Some indications will be given about the way in which the solution of the discrepancy must probably be sought.
This result is not wholly satisfactory; but the calculations, given in this chapter, which seem to be the first of this kind, are intended as a guide for future calculations rather than as a final theory.

§ 2. *Calculation of the central intensity of H_α.*
If we neglect the induced emissions, the total energy, emitted in the line H_α per cm^3 of a gas containing N_3 hydrogen atoms in the third level is

$$E_{3-2}\, d\nu d\omega = N_3\, A_{3-2}\, h\, \nu_{3-2}\, d\nu d\omega = 1{,}32.10^4\, N_3\, d\nu d\omega \text{ ergs/sec.} \qquad \text{(XIV,1)}$$

A is the EINSTEIN transition probability. Now, the central intensity of a Doppler profile normalized to unity, and with a total half width of d Angström units, is (see e.g. [65]):

$$1{,}06.10^8/d \qquad \text{(XIV,2)}$$

Since further for H_α:

$$d = 0{,}167.\omega^{-\frac{1}{2}} \text{ Angström units,} \qquad \text{(XIV,3)}$$

we find, combining (XIV,1) (XIV,2) and (XIV,3):

$$E_{3-2}\ (\Delta\lambda = 0)\ d\nu d\omega = 8{,}37.10^4 \omega^{\frac{1}{2}}\, N_3\, d\nu d\omega \qquad \text{(XIV,4)}$$

The intensity in the centre of H_α will be computed for four distances to the limb of the sun for two cases: in the first case the influence of self-absorption is entirely neglected and in the second case it is taken into account, just to shows the difference. Moreover, in the second case the calculations will be made for two dilution factors: $W = 0{,}5$ and $W = 0{,}0$.

a. Calculations, neglecting self-absorption.
The integrations have been made for
$r/R - 1 = 0{,}001$; $0{,}004$; $0{,}008$ and $0{,}012$,
for which $h =$ 700; 2800; 5600 and 8400 km.
Our model of the chromosphere, derived in the preceding chapter will be used (cf. table 79).
For the calculations of N_3, BOLTZMANN's law cannot be used since the deviations from this law are very important, especially in the high chromosphere. GIOVANELLI's tables will be used, which give the populations of the substates of principal quantum numbers 1, 2 and 3 for several values of the electron density and for several electron temperatures[53]; his results have been calculated, assuming the presence of radiation from a black body at a temperature of 5000°. These tables have been obtained for three dilution factors: 1,0; 0,5 and 0,0. In *this* calculation the dilution factor 0,5 will be used.
It must be noted that THOMAS[171,172] has also discussed the problem of the deviations of the hydrogen populations from thermodynamic equilibrium; since his results agree roughly with those of GIOVANELLI, we think it permitted to use GIOVANELLI's tables, which are given in a form, suitable to our calculations.

It is not necessary to give details on the performing of the integration: the total emission has been computed by numerical integration of (XIV,4) along lines of sight with a minimum distance to the sun's limb, equal to the four

TABLE 81. Calculated and observed intensities in the centre of $H\alpha$ in the chromosphere, as a function of the distance to the sun's limb.
All intensities are expressed in ergs cm^{-2} sec^{-1}. (frequency unit)$^{-1}$.(unit of solid angle)$^{-1}$.

h(km)		700	2 800	5600	8400
without self-absorption		25600.10^{12}	103.10^{12}	808.10^{9}	33.10^{9}
with self-absorption	$W = 0,5$	133.10^{12}	100.10^{12}	808.10^{9}	33.10^{9}
	$W = 0,0$	$13,8.10^{12}$	$20,1.10^{12}$	655.10^{9}	33.10^{9}
$h(\triangleq \tau = \frac{2}{3})$ (km)	$W = 0,5$	1000	-	-	-
	$W = 0,0$	3000	3000	-	-
observed intensities		15.10^{12}	16.10^{12}	6600.10^{9}	1500.10^{9}

values given above. The results are listed in table 81.

b. Calculations with self-absorption.
To compute the influence of self-absorption, we first derive the excitation coefficient in the core of the line; it is per hydrogen atom in the second substate:

$$k = \frac{\sqrt{\pi}\, e^2}{mc^2} \frac{\lambda^2 f}{1,19\, d} = 1,16.10^{-13}\, d^{-1}$$

Hence, the absorption coefficient per cm is

$$1,16.10^{-13}.N_2\, d^{-1}.$$

Then the optical depth along the line of sight is computed, and after that the intensity in the core of $H\alpha$ is found according to

$$I\ (\Delta\lambda=0) = \int E_{3-2}\ (\Delta\lambda=0)(h).e^{-\tau(h)}\, dh,$$

in which formula the integration is performed along the line of sight. *These* calculations are made for two dilution factors: $W = 0,0$ and 0,5. The results are given in table 81.

§ 3. *Discussion.*
We note:
a. In the low chromosphere, up to a height, somewhere between 2800 km and 5600 km our observations agree to the calculations for $W = 0$.
b. In the regions above that level, the deviations between theory and observations increase with the distance to the sun's limb. The ratio between the observed and the computed intensities is already 10 at 5600 km and it is about 50 at 8400 km.
c. The importance of self-absorption is shown in rows 5 and 6 of the table. For $W = 0,0$ the observations, made at 700 km from the limb of the sun, refer in fact to layers at a true distance to the solar surface of 3000 km.

These three remarks will now be discussed:
The agreement with the observations in the low levels would suggest assuming for future calculations of $H\alpha$ a dilution factor $W = 0,0$. But from the theoretical standpoint this is not justified. The excitation coefficient in the centre of $H\alpha$ is so great that at a height of 700 km above the solar surface the "sight" is about 500 km. This means that the light from the disc of the sun does not directly influence the excitation of the hydrogen substates; the radiation field, affecting the hydrogen atoms in the chromosphere is defined only by the distribution of the absorbing and emitting H atoms in the chromosphere. This field must be calculated exactly; we wish to note that there are no basic difficulties preventing this calculation; the mathematical apparatus is developed but the computation will be rather difficult.
In the high chromosphere the observations give much greater intensities than the calculations. Tentatively we suggest the following possible solution. The dynamical character of the chromosphere, which is shown very markedly in the spicules, is important at these great heights. We must, assume, as is suggested by the spicules, a streaming of matter towards the high levels. This matter emits the light of $H\alpha$. Hence, it must be cooler or denser than the surrounding matter, since at the temperatures and densities, prevailing at these high levels, the hydrogen is mainly ionised and the $H\alpha$ emission is negligible.
Now, because of this inhomegeneous structure of the chromosphere, the temperatures and densities of our model must probably be considered as *mean* values where the "mean" has to be taken over the matter at rest and the upward moving matter. Suppose that at a height h a fraction θ of the matter is in the "normal" state (= at the temperature and pressure predicted by

the model) and a fraction (1 - θ) consists of upward moving matter.

Suppose further that the upward moving matter (which is assumed to keep the temperature and density, which it had in the layer of origin) originates from the 3000 km level. This height of 3000 km is not chosen wholly arbitrarily but it seems to be supported by the observations of the spicules and by the fact that our calculations agree with the observations up to that height. Then it is possible to make a rough estimate of the fraction θ, by comparing the intensity, observed at a height h with the intensity, observed at 3000 km, this being about 16.10^{12} ergs/sec.

This yields at 5600 km $\theta = 0,5$;
at 8400 km $\theta = 0,9$.

These two data seem to be reasonable; they are suggested already more or less by photographs of chromospheric spicules; exact photometry of spicules would give further informations.

Naturally this assumption is not entirely justified since the model has been derived from the optical and the radio measurements and gives already the *mean* values of T and Ne; it is not permitted to add a deviating component to this model. It should be necessary to assume in this case that the chromosphere consist of (*a*) streaming matter with the temperature and pressure of the matter at 3000 km, and (*b*) matter at rest with higher temperatures and lower densities than the values, given by the model CII. It is clear that in this latter case our conclusions given above remain *valid*, since the matter at rest would emit no light in H.

Finally it is noted that the existence of self absorption might be important for the interpretation of eclipse observations. So, REDMAN [144] finds that the Doppler width of H_δ, H_γ and H_δ at a distance of 1500 km to the limb corresponds with a kinetic temperature of 30000°. But it might be possible that this temperature does not correspond with a height of 1500 km but with a higher level. (N.B. This discussion is, of course, somewhat simplified: the light at the wavelengths where the intensity = ½ times the central line intensity originates from lower levels than the light from $\Delta\lambda = 0$. Only a thorough, quantitative discussion will show whether REDMAN's kinetic temperature needs correction).

§ 4. *The height of emission of the light from the core of $H\alpha$, observed in the centre of the disc.*

In chapter VIII we adopted as the mean optical depth of the light in the core of H_α ($\Delta\lambda = 0$), observed in the centre of the disc: $\tau_0 = 0,009$. This figure was calculated, neglecting a possible influence of the chromosphere. It was shown in this chapter that the influence of the chromospheric layers is probably not negligible; so the height of origin will now be estimated anew.

The excitation coefficient in the chromosphere at $\Delta\lambda = 0$ in $H\alpha$ is about 2.10^{-8} cm^{-1} at a height of 600 km above the surface of the sun. (This result follows from the model of the chromosphere and the data on the hydrogen excitation coefficient; we give this result without details on its derivation). This value remains nearly constant in the lower levels and decreases very fast in higher layers. Hence an optical depth unity will be reached at a height of 600 - $(2.10^{-8})^{-1}.10^{-5}$ = 100 km above the surface of the sun (there $\tau_0 = 0,002$).

The previously adopted value $\tau_0 = 0,009$ corresponds with a depth of 90 km below the surface; the difference with this new determination is 200 km.

However, it must be noted that this correction has no perceptible influence on the theoretical profiles, computed in chapter VIII.

If we only assume, that the layer, 100 km above the solar surface has the same temperature as the layer, 100 km below it, the resulting line intensity remains practically unchanged.

It is generally assumed that the temperature does indeed not change much in the low chromosphere and in the region of transition between chromosphere and phorosphere.

Conclusion. The calculations, presented in this chapter seem to indicate that a satisfactory, quantitative interpretation of the hydrogen spectrum of the chromosphere is possible. This requires

a. a precise knowledge of the model of the chromosphere; our model, derived in chapter XIII (table 79) does not seem to be in disagreement with the observations;

b. a quantitative calculation of the dilution factor;

c. knowledge of the distribution of the atoms over the substates; there is evidence that GIOVANELLI's calculations are correct;

d. incorporation of the dynamics of the chromosphere in the formulae.

BIBLIOGRAPHY

1 C.G. ABBOT, *Ann. Ap. Obs: Smithson. Inst.* **3**, 157, 1913.
2 C.G. ABBOT, *Ann. Ap. Obs. Smithson. Inst.* **4**, 221, 1922.
3 H. ALFVEN, *Arkiv Math. Phys. Astr.* **27A**, no 25, 1941.
4 C.W. ALLEN, *M.N.* **107**, 426, 1947.
5 C.W. ALLEN, *M.N.* **109**, 343, 1949.
6 L. d'AZAMBUJA, *Ann. Obs. Meudon* **8**, fasc. II, 1930.
7 F. BALDET, *B.S.A.F.* **38**, 383, 1924.
8 D. BARBIER, *Ann. d'Ap.* **9**, 173, 1946.
9 S. BAUMBACH, *Astr. Nachr.* **263**, 121, 1937.
10 L. BIERMANN, *Zs. für Ap.* **21**, 320, 1942.
11 L. BIERMANN, *Himmelswelt* **55**, 121, 1948.
12 E.J. BLUM and J.F. DENISSE, *C.R. Paris* **231**, 1241, 1950.
13 E.J. BLUM and J.F. DENISSE, *C.R. Paris* **232**, 387, 1950.
14 P. ten BRUGGENCATE, H. GOLLNOW, S. GUNTHER and W. STROHMEIER, *Zs. fur Ap.* **26**, 51, 1949.
15 P. ten BRUGGENCATE, H. GOLLNOW and F.W. JÄGER, *Zs. fur Ap.* **27**, 223, 1950.
16 H.C. BURGER and P.H. van CITTERT, *Zs. für Phys.* **79**, 722, 1932.
17 H.C. BURGER and P.H. van CITTERT, *Zs. für Phys.* **81**, 428, 1933.
18 I.W. BUSBRIDGE, *M.N.* **101**, 26, 1941.
19 F.W.C.A. BUYS and F.E.M. ONGERING, *B.A.N.* **10**, 347, 1948.
20 R. CANAVAGGIA, D. CHALONGE, M. EGGER-MOREAU and H. OZIOL-PELTEY, *Ann. d'Ap.* **13**, 355, 1950.
21 D. CHALONGE and R. CANAVAGGIA, *Ann. d'Ap.* **9**, 143, 1946.
22 D. CHALONGE and R. CANAVAGGIA, *Ann. d'Ap.* **9**, 149, 1946.
23 D. CHALONGE and V. KOURGANOFF, *Ann. d'Ap.* **9**, 69, 1946.
24 S. CHANDRASEKHAR, *Ap. J.* **100**, 76, 1941.
25 S. CHANDRASEKHAR and F.H. BREEN, *Ap. J.* **104**, 430, 1946.
26 G.G. CILLIE and D.H. MENZEL, *Ap. J.* **85**, 88, 1937.
27 P.H. van CITTERT, *Zs. für Phys.* **68**, 547, 1930.
28 P.H. van CITTERT, *Zs. für Phys.* **69**, 298, 1931.
29 W.J. CLAAS, *Recherches Utrecht* **12**, (1), 1951.
30 A.E. COVINGTON, *Nature* **159**, 405, 1947.
31 L.L. McCREEDY, L.J. PAWSEY and R. PAYNE-SCOTT, *Proc. Roy. Soc. London, A* **190**, 357, 1947.
33 C.R. DAVIDSON, M. MINNAERT, L.S. ORNSTEIN and F.J. M. STRATTON, *M.N.* **88**, 536, 1928.
34 A. DEMIDOVA, *Trudy G.A.O. Leningrad* **15**, 230, 1950.
36 J.F. DENISSE, *C.R. Paris* **233**, 1951.
37 J.F. DENISSE, *C.R. Paris* **234**, 1952.
38 H. DESLANDRES, *Ann. Obs. Meudon* **4**, (1), 1910.
39 R.H. DICKE, R. BERINGER, *Ap. J.* **103**, 375, 1946.
40 E. van DIEN, *Ap. J.* **109**, 452, 1949.
41 A.S. EDDINGTON, *The internal Constitution of the Stars*, Cambridge, 1926.
42 A.S. EDDINGTON, *M.N.* **89**, 620, 1929.
43 B. EDLEN, *Arkiv Math. Phys. Astr.* **28B**, no. 1. 1941.
44 D.S. EVANS, *M.N.* **99**, 156, 1939.
45 D.S. EVANS, *M.N.* **100**, 156, 1940.
46 D.S. EVANS, *M.N.* **107**, 433, 1947.
47 D.S. EVANS, *The Obs.* **67**, 138, 1947.
48 J.L. GABBARD and M. DOLE, *Journ. Amer. Chem. Soc.* **59**, 181, 1937.
49 L. GOLDBERG, O.C. MOHLER and R.R. McMATH, *Ap. J.* **109**, 28, 1949.
50 O.C. MOHLER, A.K. PIERCE, R.R. McMATH and L. GOLDBERG, *Photometric Atlas of the near Infrared Solar Spectrum*, Ann. Arbor, 1950.
51 H. GOLLNOW, *Naturwiss.* **36**, 175 and 213, 1949.
52 A. GORDON, *Ann. d. Phys.* (V), **2**, 1031, 1929.
53 R.G. GIOVANELLI, *Austr. J. Sci. Res.* **1**, 289, 1948.
54 R.G. GIOVANELLI, *M.N.* **109**, 298, 1949.
55 W. GROTRIAN, *Zs. für Ap.* **3**, 199, 1931.
56 W. GROTRIAN, *Zs. für Ap.* **8**, 124, 1934.
57 J.P. HAGEN, *Georgtown Obs. Repr.* **13**, 1949.
58 J.P. HAGEN, *Ap. J.* **113**, 547, 1951.
59 L.G. HENYEY, *Proc. Nat. Acad. Sci.* **26**, 50, 1940.
60 J. HOLTSMARK, *Ann. d. Phys.* **58**, 576, 1919.
61 J. HOLTSMARK, *Phys. Zs.* **25**, 73, 1924.
62 J. HOUTGAST, *thesis*, Utrecht, 1942.
63 J. HOUTGAST, *B.A.N.* **10**, 417, 1948.
64 H.C. van de HULST, *B.A.N.* **10**, 79, 1946.
65 H.C. van de HULST and J.J.M. REESINCK, *Ap. J.* **106**, 121, 1947.
66 H.C. van de HULST, *B.A.N.* **11**, 135, 1951.
67 H.C. van de HULST, *B.A.N.* **11**, 156, 1951.
68 C. de JAGER, *Proc. Acad. Amsterdam* **51**, 731, 1948.
69 C. de JAGER, *Proc. Acad. Amsterdam* **51**, 1159, 1948.
70 C. de JAGER and L. NEVEN, *Proc. Acad. Amsterdam* **53**, 1577, 1950 = *Comm. Obs. Roy. Belg.* **23**, 1950.
71 C. de JAGER and J.-C. PECKER, *C.R. Paris* **232**, 1645, 1951 = *Contr. I.A.P. série A*, **89**.
72 C. de JAGER and L. NEVEN, *Proc. Acad. Amsterdam* **55**, 153, 1952.
73 C. de JAGER and L. NEVEN, *Proc. Acad. Amsterdam* **55**, 1952.
74 W.H. JULIUS, *B.A.N.* **1**, 119, 1922.
75 W.H. JULIUS, *Hemel en Dampkring* **21**, 57, 1923.
76 P.C. KEENAN, *Ap. J.* **75**, 277, 1932.
77 P.C. KEENAN, *Ap. J.* **76**, 134, 1932.
78 A. KOEKELENBERGH, *Inst. d'Astr. Bruxelles* (2), **67**, 1951.
79 D. KOELBLOED, W. VELTMAN, *Proc. Acad. Amsterdam* **54**, 468, 1951 = *Circ. Ast. Inst. Amsterdam* **3**.
80 Z. KOPAL, *Ap. J.* **104**, 60, 1946.
81 V. KOURGANOFF, *C.R. Paris*, **228**, 2011, 1949 = *Contr. I.A.P. série A*, **46**.
82 T.W. KRAT, *Isw. G.A.P. Pulkowo* **137**, 1948.
83 M.K. KROGDAHL, *Ap. J.* **110**, 355, 1949.
84 G.P. KUIPER, W. WILSON and R.J. CASHMAN, *Ap. J.* **106**, 243, 1947.
85 D. LABS, *Zs. für Ap.* **28**, 150, 1951.
86 D. LABS, *Zs. für Ap.* **29**, 199, 1951.
87 R. LADENBURG, in *Muller-Pouillet, Physik;* **2**, 2nd half, chapter 40.
88 M. LAFFINEUR and J. HOUTGAST, *Ann. d'Ap.* **12**, 137, 1949.
89 M. LAFFINEUR, *C.R. PARIS*, **234**, 1952.
90 F.J. LEHANY, D.E. JABSLEY, *Austr. J. Sci. Res.* A, **2**, 48, 1949.
91 W. LENZ, *Zs. für Phys.* **25**, 299, 1924.
92 R. LUNDBLAD, *Ap. J.* **58**, 113, 1923.
93 E. LINDHOLM, *Thesis*, Uppsala, 1942.
94 B. LYOT, *B.S.A.F.* **51**, 211, 1937.
95 B. LYOT, *M.N.* **99**, 580, 1939.
96 K.E. MACHIN, *Nature*, **167**, 889, 1951.
97 D.F. MARTYN, *Proc. Roy. Soc. London, A* **193**, 44, 1948.
98 W.H. McCREA, *M.N.* **89**, 718, 1929.
99 D.H. MENZEL, *Publ. Lick Obs.* **17**, 1, 1931.
100 D.H. MENZEL and C.L. PEKERIS, *M.N.* **96**, 77, 1936.

101 R. MICHARD, *Contr. I.A.P. serie A*, **37**, 1949.
102 R. MICHARD, *Ann. d'Ap.* **12**, 143, 1949.
103 R. MICHARD, *B.A.N.* **11**, 227, 1950.
104 M. MIGEOTTE and L. NEVEN, *Mem. Soc. Roy. Sci. Liège*, **12**, 165, 1952.
105 M. MINNAERT, *B.A.N.* **2**, 75, 1924.
106 M. MINNAERT, *Zs. für Phys.* **45**, 610, 1927.
107 M. MINNAERT and G.W.F. MULDERS, *Zs. für Ap.* **2**, 165, 1931.
108 M. MINNAERT, G.W.F. MULDERS and J. HOUTGAST, *Photometric Atlas of the Solar Spectrum*; Sterrewacht Sonnenborgh, Utrecht, 1940.
109 M. MINNAERT, *B.A.N.* **10**, 403, 1948.
110 M. MINNAERT, E. van den HOVEN van GENDEREN and J. van DIGGELEN, *B.A.N.* **11**, 55, 1949.
111 M. MINNAERT, in "The Solar System", Vol **1**, 1952.
112 H.C. MINNETT, N. LABRUM, *Austr. J. Sci. Res. A* **3**, 60, 1950.
113 S.A. MITCHELL, *Ap. J.* **105**, 1, 1947.
114 S. MIYAMOTI, *Publ. Astr. Soc. Japan*, **1**, 14, 1949.
115 S. MIYAMOTO, *Mem. of Astrophysics*, Oct. 1949, pag. 8.
116 W.J.H. MOLL, H.C. BURGER and J. van der BILT, *B.A.N.* **3**, 83, 1925.
117 B. MROWKA, *Ann. d. Phys.* **12**, 756, 1932.
118 G.W.F. MULDERS, *Zs. für Ap.* **11**, 132, 1936.
119 G. MÜNCH, *Ap. J.* **109**, 275, 1949.
120 Naval Res. Lab. Comm. Cf[57].
121 L. NEVEN and C. de JAGER, *B.A.N.* **11**, 291, 1951.
122 M. NICOLET, *Ann. d'Ap.* **14**, 249, 1951.
123 A. PANNEKOEK and M. MINNAERT, *Verh. Acad. Amsterdam* **13**, no. 5, 1928.
124 A. PANNEKOEK, *M.N.* **91**, 139, 1930.
125 A. PANNEKOEK, *B.A.N.* **7**, 151, 1933.
126 A. PANNEKOEK, *M.N.* **98**, 694, 1938.
127 J.L. PAWSEY and D.E. JARSLEY, *Austr. J. Sci. Res.* **2**, 198, 1949.
128 J.-C. PECKER, *Ann. d'Ap.* **12**, 1, 1949.
129 J.-C. PECKER and Ch. PECKER, *Ann. d'Ap.* **12**, 197, 1949.
130 J.-C. PECKER, Thesis, Ch. V; *Ann. d'Ap.* **14**, 1951.
131 R. PEYTURAUX, *C.R. Paris*, **232**, 931, 1951 = *Contr. I.A.P. serie A*, **83**.
132 R. PEYTURAUX, *C.R. Paris*, **230**, 368, 1950 = *Contr. I.A.P. serie A*, **53**.
133 J.H. PIDDINGTON and H.C. MINNETT, *Austr. J. Sci. Res. A* **2**, 539, 1949.
134 J.H. PIDDINGTON and J.V. HINDMAN, *Austr. J. Sci. Res. A* **2**, 524, 1949.
135 J.H. PIDDINGTON and H.C. MINNETT, *Proc. Roy. Soc. London, A* **203**, 417, 1950.
136 J.H. PIDDINGTON, *Proc. Roy. Soc. London, A* **203**, 421 1950.
137 A. PIERCE, R.R. McMATH, L. GOLDBERG, O.C. MOHLER, *Ap. J.* **112**, 289, 1950.
138 A. PIERCE and L.H. ALLER, *Ap. J.* **114**, 145, 1951.
139 H.H. PLASKETT, *M.N.* **96**, 402, 1936.
140 H.H. PLASKETT, *M.N.* **101**, 3, 1941.
141 H. RAUDENBUSCH, *A.N.* **266**, 301, 1938.
142 G. REBER and J.L. GREENSTEIN, *Obs.* **67**, 15, 1947.
143 R.O. REDMAN, *M.N.* **97**, 552, 1937.
144 R.O. REDMAN, *M.N.* **102**, 140, 1942.
145 R.O. REDMAN, *M.N.* **102**, 146, 1942.
146 R.O. REDMAN, *M.N.* **103**, 173, 1943.
147 W.O. ROBERTS, *Ap. J.* **101**, 101, 1945.
148 W.O. ROBERTS, V.K. BRENTON, M.B. SHARPLEY and Z. KOPAL, *P.A.S.P.* **61**, 160, 1949.
149 A. ROSA, *Zs. für Ap.* **24**, 38, 1947.
150 S. ROSSELAND, *Ap. J.* **63**, 218, 1926.
151 T. ROYDS and A.L. NARAYAN, *Kodaikanal Obs. Bull.* **109**, 1936.
152 R. RUDKJØBING, *Ann. d'Ap.* **9**, 7, 1946.
153 M. RYLE and D.P. VONBERG, *Proc. Roy. Soc. Londen, A*, **193**, 98, 1948.
154 K.F. SANDER, *Nature*, 159, 506, 1947.
155 E. SCHATZMAN, *Ann. d'Ap.* **12**, 203, 1949.
156 P. SCHMALJOHANN, Cf. Unsold[177], pag. 182.
157 E. SCHRÖDINGER, *Ann. d. Phys.* (IV) **80**, 486, 1926.
158 W.W. SOBOLEW, *Astr. Zjurn.* **26**, 129, 1949.
159 G.C. SOUTHWORD, *Journ. Franklin Inst.* **239**, 285, 1945.
160 L. SPITZER, M.N. **96**, 794, 1936.
161 L. SPITZER, *Phys. Rev.* **55**, 694, 1939.
162 L. SPITZER, *Phys. Rev.* **56**, 39, 1939.
163 L. SPITZER, Ap. J. **99**, 1, 1944.
164 H.M. STANIER, *Nature*, **165**, 354, 1950.
165 B. STRÖMGREN, *Zs. für Ap.* **10**, 237, 1935.
166 B. STRÖMGREN, *Festschrift für E. Stromgren*, 1940.
167 B. STRÖMGREN, *Publ. København* **138**, 1944.
168 O. STRUVE and C.T. ELVEY, *Ap. J.* **72**, 277, 1930.
169 Z. SUEMOTO, *Publ. Astr. Soc. Japan* **1**, 78, 1949.
170 A.D. THACKERAY, *M.N.* **95**, 293, 1935.
171 R.N. THOMAS, *Ap. J.* **108**, 142, 1948.
172 R.N. THOMAS, *Ap. J.* **109**, 480, 1949.
173 R.N. THOMAS, *An. J.* **54**, 196, 1949.
174 R.N. THOMAS, *Ap. J.* **111**, 165, 1950.
175 A. UNSÖLD, Zs. *für Phys.* **59**, 353, 1929.
176 A. UNSÖLD, *Zs. für Ap.* **4**, 319, 1932.
177 A. UNSÖLD, *Physik der sternatmosphären*,, Springer, Berlin, 1938.
178 A. UNSÖLD, *V.J.S.* **78**, 213, 1943.
179 A. UNSÖLD, *Nachr. Akad. Wiss. Göttingen*, Math. Phys. Kl. **71**, 1945.
180 A. UNSÖLD, *Ann. d. Phys.* (VI) **3**, 124, 1948.
181 A. UNSÖLD, *Zs. für Naturforschung* **3a**, 486, 1948.
182 A. UNSÖLD, *Zs. für Naturforschung* **7a**, 121, 1952.
183 S. VERWEY, *Publ. Astr. Inst. Amsterdam* **5**, 1936.
184 H.H. VOIGT, *Zs. für Ap.* **27**, 82, 1950.
185 M. WALDMEIER, *Helv. Phys. Acta* **13**, 14, 1940.
186 M. WALDMEIER, *Experientia* **2**, no. 12, 1946.
187 M. WALDMEIER, *Ast. Mitt. Zürich* **149**, 1947.
188 A.J.M. WANDERS, *Thesis, Utrecht*, 1933.
189 A.J.M. WANDERS, *Zs. für Ap.* **8**, 108, 1934.
190 V. WEISZKOPF, *Zs. für Phys.* **75**, 287, 1932.
191 V. WEISZKOPF, *Phys. Zs.* **34**, 1, 1933.
192 A.J. WESSELINK, *B.A.N.* **9**, 81, 1940.
193 R. v.d. WOOLLEY, *M.N.* **94**, 631, 1934.
194 R. v.d. WOOLLEY, *M.N.* **101**, 58, 1941.
195 R. v.d. WOOLLEY and C.W. ALLEN, *M.N.* **110**, 358, 1950.
196 R. WILDT, *Ap. J.* **105**, 36, 1947.
197 K.O. WRIGHT, *Ap. J.* **99**, 249, 1944.
198 H. ZANSTRA, *M.N.* **101**, 250, 1941.
199 H. ZANSTRA, *M.N.* **101**, 273, 1941.
200 H. ZANSTRA, *Proc. Amsterdam* **53**, 1289, 1950 = *Circ. Astr. Inst. Amsterdam* **1**.
201 C.G.J. ZWANIKKEN, *Thesis, Utrecht*, 1947.

202 H. KRISTENSON, *Stockholm Obs. Ann.* **17**, 1, 1951.
203 H.N. RUSSELL and J.Q. STEWART, *Ap. J.* **59**, 197, 1924.
204 M. WALDMEIER, *Zs. fur Ap.* **30**, 137, 1952.
205 J.L. PAWSEY, *Nature* **158**, 633, 1946.
206 A. REULE, *Zs. für Naturforschung* **7a**, 234, 1952.
207 R. PEYTURAUX, *C.R. Paris*, **233**, 1083, 1951 = *Contr. I.A.P. série A*, **98**.
208 Ch. PECKER, *C.R. Paris*, **232**, 1285, 1951 = *Contr. I. A.P. série A*, **87**.
209 R. CAYREL, *Ann. d'Ap.* **14**, 1, 1951.
210 J.P. HAGEN, F.T. HADDOCK and G. REBER, *Sky and Tel.* **10**, 11, 1951.
211 J.F. DENISSE, E.J. BLUM and J.L. STEINBERG, *Nature* **170**, 192, 1952.